The anthelmintic niclosamide is a potent TMEM16A antagonist that fully bronchodilates airways

Kent Miner[1], Benxian Liu[1], Paul Wang[2], Katja Labitzke[2,†], Kevin Gaida[1], Jian Jeffrey Chen[3], Longbin Liu[3,†], Anh Leith[1,†], Robin Elliott[1], Kathryn Henckels[1], Esther Trueblood[4,†], Kelly Hensley[4], Xing-Zhong Xia[1], Oliver Homann[5], Brian Bennett[1], Mike Fiorino[1], John Whoriskey[1], Sabine Escobar[1], Gang Yu[1], Joe McGivern[2], Min Wong[1], Teresa L. Born[1,†], Alison Budelsky[1,†], Mike Comeau[1], Dirk Smith[1,†], Jonathan Phillips[1], James A. Johnston[1], Kerstin Weikl[2,†], David Powers[2], Deanna Mohn[1,*], Andreas Hochheimer[2,†,*], John K. Sullivan[1,†,*]

[1]Department of Inflammation Research, Amgen Inc., Thousand Oaks, CA and Seattle, WA, USA
[2]Department of Therapeutic Discovery, Amgen Inc., Thousand Oaks, CA, USA and Regensburg, Germany
[3]Department of Medicinal Chemistry, Amgen Inc., Thousand Oaks, CA, USA
[4]Department of Comparative Biology and Safety Sciences, Amgen Inc., Seattle, WA, Thousand Oaks, CA and South San Francisco, CA, USA
[5]Genome Analysis Unit, Amgen Inc., South San Francisco, CA, USA
[†]Present address; see Additional Information section

*Corresponding authors. E-mails: jksullivan@polestarbio.com (J.K.S); ahochheimer@web.de (A.H.); dmohn@amgen.com (D.M.)

Abstract There is an unmet need in severe asthma where approximately 40% of patients exhibit poor β-agonist responsiveness, suffer daily symptoms and show frequent exacerbations. Antagonists of the Ca^{2+}-activated-Cl^{-} channel, TMEM16A, offers a new mechanism to bronchodilate airways and block the multiple contractiles operating in severe disease. To identify TMEM16A antagonists we screened a library of ~580,000 compounds. The anthelmintics niclosamide, nitazoxanide and related compounds were identified as potent TMEM16A antagonists that blocked airway smooth muscle depolarization and contraction. To evaluate whether TMEM16A antagonists resist use- and inflammatory-desensitization pathways limiting β-agonist action, we tested their efficacy under harsh conditions using maximally contracted airways or airways pretreated with a cytokine cocktail. Stunningly, TMEM16A antagonists fully (>92%) bronchodilated airways, while the β-agonist isoproterenol showed only partial (26-43%) effects. TMEM16A antagonists and repositioning of niclosamide or nitazoxanide could represent an important additional treatment for uncontrolled severe disease.

Introduction

Asthma afflicts over 300 million people worldwide, with 5-10% of patients suffering from severe disease which remains poorly controlled despite maximal treatment with an inhaled corticosteroid (ICS) and long-acting β-agonist (LABA). Inflammation is poorly controlled in severe asthmatics, which often necessitates addition of oral corticosteroids, and ~40% of patients show poor β-agonist responsiveness (***Moore et al.***, ***2007; Moore et al.***, ***2010***). Agonists of the β2-adrenergic receptor (β2AR) signal through the stimulatory G-protein, $G_s\alpha$, to activate adenylate cyclase (AC), increase cAMP levels and activate PKA. While this mechanism offers the advantage of delivering a negative intracellular signal (cAMP/PKA) to airway smooth muscle (ASM) cells that blocks multiple contractants, repeated β-agonist use and poorly controlled inflammation can cause desensitization of this pathway. Phosphodiesterases (PDE) can degrade cAMP, and increased levels of PDE4D have been detected in biopsies of asthmatic ASM cells leading to reduced β-agonist cAMP responses (***Trian et al.***, ***2011***). Proinflammatory cytokines or allergic inflammation has been found to increase expression of the inhibitory G-protein, $G_i\alpha$ (***Hakonarson et al.***, ***1996***), uncouple the β2AR from $G_s\alpha$-induced activation of adenylate cyclase (***Shore et al.***, ***1997***) and upregulate COX-2 and PGE2 production inducing heterologous β2AR desensitization of ASM cells and reduced β-agonist responsiveness (***Moore et al.***, ***2001***).

Ion channels represent an alternative target class to modulate contraction which may resist these desensitization pathways, but it has been poorly understood what channels control excitation-contraction coupling in ASM cells. In vascular and airway smooth muscle, bronchoconstrictors have been recognized for years to induce calcium-activated chloride channels (CaCCs) promoting chloride efflux and spontaneous transient inward currents (STICs)

contributing to depolarization and contraction, but the molecular identity of the channel has remained elusive (***Janssen et al.***, ***1995; Large et al.***, ***1996; Wellman et al.***, ***2003***).

In 2008, three separate groups employing distinct methods identified TMEM16A as the long sought-after calcium-activated chloride channel recognized in secretory epithelial cells, smooth muscle cells and sensory neurons (***Caputo et al.***, ***2008; Schroeder et al.***, ***2008; Yang et al.***, ***2008***). While these initial studies solidified TMEM16A's role in the bronchial epithelium as responsible for the elevated Ca^{2+}-dependent chloride secretion induced by Th2 cytokines, subsequent studies by ***Huang et al.***(***2012***) expanded this perspective demonstrating TMEM16A had a dual role in controlling both ASM contraction and epithelial mucin secretion, a hallmark of allergic asthma. Since this time investigations of its role in ASM cells has steadily progressed with biophysical studies, experiments with cells from knockout mice and pharmacological inhibitors firmly establishing its role in controlling STICs and airway smooth muscle contractility (***Danielsson et al.***, ***2015; Yim et al.***, ***2013; Zhang et al.***, ***2013; Zhuge et al.***, ***2010***). While these pivotal studies introduced TMEM16A antagonists as a promising new method to bronchodilate airways, only a limited number of compounds were explored and details of their relative efficacy compared to β-agonists remained unclear.

To identify additional TMEM16A antagonists and characterize their potential as novel bronchodilators, we screened a library of over half a million compounds. For the first time, we describe the approved drug niclosamide, nitazoxanide and related compounds as potent TMEM16A antagonists that provided robust bronchodilation of airways and resist use- and inflammatory-desensitization pathways limiting β-agonist action. We also discuss separate research from drug-repurposing screens finding the anthelmintics niclosamide and nitazoxanide have efficacy for treating a variety of other disorders, including cancer, and discuss this in the

context of TMEM16A, where antagonists have similarly been proposed as a promising new treatment for a variety of diseases including, cancer, pulmonary hypertension, secretory diarrhea, polycystic kidney disease and pain.

Results

Discovery of TMEM16A antagonists

To identify novel inhibitors of the TMEM16A channel we performed high-throughput screening of a library comprising ~580,000 compounds using a halide-sensitive YFP (eYFP) assay (***Fig. 1A***, ***Figure 1–figure supplement 1***). TMEM16A inhibitors were identified by measuring TMEM16A-dependent quenching of eYFP fluorescence intensity. HEK293T cells stably co-expressing the 'abc' splice variant of human TMEM16A and the YFP [H148Q,I152L] mutant (***De La Fuente et al.***, ***2008***) were pre-incubated either with test compound (5 μM final), buffer as 'Neutral Control' or an 'Inhibitor Control' (20 μM benzbromarone) (***Huang et al., 2012***) prior to addition of the iodide and ionomycin stimulus (***Fig. 1A***, ***Figure 1–figure supplement 1***). Ionomycin triggers the Ca^{2+}-dependent activation of TMEM16A, which allows iodide ions to enter the cell and quench eYFP fluorescence. Assay results were normalized based on the benchmark TMEM16A inhibitor benzbromarone providing 100 percent of inhibition (POI) or 0 percent of control (POC) response to the ionomycin (plus vehicle) stimulation alone which is defined as full activation of the channel (POC=100, POI=0). The entire library was screened at a single concentration and yielded 1,445 primary hits with an activity of POC<72.6% or >27.4% inhibition of TMEM16A activity. All primary hits were tested again in three independent, consecutive runs and confirmed 673 hits. In order to eliminate false-positive TMEM16A inhibitors, auto-fluorescent compounds were eliminated revealing 491 non-fluorescent hits. Dose

response assays using a Ca^{2+} flux assay further eliminated compounds, which non-specifically interfered with ionomycin-triggered calcium signaling. Dose response testing of these hits using the eYFP assay yielded 145 hits with an IC50<5μM (***Fig. 1B***). Finally, the HTS campaign delivered 130 TMEM16A inhibitors as validated hits, which also passed quality control by mass spec analysis. Niclosamide (Compound 1) and a related analog Compound 4 (***Fig. 1D***) were identified as interesting new antagonists with sub-μM potency, but partial block (31-39% inhibition) of TMEM16A halide-sensitive response. In fact, many of the hits provided less than 50% inhibition of the iodide eYFP quenching after ionomycin-activation of TMEM16A (***Fig. 1B***). This contrasts with the benchmark antagonist benzbromarone (***Huang et al.***, ***2012***), which fully blocked the halide-sensitive response as shown in the FLIPR kinetic fluorescence traces in ***Figure 1C*** and the representative dose-response curve provided in ***Figure 1E***. Interestingly, the TMEM16A benchmark antagonist 1PBC (***Fig. 1D***) described earlier by ***Peters et al.*** (***2015***) was also within our compound library, but with a POC of 74.8 it did not pass our hit cut-off of POC <72.6. To characterize this compound more thoroughly, however, we performed a dose-response analysis to determine its potency in blocking the halide-sensitive YFP response. As shown in the representative dose-response curve (DRC) in ***Figure 1G***, 1PBC, like niclosamide (***Fig. 1F***) and Compound 4 (***Fig. 1H***) only partially blocked the TMEM16A halide-sensitive response. The results of repeat tests are shown in ***Figure 1–figure supplement 3*** which provides composite dose-response curves for these compounds. With an average IC_{50} of 132 ± 67 nM (n=42), niclosamide represents one of the most potent TMEM16A antagonists described to date (***Table 1*** and ***Figure 1–figure supplement 3C***). Compound 4 inhibited the TMEM16A halide-sensitive response with an average IC_{50} of 0.901 ± 0.524 μM (n=53) while 1PBC and benzbromarone

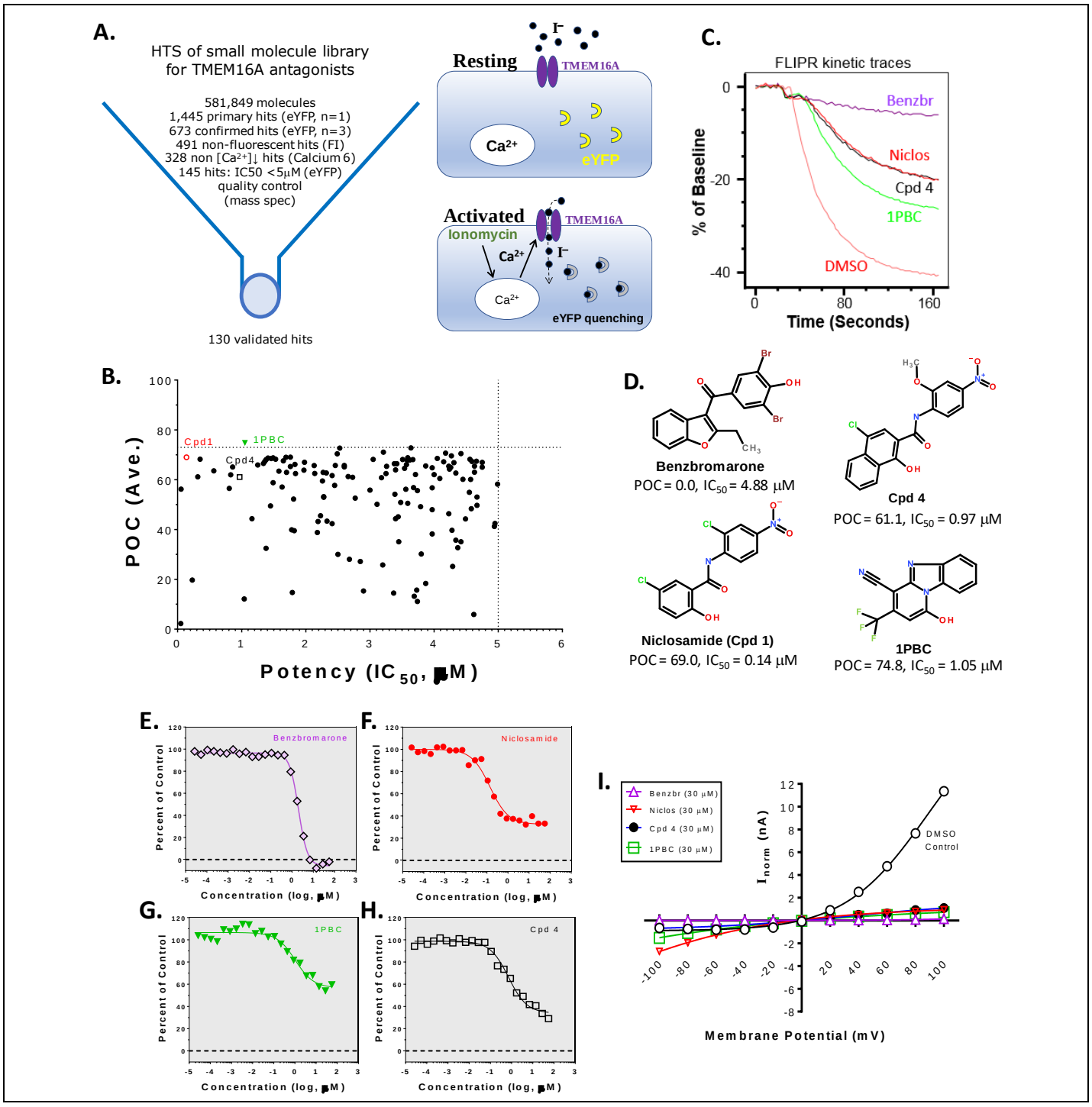

Figure 1. Discovery of inhibitors of the calcium-activated chloride channel TMEM16A by high-throughput screening. (**A**) TMEM16A eYFP assay principle and process flow scheme to identify validated hits. (**B**) Potency range of hits with IC50 < 5 µM and POC<72.6 (n=4) in halide-sensitive YFP assay. Representative FLIPR kinetic traces (**C**) and dose-response curves showing niclosamide (**F**), 1PBC (**G**) and Cpd 4 (**H**) only partially blocked the ionomycin-induced eYFP quenching (DMSO) using iodide as permeant anion compared to full block by benzbromarone (**E**), with compound structures provided in (**D**). In contrast, QPatch electrophysiology analysis of TMEM16A current-voltage response using 170 nM intracellular calcium shows the typical voltage-dependent response and reveals all the compounds were capable of fully blocking the chloride current (**I**).

Figure 1 continued on next page

Figure 1 continued

The following figure supplements are available for Figure 1:

Figure supplement 1. High-throughput-screening for TMEM16A antagonists and hit triaging
DOI:
Figure supplement 2. Signal distribution and quality control metrics of the TMEM16A HTS campaign
DOI:
Figure supplements 3 and **4.** Replicate compound dose-response data in TMEM16A eYFP assay
DOI:
Figure supplement 5. Distribution of potency of 304 niclosamide analogs in the TMEM16A eYFP assay
DOI:
Figure supplement 6 and **7.** TMEM16A QPatch voltage protocol and representative current-voltage raw traces versus time for the DMSO vehicle control or the benzbromarone positive control antagonist
DOI:
Figure supplement 8 and **9.** Representative TMEM16A current-voltage responses and impact of antagonists
DOI:

---

were of similar potency with IC_{50} of 1.523 ± 1.360 (n=17) and 1.508 ± 0.504 (n=58) μM, respectively (***Table 1*** and ***Figure 1–figure supplement 3***).

Antagonists partially block the TMEM16A iodide eYFP response but fully inhibit the calcium-activated chloride current

While our screen identified potent TMEM16A antagonists, many just partially inhibited the ionomycin-induced iodide quenching of the YFP halide sensor (***Fig. 1B-1H***), which was concerning. Therefore, we performed automated patch clamp electrophysiology to evaluate niclosamide, Cpd 4 and 1PBC for efficacy in inhibiting the TMEM16A chloride current. Importantly, these compounds at 30 μM fully inhibited the TMEM16A Ca^{2+}-activated Cl^{-} current by QPatch electrophysiology using 170 nM free $[Ca^{2+}]i$ (***Fig. 1I***) to same level as benzbromarone. At a lower concentration of 1.2 μM, these compounds still provided significant block of the TMEM16A outward chloride current (***Figure 1–figure supplements 8*** *and* ***9***). Significantly, the iodide/eYFP response (***Fig. 1F-1H***) was only partially inhibited despite doses

as high as 55.6 μM. This would suggest the efficacy of niclosamide, Cpd 4 and 1PBC in blocking TMEM16A depends on the permeate anion, with there being greater impact on chloride versus iodide permeation. Interestingly, ***Peters et al.*** (***2015***) report 1PBC interacts with four basic residues of the TMEM16A ion selectivity filter and provide supplementary data it only partially blocks the iodide eYFP response, but fully inhibited the chloride current. As shown in ***Figure 1,*** we have similar findings which could suggest niclosamide shares this mechanism as a pore blocker. Similarly, niflumic acid (NFA), which has been widely used as an antagonist of Ca^{2+}-activated Cl^{-} channels, has an apparent affinity for inhibiting TMEM16A that is inversely proportional to the channel permeability ratios for anions, with NFA showing significantly less potency in blocking iodide versus chloride (***Ni et al.***, ***2014***). We also found NFA was routinely about 3-fold less active in blocking the TMEM16A iodide eYFP response versus the TMEM16A chloride current, IC_{50} of 26.57 and 8.54 μM, respectively (***Table 1; Figure 1–figure supplement 4*** *and* ***Figure 2–figure supplement 5***).

It is clear from these studies that niclosamide, Cpd4 and 1PBC exhibit a distinct pharmacology from the benchmark antagonist benzbromarone, which fully inhibited both the iodide eYFP response and the TMEM16A chloride current. Besides benzbromarone, we also evaluated the TMEM16A antagonists dichlorophen, CaCCinh-A01, MONNA and T16Ainh-A01 described earlier as additional benchmarks (***De La Fuente et al.***, ***2008; Huang et al.***, ***2012; Namkung et al.***, ***2011b; Oh et al.***, ***2013***). Like benzbromarone, these compounds fully blocked the TMEM16A halide-sensitive YFP response with IC_{50} ranging from 4-8 μM, with the exception of T16Ainh-A01 which was inactive (***Table 1; Figure 1–figure supplements 3*** *and* ***4***). We also were unable to show significant activity of T16Ainh-A01 by QPatch electrophysiology using HEK293/TMEM16A cells and elevated intracellular calcium (***Table 1; Figure 2–figure***

supplement Fig. 4), while the three other benchmark antagonists were confirmed active in this ephys assay (***Table 1; Figure 2–figure supplements 1 - 3***). Our findings are consistent with those from ***Liu et al.*** (***2015***) who found T16Ainh-A01 had just minor effects in blocking TMEM16A expressed in CHO cells compared to other benchmark antagonists, including CaCCinh-A01. In support of these findings, studies with knock-out mice have clearly established a role of TMEM16A in controlling calcium-activated chloride secretion in airway and intestinal epithelial cells (***Ousingsawat et al.***, ***2009; Schreiber et al.***, ***2015***), yet T16Ainh-A01 had only weak effects on these cell types (***Namkung et al.***, ***2011a***). Additionally, studies with knock-out mice have demonstrated TMEM16A is responsible for slow waves in the gastrointestinal tract, yet ***Hwang et al.*** (***2016***) find antral and intestinal slow waves were blocked by the antagonists CaCCinh-A01 and benzbromarone, but insensitive to T16Ainh-A01.

In summary, a direct comparison of niclosamide to the five distinct TMEM16A antagonists described here indicated niclosamide, with an IC_{50} of 132 nM in the halide-sensitive YFP assay, is 10 to 60 times more potent than the other antagonists and may provide a unique mechanism for channel block. These findings motivated us to perform additional studies testing chemically similar compounds, selectivity against other chloride channels and effects in blocking airway smooth muscle cell depolarization and contraction of airways.

The niclosamide related compounds nitazoxanide and its metabolic product tizoxanide are also TMEM16A antagonists

The structure and activity of additional niclosamide-related compounds are provided in ***Figure 2***. Compounds 2, 3 and 5 provided sub-μM block of the TMEM16A eYFP response (***Fig. 2C*** *and* ***Table 1***), but like niclosamide only partially inhibited this *iodide* response while fully

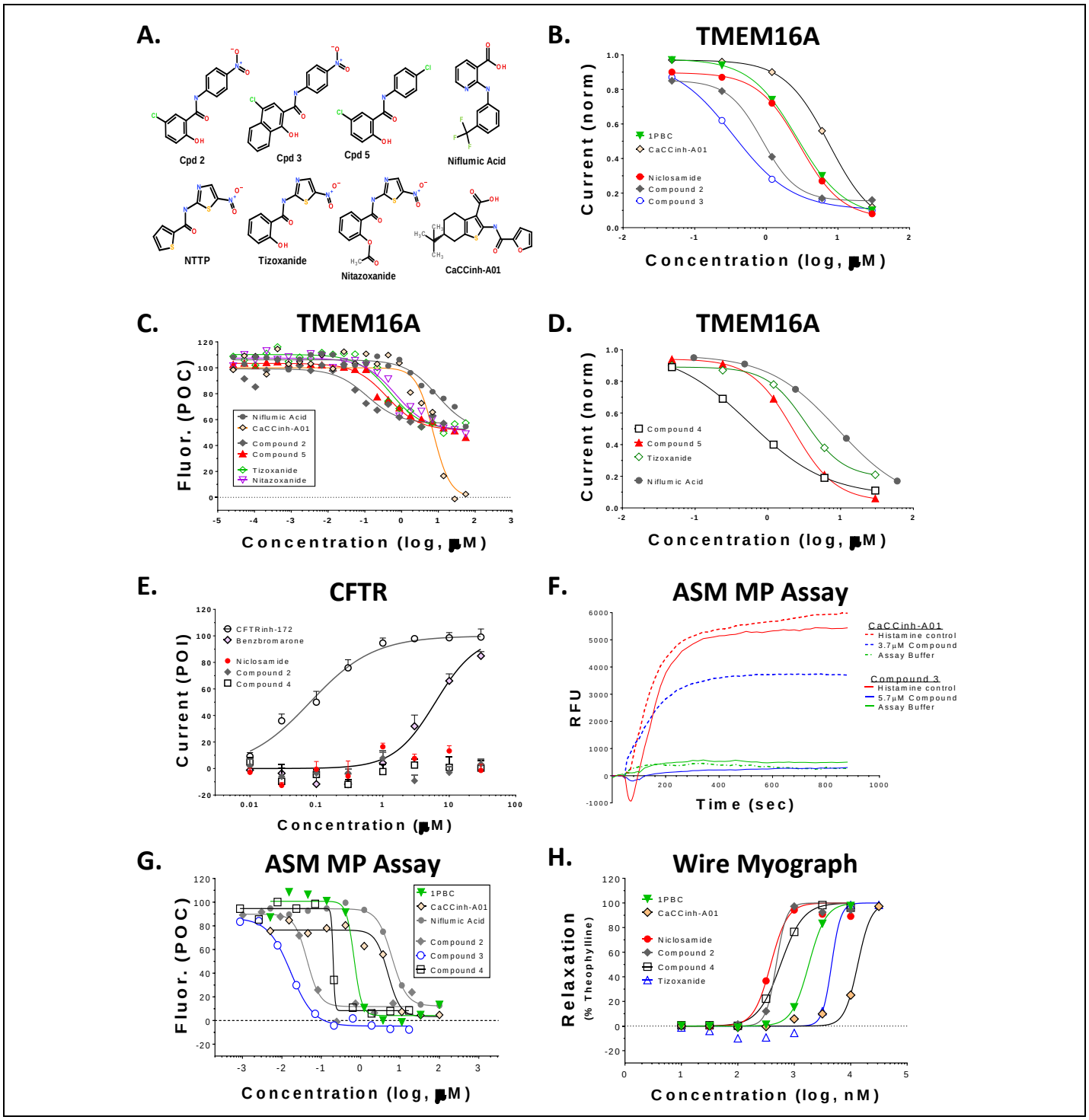

Figure 2. Niclosamide related compounds are potent and selective TMEM16A antagonists that block histamine depolarization of airway smooth muscle cells and provide robust bronchodilation of airway rings. (**A**) Structure of niclosamide, nitazoxanide and analogs. While niclosamide and relateds only partially blocked the ionomycin-induced TMEM16A eYFP response to iodide (**C**), they fully inhibited the TMEM16A calcium-activated chloride current (**B, D**), yet spared the cAMP-induced CFTR chloride current (**E**). Histamine depolarization of human ASM cells was fully blocked by TMEM16A antagonists as shown in kinetic traces in (**F**) and dose-response studies in (**G**). Carbachol pre-contracted mouse tracheal rings were fully relaxed by niclosamide-related analogs and benchmark TMEM16A antagonists (**H**). Mean±SEM, n=3-4 (**E**), representative data (**B-D**, **F-H**).

Figure 2 continued on next page

Figure 2 continued

The following figure supplements are available for Figure 2:

Figure supplements 1 - 16. Representative TMEM16A (acd) QPatch electrophysiology raw data showing the dose-dependent effect of antagonists in blocking TMEM16A calcium-activated chloride currents.

DOI:

Figure supplement 17 and **18.** Effect of 1PBC and benzbromarone in blocking endogenous TMEM16A calcium-activated chloride currents in COLO205 cells as measured by QPatch electrophysiology.

DOI:

Figure supplement 19. Effects of 1PBC in blocking TMEM16A (abc) calcium-activated chloride currents

DOI:

Figure supplement 20 and **21.** Benzbromarone, niflumic acid, 1PBC and Compound 4 block the ionomycin-induced TMEM16A (abc) inward current at -100 mV as measured by IonWorks Barracuda perforated patch clamp electrophysiology.

DOI:

Figure supplement 22. Voltage protocol for measuring compound impact on CFTR chloride currents and raw data showing relative impact of CFTR benchmark antagonist CFTRinh-172 versus TMEM16A antagonists niclosamide and Compound 4.

DOI:

Figure supplement 23. Patch clamp electrophysiology analysis of the dose-dependent effects of 1PBC, benzbromarone and CaCCinh-A01 on the TMEM16A calcium-activated chloride current versus the cAMP-activated CFTR chloride current.

DOI:

Figure supplement 24 and **25.** FLIPR membrane potential assay showing histamine causes dose-dependent depolarization of airway smooth muscle cells, a response that is inhibited by the TMEM16A antagonists dichlorophen and benzbromarone.

DOI:

Figure supplement 26. The antagonists dichlorphen and benzbromarone also block methacholine depolarization of ASM cells.

DOI:

Figure supplement 27. The TMEM16A opener, Eact, causes robust depolarization of ASM cells like the contractant carbachol and shows a similar EC50 to that described earlier for activation of TMEM16A.

DOI:

Figure supplement 28. The TMEM16A opener, Eact, and methacholine induce calcium mobilization in ASM cells, a response which is blocked by benchmark TMEM16A antagonists.

DOI:

---

suppressing the calcium-activated *chloride* current by QPatch ephys (***Fig. 2B,D; Figure 2–figure supplements 7-13***). The TMEM16A antagonist CaCCinh-A01 fully inhibited the ionomycin-induced iodide eYFP quenching (***Fig. 2C***) like benzbromarone, as did the benchmark antagonists MONNA and dichlorophen (***Figure 1–figure supplement 4***). From these parallel studies, it's apparent that the pharmacology of niclosamide and related compounds is more like 1PBC in partially inhibiting the iodide eYFP response, compared to other benchmark antagonists. Importantly, however, niclosamide and Compounds 2 - 5 fully inhibited the TMEM16A calcium-activated chloride current yet were inactive in blocking the cAMP-induced

CFTR chloride current as measured by IonWorks Barracuda (IWB) electrophysiology (***Fig. 2E; Figure 2–figure supplement 22; Table 1***). In contrast, IWB studies indicated the TMEM16A inhibitors benzbromarone, CaCCinh-A01 and MONNA were dual antagonists as they also blocked the CFTR chloride current (***Table 1*** *and* ***Figure 2–figure supplement 23***). Interestingly, 1PBC and niflumic acid which exhibit a similar pharmacology to niclosamide, also showed selectivity in blocking TMEM16A and sparing CFTR (***Table 1***). While we haven't screened other chloride channels, in concordance with our findings ***Liu et al.*** (***2015***) report niflumic acid is more selective in blocking TMEM16A than CaCCinh-A01 which also had off-target impacts on the calcium-activated chloride channel, bestrophin-1 (BEST1).

The niclosamide-related Compounds 2-5 represent only a small subset of compounds we've tested in this series to develop a structure-activity relationship. ***Figure 1–figure supplement 5*** shows the potency distribution of 304 compounds of this series in blocking TMEM16A. Compounds 2 and 5 are instructive in showing the nitro group is unnecessary for TMEM16A bioactivity and can be replaced with a chloride atom (***Fig. 2A***). The World Health Organization includes niclosamide (Compound 1) on its list of Essential Medicines based on its efficacy, safety and cost-effectiveness (***WHO***, ***2015***). In evaluating published literature pertaining to this compound we became aware of another approved drug, nitazoxanide, which was synthesized in the early 1970s using the scaffold of niclosamide (***Rossignol***, ***2014***). Given nitazoxanide and its metabolic product tizoxanide appear structurally similar to niclosamide (***Fig. 2A***), we decided to test these drugs for activity in blocking TMEM16A. Both nitazoxanide and tizoxanide were found to be antagonists of TMEM16A (***Fig. 2C*** *and* ***2D; Table 1*** *and* ***Figure 2–figure supplement 15***) and exhibit a pharmacology similar to niclosamide in partially inhibiting the iodide/eYFP response, yet fully blocking the chloride current. It is noteworthy

Peters et al. (***2015***) describe a second compound, NTTP, which shares the mechanism of 1PBC in binding four basic residues in the TMEM16A selectivity filter to block channel conductivity. We have confirmed NTTP blocks TMEM16A conductivity (***Figure 2–figure supplement 14***). Interestingly, an examination of the chemical structure of NTTP reveals it is a highly similar analog of tizoxanide (***Fig. 2A***). Thus, nitazoxanide and its metabolic product tizoxanide may share the mechanism of NTTP in binding the pore region of TMEM16A to block channel conductivity. It is worth mentioning the data from the ***Peters et al.*** (***2015***) screen of 306,595 compounds to identify TMEM16A antagonists is deposited in PubChem as AID#588511. Approximately 3600 compounds were identified as hits from their TMEM16A/eYFP primary screen and ~2300 compounds advanced for counterscreens. While only limited follow-up and dose-response data is available, we've tested a subset of hits from this screen and can confirm it represents a source of additional TMEM16A antagonists. ***Figure 2–figure supplement 16*** shows QPatch ephys dose-response results on one compound, CID# 2806957, which resembles NTTP structurally, demonstrating it is an active antagonist of TMEM16A. It should be noted our compound library and that tested by ***Peters et al.*** (***2015***) are distinct. While niclosamide was a hit from our collection, it was not present in the PubChem collection screened.

Drug repurposing represents an attractive approach to reduce the time and cost of drug development as it exploits preexisting clinical data on the pharmacokinetics, pharmacodynamics and safety of a compound. To further evaluate the TMEM16A antagonists niclosamide, nitazoxanide and relateds as a new mechanism for bronchodilation we performed additional test to evaluate their efficacy in blocking ASM contractility.

TMEM16A antagonists block ASM depolarization and bronchodilate airways

Pro-contractiles such as histamine and methacholine signal through Gq-coupled GPCRs on the cell surface to cause membrane depolarization and contraction of airway smooth muscle cells. To enable high-throughput measures of the impact of TMEM16A antagonists on ASM responses, we developed a membrane potential assay using primary human ASM cells. As demonstrated in the FLIPR-Tetra kinetic traces shown in ***Figure 2F***, histamine causes a rapid increase in fluorescence in the membrane potential assay related to ASM depolarization that is fully suppressed by the TMEM16A antagonist, Compound 3. ***Figure 2G*** provides representative dose-response results on six TMEM16A antagonists indicating they fully inhibited the depolarization induced by an EC_{90} amount of histamine (***Figure 2–figure supplement 24***). The niclosamide-related compounds, Cpd2 - Cpd4, exhibited significantly greater potency than the benchmark antagonists CaCCinh-A01 and niflumic acid in blocking ASM depolarization. Heartened by these results we advanced compounds to tissue studies using mouse tracheal rings to evaluate their effect in bronchodilating airways. As shown in ***Figure 2H***, niclosamide, Cpd2 and Cpd 4 were highly potent (sub-μM) in providing full relaxation (bronchodilation) of carbachol precontracted airways. ***Table 1*** provides the full results from these studies, where it can be seen the enhanced efficacy of niclosamide and related compounds in blocking TMEM16A corresponds to improved potency in bronchodilating airways. For the first time, we also provide data exploring the effects of 1PBC on ASM physiology. While 1PBC to date has only been explored for effects on TMEM16A, our data would suggest it is one of the most promising compounds in blocking depolarization and contraction of ASM cells (***Fig. 2G,H***). For over 50 years there has been no new bronchodilators, with β-agonists remaining the only agent and mechanism for blocking the multiple contractiles operating in disease. Antagonists of

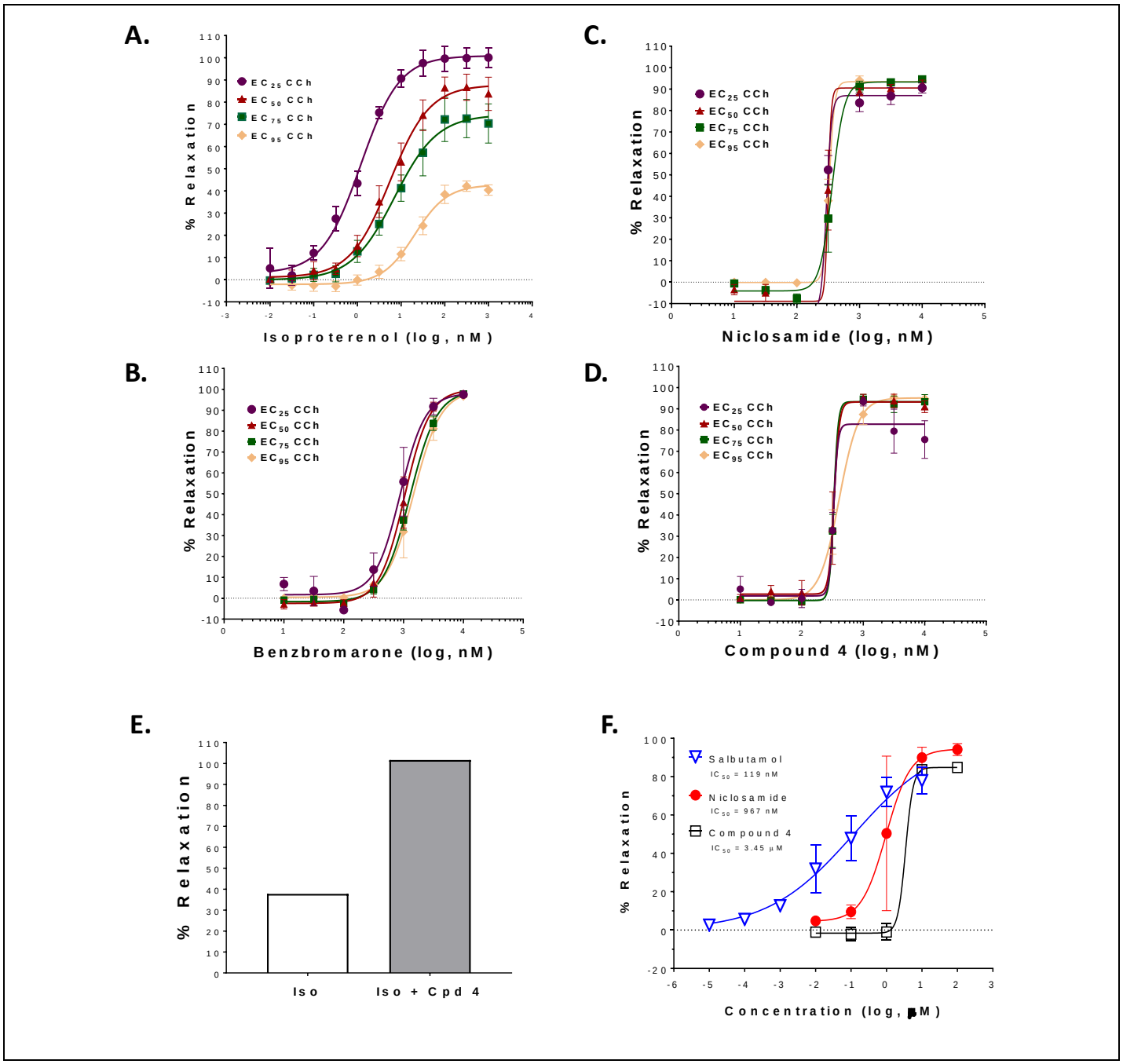

Figure 3. TMEM16A antagonists fully relax mouse airways maximally contracted with carbachol, work with β-agonists to improve bronchodilation and relax human 4th order bronchi precontracted with histamine. Mouse tracheal rings were pre-contracted with EC_{25} − EC_{95} concentrations of carbachol and then treated with the β-agonist isoproterenol (**A**), or the TMEM16A antagonists benzbromarone (**B**), niclosamide (**C**) or Compound 4 (**D**) to measure bronchodilation using a DMT wire myograph (n=3-5 rings per condition). Addition of 10 µM of the TMEM16A antagonist Compound 4 to a maximally contracted (EC_{95}) tracheal ring exhibiting just partial relaxation with 1 µM isoproterenol resulted in full bronchodilation (**E**). The TMEM16A antagonists niclosamide and Compound 4 also provided robust bronchodilation of human 4th order bronchi pre-contracted with histamine (n of 2-3 donors). The average response of three donors to salbutamol is provided for comparison (**F**). Mean±SEM.

Figure 3 continued on next page

Figure 3 continued

The following figure supplements are available for Figure 3:

Figure supplement 1. Experimental procedure for determining mouse tracheal ring sensitivity to carbachol.
DOI:
Figure supplement 2. Mouse tracheal rings maintain contraction to carbachol for hours and do not fatigue.
DOI:
Figure supplement 3. Example of additional TMEM16A antagonists from screen that fully bronchodilate mouse airways.
DOI:
Figure supplement 4. TMEM16A antagonists NTTP and benzbromarone have similar efficacy in fully relaxing mouse airways.
DOI:
Figure supplement 5. Wire myograph can be used to measure if compounds provide long lasting or sustained bronchodilation.
DOI:
Figure supplement 6. Impact of isoproterenol, benzbromarone and niclosamide-related compounds in relaxing human 4th order bronchi pre-contracted with histamine.
DOI:
Figure supplement 7 and **8.** TMEM16A antagonists also fully relax human bronchial rings pre-contracted with carbachol.

Table 1. Niclosamide and related compounds are potent inhibitors of TMEM16A conductivity and airway smooth muscle contraction relative to benchmark antagonists described earlier.

Name	TMEM16A eYFP Assay (FLIPR)	Block of Histamine Depolarization of hASM Cells (FLIPR)	Bronchodilation of Tracheal Rings Pre-Contracted with Carbachol (EC95* or EC75$^{\Psi}$)	TMEM16A ePhys Assay (Qpatch)	CFTR ePhys Assay (IWB)
Niclosamide (Cpd 1)	0.132 (0.067, 42)	0.389 (0.478, 3)	0.379 (0.082, 5)*	2.37 (2.11, 7)	>30
Cpd 2	0.196 (0.105, 3)	0.044	0.483*, 0.585$^{\Psi}$	0.70 (0.53, 11)	>30
Cpd 3	0.184 (0.089, 4)	0.017 (0.000, 2)	0.606 (0.003, 2)$^{\Psi}$	0.61 (0.62, 6)	nd
Cpd 4	0.901 (0.524, 53)	0.178 (0.007, 3)	0.467 (0.167, 4)*	0.62 (0.37, 9)	>30
Cpd 5	0.370 (0.131, 42)	0.071 (0.020, 26)	1.125*	2.26 (0.65, 3)	nd
Nitazoxanide	1.23	nd	nd	1.26 (1.31, 3)	nd
Tizoxanide	0.398	nd	3.902*	4.42 (2.40, 2)	nd
Niflumic Acid	26.570 (11.800, 55)	6.285 (1.59, 4)	51.204*	8.54 (6.75, 7)	>30
Dichlorophen	4.365 (1.210, 58)	0.938 (0.36, 29)	2.012*	4.66 (2.20, 3)	nd
Benzbromarone	1.508 (0.504, 58)	0.208 (0.248, 6)	1.285 (0.211, 4)*	4.09 (2.08, 6)	5.2
1PBC	1.523 (1.360, 17)	0.964 (0.756, 7)	1.769*	2.81 (1.25, 6)	>30
CaCCinh-A01	8.125 (2.720, 58)	4.761 (1.23, 9)	13.529*	7.57 (3.96, 7)	10.08
MONNA	6.295 (1.470, 19)	0.201 (0.162, 2)	3.023*	13.60 (9.76, 4)	18.99
T16Ainh-A01	>50.000 (0.0, 16)	>30 (partial)	>50.000 (0.000, 2)*	>30.000 (0.0, 7)	>30

Values shown are the average IC_{50} (μM) for inhibition of responses (nd = not done). The standard deviation and n number are provided in parentheses. All CFTR IWB electrophysiology studies (n = 3-4) included the benchmark inhibitor CFTRinh-172 on every assay plate, which had an average IC_{50} of 0.080 ± 0.014 μM (n=5).

TMEM16A offer a new mechanism, thus it's important to point out our studies with ASM cells using histamine and our studies with mouse trachea using the cholinergic carbachol support the idea that TMEM16A antagonists block the multiple contractiles that can operate in disease. To extend our bronchodilation studies to human tissue and smaller airways, we've also tested antagonists for relaxation of human 4th order bronchi. Niclosamide and Compound 4 fully relaxed human bronchial rings pre-contracted with histamine (***Fig. 3F*** *and* ***Figure 3–figure supplement 6***) or carbachol (***Figure 3–figure supplement 7***). Of the TMEM16A antagonists, niclosamide routinely provided the most potent bronchodilation with EC_{50} values of 0.305, 0.734 and 3.267 μM in tests on three donors. In the latter case, poor solubility of niclosamide after step-dilution into saline as opposed to DMSO is thought to explain the reduced potency. In general, the efficacy of niclosamide in relaxing human bronchi compared favorably to its efficacy in relaxing mouse tracheal rings where it averaged an EC_{50} of 0.379 μM (***Table 1***). Of the benchmark TMEM16A antagonists, 1PBC had the greatest potency in relaxing carbachol precontracted human bronchial rings with EC_{50} of 0.8 - 1.0 μM, followed by benzbromarone, CaCCinh-A01, NFA and dichlorophen with EC_{50} values of 3.45, 9.24, 13.86 and 19.12 μM, respectively (***Figure 3–figure supplements 7*** *and* ***8***). The short-acting β-agonist salbutamol had an average EC_{50} of 0.119 μM for bronchodilating histamine precontracted human airways (***Fig. 3F***), while the average EC_{50} for the β-agonist isoproterenol was 0.072 μM, but varied widely amongst the four donors tested ranging from 0.009 - 0.133 μM (***Figure 3–figure supplement 6***). The reduced potency of isoproterenol in this latter case (donor 6) which was also accompanied by incomplete maximal bronchodilation of just 77% (***Figure 3–figure supplement 6D***), may reflect differences in donor hypersensitivity to the contractant. In contrast, the TMEM16A antagonist niclosamide provided near complete (97%) relaxation of this donor.

Antagonists resist use- and inflammatory-desensitization mechanisms

TMEM16A antagonists offer a new mechanism to bronchodilate airways that we'd expect to resist use- and inflammatory-desensitization mechanisms that limit β-agonist action. To test this hypothesis, we employed mouse tracheal rings which can be readily attained and compared TMEM16A antagonists versus the β-agonist isoproterenol for bronchodilation after various challenges meant to reflect the situation of severe asthma with poorly controlled inflammation and airway hyperresponsiveness (AHR), which reflects increased sensitivity to contractants. While β-agonists fully relax partially precontracted airways, it's been shown earlier they only partially relax maximally precontracted airways (***Lemoine et al.***, ***1992***), which may be relevant to drug therapy and disease control. We have confirmed this desensitization phenomena using the β-agonist isoproterenol, but importantly find TMEM16A antagonists fully bronchodilate airways irrespective of the level of carbachol precontraction (***Fig. 3***). To accomplish these studies, the EC_{25}, EC_{50}, EC_{75} and EC_{95} for carbachol bronchoconstriction is first determined for each airway ring (***Figure 3–figure supplement 1***), the tissue is then washed to return tissue to baseline tension and then treated with various levels of contractant. As shown in ***Figure 3A***, the β-agonist isoproterenol fully (100%) relaxed airway rings treated with an EC_{25} level of carbachol, but caused only a partial 42% relaxation of airways treated with an EC_{95} level of carbachol. In contrast, the TMEM16A antagonists benzbromarone, niclosamide and Compound 4 fully relaxed maximally (EC_{95}) contracted airways, provided roughly 100% bronchodilation irrespective of contractile force (***Figs. 3B-3D***). Thus, TMEM16A antagonists as an add-on therapy operating with a distinct MOA may help patients retain disease control when β-agonists are functioning sub-optimally. Indeed, an airway ring maximally contracted with an EC_{95} level of carbachol showing just 38% bronchodilation with 1 μM isoproterenol, achieved roughly 100%

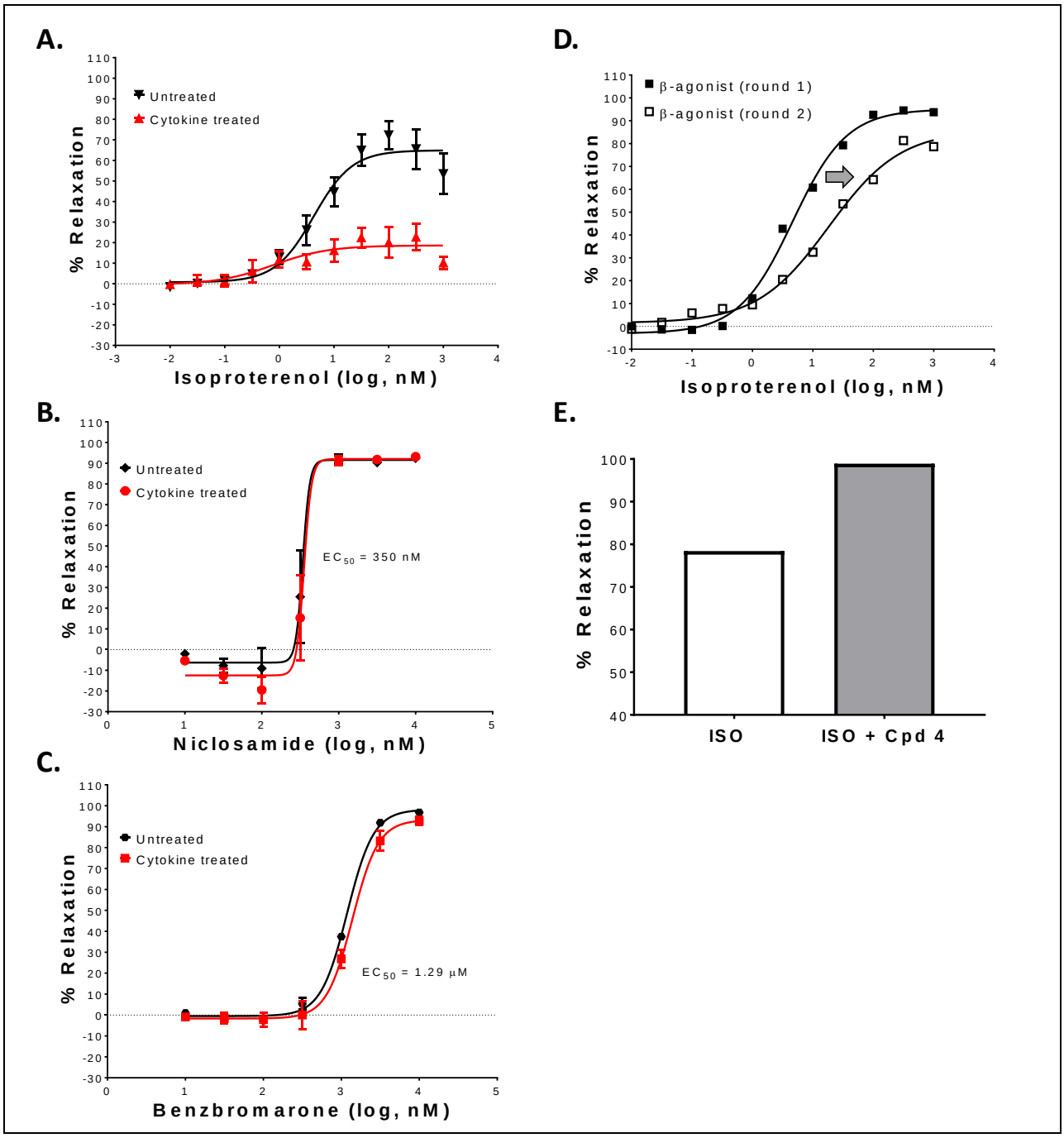

Figure 4. TMEM16A antagonists fully bronchodilate airways and resist use- and inflammatory-desensitization pathways that limit β-agonist efficacy. Treatment of mouse tracheal rings overnight with a cytokine cocktail of IL-1β, IL-13 and TNFα strongly reduced isoproterenol (**A**) bronchodilation of carbachol pre-contracted airways, while the TMEM16A antagonists niclosamide (**B**) and benzbromarone (**C**) remained effective in fully relaxing the cytokine treated airways (n=4; 2 rings/group, 2 experiments; Mean±SEM). As a model of β-adrenergic receptor use-dependent desensitization, CCh pre-contracted mouse tracheal rings were treated with the β-agonist isoproterenol (round 1), washed, re-contracted with carbachol and tested again (round 2) for bronchodilation. Isoproterenol showed a rightward shift in potency after the 2nd treatment and a reduction in maximal efficacy in bronchodilation (**D**). Addition of the TMEM16A antagonist Cpd 4 (10 µM) after the 2nd isoproterenol treatment and final highest dose induced full relaxation of the airways (**E**).

bronchodilation after subsequent treatment with the TMEM16A antagonist, Cpd 4 (***Fig. 3E***).

Severe asthma and COPD is associated with poorly controlled inflammation. Using a cocktail of cytokines (IL-1β, TNFα, IL-13) to mimic this process, we show the efficacy of isoproterenol in bronchodilating airways is dramatically reduced when airways are pretreated with cytokines (***Fig. 4A***). In contrast niclosamide and benzbromarone fully bronchodilated cytokine-treated airways (***Fig. 4B,C***), suggesting TMEM16A antagonists offer a new mechanism to resist the inflammatory desensitization pathways that limit β-agonist action. Repeat treatment with β-agonists are also known to induce tachyphylaxis or use-dependent desensitization, which involves β2-adrenergic receptor phosphorylation, arrestin recruitment and receptor internalization and degradation resulting in reduced bronchodilation. To ascertain whether these pathways leading to β-agonist desensitization also interfere with bronchodilation by TMEM16A antagonists, we measured the degree of bronchodilation after repeated treatment with isoproterenol. As shown in ***Figure 4D***, there was less bronchodilation and a rightward shift in potency after the 2nd round of β-agonist treatment which reflected use-dependent desensitization. Subsequent addition of Compound 4 to this same tissue resulted in full bronchodilation indicating TMEM16A antagonists restore bronchodilation of airways undergoing β-agonist use dependent desensitization (***Fig. 4E***).

The combined data indicates TMEM16A antagonists provide a new mechanism for robust bronchodilation of airways, even when they encounter high levels of contractants or are exposed to inflammatory conditions that limit β-agonist action. The duration of bronchodilation is another critical parameter for development of new asthma maintenance therapies. The wire myograph technique can also be applied to evaluate a compounds duration of bronchodilation. ***Figure 3–figure supplement 5*** shows a preliminary example of this approach applied to

isoproterenol, niclosamide and benzbromarone indicating some TMEM16A antagonists may have characteristics allowing for prolonged bronchodilation.

Effects of antagonists on endogenous TMEM16A currents in cancer cells

Owing from its overexpression in several cancers, TMEM16A was originally named DOG1 (discovered on gastrointestinal stromal tumors protein 1), TAOS2 (tumor-amplified and overexpressed sequence 2) and ORAOV2 (oral cancer overexpressed 2). TMEM16A is located within the 11q13 amplicon, one of the most frequently amplified chromosomal regions in human cancer that correlates with a poor prognosis. TMEM16A overexpression contributes directly to tumorigenesis and cancer progression and its knockdown with shRNA or small molecule antagonists ameliorates disease (***Britschgi et al.***, ***2013; Duvvuri et al.***, ***2012; Liu et al.***, ***2012; Wang et al.***, ***2017***). It associates with EGFR to regulate cancer cell proliferation and activates several pathways important for tumor growth (***Bill et al.***, ***2015; Britschgi et al.***, ***2013***). TMEM16A has been implicated in numerous cancers, including head and neck, esophageal, gastric, colorectal, lung, breast, prostate, pancreatic and glioma (reviewed recently by Wang (***Wang et al.***, ***2017***). To explore the impact of antagonists on native calcium-activated chloride currents, we profiled RNAseq data on cancer cell lines to identify high expressers. Of the 110 cell lines showing the most elevated TMEM16A expression (***Figure 5–figure supplement 8***), roughly 18 % were colorectal cancer cell lines and 6% were gastric cancer cell lines. We chose the colorectal cancer (CRC) cell line COLO205 for further evaluation by QPatch electrophysiology. COLO205 cells gave good seals and a robust TMEM16A current with the characteristic calcium and voltage-dependence. Application of three benchmark TMEM16A antagonists (benzbromarone, CaCCinh-A01 and 1PBC) fully blocked this native chloride current

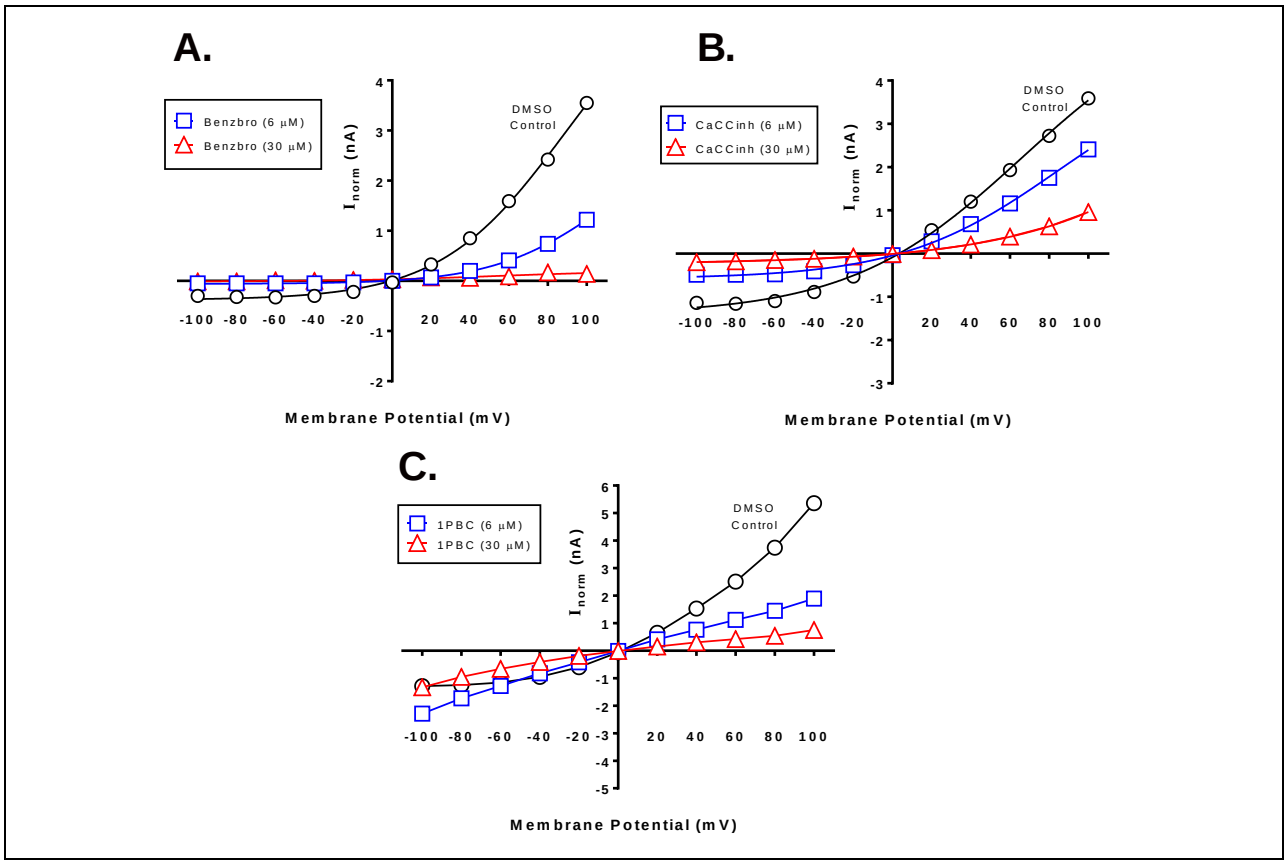

Figure 5. TMEM16A antagonists block endogenous calcium-activated chloride currents in the colorectal cancer cell line, COLO205. RNAseq identified several colorectal cancer cell lines as overexpressing TMEM16A (Figure 5–figure supplement 8). Shown are results from QPatch electrophysiology studies indicating COLO205 cells exhibit the characteristic current-voltage relationship of TMEM16A which was sensitive to the TMEM16A antagonists benzbromarone (**A**), CaCCinh-A01(**B**) and 1PBC (**C**).

The following figure supplements are available for Figure 5:

Figure supplement 1. RNAseq analysis of TMEM16A expression in human ASM and bronchial epithelial cells.
DOI:

Figure supplement 2. RNAseq analysis of TMEM16A, Muc5AC and FoxA3 expression in human bronchial epithelial (HBE) ALI cultures untreated or treated with the Th2 cytokine IL-13.
DOI:

Figure supplement 3. Strand-specific RNAseq analysis of TMEM16A splice variant expression in HBE and ASM.
DOI:

Figure supplement 4. TMEM16A is increased after IL-4 or IL-13 treatment of HBE ALI cultures (IHC).
DOI:

Figure supplement 5 and **6.** Increased TMEM16A expression in lung of asthmatic cynomolgus monkeys.
DOI:

Figure supplement 7. The TMEM16A opener Eact induces Muc5AC and leukotriene secretion from HBE ALIs.
DOI:

Figure supplement 8. RNAseq analysis of TMEM16A expression in cancer cell lines.
DOI:

Figure supplement 9. Comparing niclosamide analogs for activity on TMEM16A versus Wnt/β-catenin.
DOI:

(***Fig. 5; Figure 2–figure supplements 17*** *and* ***18***), providing important confirmation of our earlier results with cloned TMEM16A in HEK293 cells. To our knowledge this represents the first description that COLO205 cells express a functional TMEM16A calcium-activated chloride current. While we haven't yet extended these studies to other antagonists, it's worth noting ***Li et al.*** (***2014***) report niclosamide inhibits proliferation of the colon cancer cell lines HCT116, COLO205 and HT29 with an IC_{50} of 0.37, 0.98 and 4.17 μM, respectively, which falls within the range of potency we find for blocking TMEM16A conductivity (***Table 1***). ***Osada et al.*** (***2011***) report a similar potency of niclosamide in inhibiting HT29 and HCT116 proliferation *in vitro* and observed minimal toxicity on normal fibroblasts, PBMCs or immortalized mammary epithelial cells. Importantly, these authors also found niclosamide inhibited CRC tumor growth in mice and was well tolerated. While chloride currents have only been measured in a subset of cancer cell lines, it is notable HT29 cells were also shown to express a functional calcium-activated chloride current which was exploited to screen for antagonists (***De La Fuente et al.***, ***2008***). Interestingly, in a drug repositioning effort ***Senkowski et al.*** (***2015***) employed HCT116 spheroid cultures to screen 1600 clinical compounds and identified the FDA-approved drugs nitazoxanide and niclosamide as promising new anticancer agents.

Wnt/β-catenin signaling is commonly altered in cancer and is consider a principle driver of colorectal carcinomas (***Ahmed et al.***, ***2016***). Niclosamide was found to downregulate Wnt signaling and elicit colorectal antitumor responses (***Osada et al.***, ***2011***). Because niclosamide's efficacy in suppressing the Wnt pathway (IC_{50} of 0.2-0.4 μM) correlated with its efficacy in inhibiting cancer cell growth (IC_{50} of 0.33-0.75 μM), it has been suggested Wnt inhibition may underlie niclosamide's promising anticancer effects (***Ahmed et al.***, ***2016; Lu et al.***, ***2011***). To investigate this further, ***Mook et al.*** (***2015***) synthesized over 35 niclosamide

analogs to understand its SAR for inhibition of Wnt and to identify compounds with improved systemic exposure. A comparison of the 304 niclosamide analogs we've characterized for TMEM16A activity (***Figure 1–figure supplement 5***), indicates sixteen were identical to compounds characterized by ***Mook et al.*** (***2015***) and many were potent antagonists of both TMEM16A and Wnt signaling (***Figure 5–figure supplement 9***). Niclosamide had an IC_{50} of 0.34 μM for inhibition of Wnt/β-catenin transcription using a TOPFlash reporter assay (***Mook et al.***, ***2015***), which matches closely the IC_{50} of 0.13 μM we calculate for inhibition of the TMEM16A halide-sensitive YFP response.

Discussion

For the first time, we identify the approved drugs niclosamide and nitazoxanide as TMEM16A antagonists. With an IC_{50} of 132 nM in blocking the TMEM16A halide sensitive YFP response, niclosamide is one of the most potent antagonists described to date. We also characterized four niclosamide analogs and eight benchmark TMEM16A antagonists described earlier. The pharmacology of niclosamide and relateds in providing potent but partial block of the iodide eYFP response yet full block of the TMEM16A chloride current appears most similar to the benchmark antagonists 1PBC and NTTP. Thus, niclosamide and relateds may share their mechanism as pore blockers. While we provide details on four analogs (Cpds 2-5) that show similar effects, over 300 niclosamide analogs have been tested and the partial block of the iodide eYFP response is characteristic of this chemotype. This detailed evaluation of niclosamide SAR motivated us to also analyze the approved drug nitazoxanide and its metabolic product tizoxanide for activity on TMEM16A since nitazoxanide was synthesized in early 1970s using the niclosamide scaffold. Remarkably, nitazoxanide and tizoxanide also blocked TMEM16A

with low single digit μM potency and showed a similar pharmacology to niclosamide in the YFP and ephys assays. Because tizoxanide is a highly similar structural analog of NTTP, we suggest this provides further evidence they are pore blockers and propose they may interact with the same charged residues, Arg 511 and Lys 599, which ***Peters et al.*** (***2015***) find are important for NTTP and 1PBC inhibition of TMEM16A. These two basic residues along with Arg 531 which upon mutation to alanine alter anion selectivity of TMEM16A (***Peters et al.***, ***2015***) have been confirmed recently in the cryoEM structures of mouse TMEM16A to reside near the external narrow neck of the channel pore where the positive charges facilitate anion entrance and permeability (***Dang et al.***, ***2017; Paulino et al.***, ***2017a; Paulino et al.***, ***2017b***). To our knowledge the mechanism of action of CaCCinh-A01, benzbromarone, dichlorophen and MONNA on TMEM16A remains unknown, but because these compounds show a distinct pharmacology from niclosamide and relateds it is likely they have different site/s of action. Niflumic acid which has a pharmacology similar to niclosamide, 1PBC and NTTP in preferentially blocking larger versus smaller halides (***Ni et al.***, ***2014***), interestingly was proposed over a decade earlier to be a pore blocker (***Piper et al.***, ***2002***). At this time, we've run only limited counterscreens for selectivity over other chloride channels, but promisingly find niclosamide and relateds showed little impact on the CFTR chloride current, as did the other pore blockers 1PBC and niflumic acid. Thus, compounds which are TMEM16A pore blockers may offer a unique mechanism for selective impact on TMEM16A versus other chloride channels.

To further evaluate niclosamide for physiological effects in modulating airway smooth muscle contractility we used cultured primary human ASM cells and tissue rings from large and small airways. TMEM16A is expressed on airway smooth muscle cells which display the classical electrophysiology properties of CaCC (***Gallos et al.***, ***2013; Zhang et al.***, ***2013***),

including a rapid calcium-dependent inactivation (***Wang et al.***, ***1997***) which we also observe after ionomycin-activation of cloned TMEM16A in HEK293 cells (***Figure 2–figure supplements 20*** *and* ***21***). We have confirmed TMEM16A expression in ASM cells and human bronchial epithelial (HBE) cells by RNAseq (***Figure 5–figure supplement 1*** *and* ***2***), detecting almost exclusively the 'abc' splice variant lacking segment 'd' in HBE cells as reported earlier (***Caputo et al.***, ***2008***), but find ASM cells express a mixture of splice variants with variable amounts of segment 'b' and 'd' (***Figure 5–figure supplement 3***). In this later case, this may include the 'acd' variant we used for QPatch ephys studies, while in the former it would include the 'abc' variant used in our eYFP screen. While we've primarily used the 'acd' variant for patch clamp electrophysiology studies on antagonists, it's worth noting the pore blocker 1PBC showed similar efficacy in blocking TMEM16A 'acd' and 'abc' Ca^{2+}-activated Cl^{-} currents (***Figure 2–figure supplements 6, 19, and 21)***. Irrespective, since pro-contractiles such as histamine and methacholine activate calcium-activated chloride channels leading to membrane depolarization, calcium mobilization and contraction of smooth muscle cells, we advanced TMEM16A antagonists for direct interrogation of impacts on these processes. Niclosamide and related compounds blocked histamine depolarization of ASM cells at sub-micromolar concentrations. These studies confirm earlier findings that TMEM16A antagonists hyperpolarize human ASM cells (***Danielsson et al.***, ***2015; Danielsson et al.***, ***2014; Yim et al.***, ***2013***) and extend them to demonstrate antagonists also reverse the depolarization induced by contractants.

To provide perspective on the activity of niclosamide and related compounds, we compared them to seven small molecule antagonists described earlier of distinct chemotypes. Consistent with TMEM16A's role in controlling ASM excitation-contraction coupling, we find antagonists characteristically blocked pro-contractile depolarization and importantly provided

robust bronchodilation of mouse tracheal rings and human small airways. In alignment with their enhanced potency on TMEM16A, niclosamide and relateds showed improved activity in relaxing airways. Our findings extend earlier studies demonstrating niflumic acid relaxes TEA or K+ gluconate pre-contracted guinea pig tracheal rings, rat small airways and human tracheal smooth muscle strips (***Danielsson et al.***, ***2014; Yim et al.***, ***2013***), benzbromarone and tannic acid suppress Substance P contraction of guinea pig tracheal rings (***Gallos et al.***, ***2013***) and benzbromarone relaxes methacholine contracted mouse peripheral airways or human airway smooth muscle strips pre-contracted with acetylcholine- or LTD4 (***Danielsson et al.***, ***2015***). Importantly, these findings and our results using carbachol and histamine indicate TMEM16A antagonists offer a new mechanism to block the multiple contractiles operating in disease.

Asthma is a chronic inflammatory disorder characterized by airway hyperresponsiveness (AHR). Significantly, ***Zhang et al. (2013)*** find in mouse model of asthma, ovalbumin-sensitization upregulates TMEM16A expression in ASM cells and benzbromarone and niflumic acid prevented AHR and contractions evoked by methacholine. We also have devised schemes to evaluate the efficacy of TMEM16A antagonist under extreme conditions of contraction and inflammation that reduce β-agonist action (***Lemoine et al.***, ***1992; Shore et al.***, ***1997***). Remarkably, maximally contracted mouse airways were fully relaxed by the TMEM16A antagonists niclosamide, Cpd 4 and benzbromarone, while the β-agonist isoproterenol showed on partial bronchodilation which importantly converted to full bronchodilation with add-on of a TMEM16A antagonist (***Fig. 3***). These findings are similar to those from ***Danielsson et al.*** (***2015***) who found benzbromarone improved the efficacy of the β-agonists isoproterenol and albuterol in relaxing acetylcholine contracted guinea pig tracheal rings. Severe asthma and COPD are also associated with poorly controlled inflammation, steroid insensitivity and reduced

β-agonist responsiveness. Thus, there is a need for new bronchodilators with a distinct MOA that can operate amidst this inflammation. The cytokines IL-1β and TNFα were shown earlier to reduce β-agonist relaxation of airway smooth muscle (***Moore et al.***, ***2001; Shore et al.***, ***1997***). More recently bitter taste receptors were shown to provide a new mechanism to bronchodilate airways which resists IL-13 desensitization events limiting β-agonist action (***Robinett et al.***, ***2014***). Using mouse tracheal rings pre-treated with an IL-1β, IL-13 and TNFα cytokine cocktail we demonstrate β-agonist bronchodilation is profoundly reduced, yet TMEM16A antagonists remain remarkably effective in fully relaxing airways (***Fig. 4***). Finally, because asthma treatment guidelines include β-agonists as a standard of care but allow for add-on therapies for poorly controlled disease, we investigated if TMEM16A antagonists can operate with β-agonists, including under situations of tachyphylaxis or use-dependent desensitization. Promisingly, airways exhibiting hyporesponsiveness after repeat β-agonist treatment were fully relaxed upon addition of the TMEM16A antagonist, Cpd 4.

Secretory epithelial cells, smooth muscle cells and sensory neurons express the calcium-activated chloride channel TMEM16A. In the bronchial epithelium, TMEM16A is strongly upregulated by Th2 cytokines which correlates with goblet cell hyperplasia and mucin hypersecretion, as well as, increased calcium-dependent chloride secretion (***Caputo et al.***, ***2008; Huang et al.***, ***2012; Scudieri et al.***, ***2012***). We have confirmed these results finding TMEM16A is dramatically upregulated in the bronchial epithelium after IL-13 treatment and expressed on the apical surface of goblet cells, but also show cynomolgus monkeys with allergic asthma have elevated TMEM16A staining within the submucosal glands which are an underappreciated but major source for excessive mucin production in disease (***Figure 5–figure supplements 2-6***). Interestingly, like our findings with IL-13, ***Gorrieri et al.*** (***2016***) similarly find TMEM16A

expression peaks quickly, 24 hours after IL-4 treatment, a time frame we find precedes maximum Muc5AC expression occurring 5-7 days later (***Figure 5–figure supplement 2***). Notably, using an IL-13 mouse model of asthma, ***Nakono et al.***(***2006***) reported that niflumic acid inhibited goblet cell hyperplasia and airway hyperresponsiveness. ***Huang et al.*** (***2012***) extended these findings in their pivotal study demonstrating TMEM16A is upregulated in the asthmatic bronchial epithelium and its inhibition with benzbromarone and dichlorophen blocked mucin secretion and ASM contraction. More recently, TMEM16A inhibition with antagonists or siRNA has been reported to reduce IL-13 induced Muc5AC production and goblet cell hyperplasia (***Lin et al.***, ***2015; Qin et al.***, ***2016; Zhang et al.***, ***2015***), while TMEM16A overexpression had opposite effects in increasing Muc5AC expression (***Lin et al.***, ***2015; Qin et al.***, ***2016***). Thus, TMEM16A inhibitors may repress two of the key features leading to airway obstruction in severe asthma and COPD, bronchoconstriction and mucin hypersecretion.

In contrast for cystic fibrosis, activation of TMEM16A on the apical membrane of epithelial cells has been proposed as one strategy to bypass the CFTR chloride secretory defect to improve hydration and mucociliary clearance, but bronchoconstriction and pain have been pointed out as possible unwanted side effects (***Liu et al.***, ***2016; Sondo et al.***, ***2014***). To evaluate the effects of direct channel activation, we employed the TMEM16A opener, Eact (***Namkung et al.***, ***2011b***), and investigated its effects on airway smooth muscle and the bronchial epithelium. Interestingly, Eact induced robust ASM cell depolarization and calcium flux like contractants, which was blocked by antagonists (***Figure 2–figure supplement 27*** *and* ***28***). The average EC_{50} of 1.6 μM for Eact induced ASM depolarization, closely matched its EC_{50} of 3.0 μM in activating TMEM16A (***Namkung et al.***, ***2011b***). These findings are consistent with those from ***Danielsson et al.*** (***2015***), who found Eact depolarized ASM cells like contractants, while

antagonists hyperpolarized ASM cells. To investigate its effects on bronchial epithelial cells, we incubated mature bronchial epithelial air-liquid interface (ALI) cultures for 2-3 days with the Eact opener. Muc5AC and leukotriene (LTC4, LTB4) secretion from bronchial epithelial ALI cultures was significantly increased following treatment with the TMEM16A opener, Eact (***Figure 5–figure supplement 7***). While these findings supported the concept that agonists may have reciprocal effects to antagonists, our enthusiasm with these results was tempered by recent findings Eact was also a direct activator of TrpV1 (***Liu et al.***, ***2016***), which can physically associate with TMEM16A in sensory neurons to enhance pain sensation (***Takayama et al.***, ***2015***). As TrpV1 is also expressed by bronchial epithelial and ASM cells (***McGarvey et al.***, ***2014; Yocum et al.***, ***2017***), it's activation alone, or with TMEM16A, could also explain some of our findings with Eact. Interestingly, ***Beneditto et al.*** (***2017***) also recently report TMEM16A and CFTR physically interact and cross-regulate each other in differentiated epithelial cells. Tissue specific knockout of TMEM16A in mouse intestine and airways abolished not only Ca^{2+}-activated Cl^{-} secretion, but also abrogated CFTR-mediated Cl^{-} secretion. Somewhat surprising, there was no overt phenotype despite the complete absence of chloride currents in knockout tissues and mucociliary clearance was not compromised, but unexpectedly enhanced in tracheas from knockout mice. While this may support airway Na^{+} transport is physiologically more relevant for hydration, further studies are needed to understand TMEM16A's role under disease conditions and the effects of pharmacological agents in modulating goblet cell hyperplasia and mucin hypersecretion. Although many antagonists have been described to date, it's clear there remains a need for additional TMEM16A openers for direct channel activation.

Beyond respiratory disease, antagonists of TMEM16A have been proposed to have utility in treating a wide variety of other diseases including, pulmonary hypertension (***Forrest et***

al., ***2012; Heinze et al.***, ***2014; Namkung et al.***, ***2010***), secretory diarrhea (***Ousingsawat et al.***, ***2011; Thiagarajah et al.***, ***2015***), polycystic kidney disease (***Buchholz et al.***, ***2014***), pain (***Cho et al.***, ***2012; Lee et al.***, ***2014; Pineda-Farias et al.***, ***2015***) and cancer (***Britschgi et al.***, ***2013; Duvvuri et al.***, ***2012; Liu et al.***, ***2012; Wang et al.***, ***2017***). Interestingly, drug repurposing efforts have similarly found the anthelmintics niclosamide and nitazoxanide hold great promise for treatment of numerous other disorders, including hypertension, secretory diarrhea, cancer and as a broad spectrum anti-infective agent (***Chen et al.***, ***2017; Li et al.***, ***2014; Rossignol***, ***2014; Rossignol et al.***, ***2006***). Underlying mechanisms proposed for its action have included uncoupling of oxidative phosphorylation, modulation of Wnt/β-catenin, mTORC1, STAT3, NF-κB and Notch signaling, but identifying a unifying mechanism for niclosamide's action has remained elusive (***Chen et al.***, ***2017***). We'd suggest antagonism of TMEM16A should now be considered as a possible contributing factor. This is especially so for secretory diarrhea and cancer where the role of TMEM16A has been well established. Activation or upregulation of the calcium-activated chloride channel TMEM16A, an upstream target on the cell surface, can initiate a variety downstream signaling pathways affecting various pathophysiological processes (e.g. as shown for Ras-Raf-MEK-ERK in cancer (***Duvvuri et al.***, ***2012***)). Channels can also associate with other cell surface molecules to form large macromolecular signaling complexes. Indeed, TMEM16A has been shown to interact with the ezrin-radixin-moesin network (***Perez-Cornejo et al.***, ***2012***) and with TrpV1 (***Takayama et al.***, ***2015***), TrpC6 (***Wang et al.***, ***2016***) and the IP3 receptor (***Jin et al.***, ***2013***) for coupled GPCR and ion channel signaling. Interestingly, the key signaling molecule β-catenin involved in numerous cancers was also found recently to associate with the ion channels KCNQ1 (***Rapetti-Mauss et al.***, ***2017***) and BKCa (***Bian et al.***, ***2011***) to modulate Wnt signaling.

TMEM16A antagonists offer an exciting new strategy to treat a wide variety of disorders. We demonstrate antagonists block airway smooth muscle depolarization and contraction, offering a promising new mechanism to bronchodilate airways that resists use- and inflammatory-desensitization pathways limiting β-agonist efficacy in severe asthma and COPD. We identify the approved drugs niclosamide, nitazoxanide and related compounds as some of the most potent TMEM16A antagonist described to date and provide a molecular target to compounds of high interest from drug repurposing efforts. Further studies will be needed to assess their efficacy in respiratory or other diseases, but the safe track record of niclosamide and nitazoxanide in man position these chemical series as a good starting point for further studies.

Materials and methods

Reagents sources, compound synthesis and characterization

Niclosamide (Cpd 1, PubChem CID: 4477), Cpd 2 (CID 487721), Cpd 3 (CID 289367), Cpd 4 (CID 44724361), niflumic acid (CID 4488), dichlorophen (CID 3037), benzbromarone (CID 2333), nitazoxanide (CID 41684), 1PBC (CID 711253), NTTP (CID 19646) and CID# 2806957 were from the Amgen small molecule compound collection. CaCCinh-A01 (CID 747219) was purchased from Sigma-Aldrich, MONNA (CID 72165188) was purchased from Sigma-Aldrich, T16Ainh-A01 (CID 3193184) was purchased from Sigma-Aldrich, and tizoxanide (CID 394397) was purchased from J&W Pharmlab LLC. Cpd 5 (CID 24326) was synthesized according to a literature procedure (***Macielag et al.***, ***1998***). The source for other compounds and reagents is provided in each experimental section.

Generation of TMEM16A HTS clone by functional clone selection

The High-Throughput-Screening clone HEK293T:eYFP:TMEM16A(abc) stably expressing eYFP (H149Q,I153L) and human TMEM16A(abc) was generated by stable transfection followed by functional clone selection. HEK293T:eYFP (H149Q,I153L) was cultivated in propagation medium DMEM (PAN #P04-03550) containing 10% FBS (PAN #3302-P281402), 1x Pen/Strep (PAN #P06-07100), 1x L-glutamine (PAN #P04-80100), 10mM HEPES (PAN #P05-01100) and 0.5µg/ml puromycin (Sigma #P7255) and transfected with pIREShyg3:huTMEM16A(abc). Stable cell pool was generated by cultivation in propagation medium containing 0.5µg/ml puromycin and 200µg/ml hygromycin B for 20 days. Cell pool was then diluted in the same medium and seeded in 384-well microtiter plates. Grown clones were replicated into daughter plates using a CyBio Felix pipetting platform (Analytik Jena AG). Daughter plates were analyzed using the eYFP assay essentially as described in the HTS protocol below using a FLIPR-Tetra. Clones showing maximal quenching of eYFP fluorescence intensity after addition of trigger solution (assay buffer containing NaI and ionomycin) were selected for propagation from the mother plate and further characterized with regard to HTS assay development performance parameters including inhibition by the benchmark compound benzbromarone, S/B and relevant HTS quality control statistics (Z-factor, Z'-factor, RZ-factor, RZ'-factor). One clone was finally selected as HTS clone and used throughout the entire HTS campaign to identify TMEM16A antagonists.

High-Throughput-Screening for TMEM16A antagonists using the halide-sensitive YFP (eYFP) assay

Screening cell line HEK293T:eYFP(H149Q,I153L):TMEM16A(abc) stably expressing halide sensitive YFP (eYFP (H149Q,I153L)) and human TMEM16A(abc) were propagated in DMEM

(PAN #P04-03550) containing 10% FBS (PAN #3302-P281402), 1x Pen/Strep (PAN #P06-07100), 1x L-glutamine (PAN #P04-80100), 10mM HEPES (PAN #P05-01100), 0.5µg/ml puromycin (Sigma #P7255) and 150 µg/ml hygromycin B (Life Technologies #10687-010) in Corning TC-treated flasks. 24 hours prior to the assay 11,000 cells were seeded per well in 30µl assay plating medium (propagation medium containing 0.01% Pluronic F-68 (PAN #P08-2100)) in Corning CellBIND 384-Well Flat Clear Bottom Black Polystyrene Microplates (Corning #3683) and cultivated for 24 hours at 37°C. Before initiating the fully automated and scheduled HTS sequence, cell plates were transferred to an incubator and stored at RT and 0% CO_2. Library compounds were delivered in Greiner 384 PP plates (Greiner #784201) containing 1mM compound dissolved in DMSO in columns 1–22 and DMSO in columns 23 and 24 and were stored in a stacker at RT. Further dilutions of compounds were generated by fully automated liquid handling using a CyBio 384-well/25µl pipetting head (Analytik Jena AG) by diluting 0.5µl compound (1mM in DMSO) in 20µl assay buffer (1xHBSS (Life Technologies #14025050) containing 10mM HEPES (PAN #P05-01100) and 0.01% Pluronic F-68 (PAN #P08-2100), adjusted to pH 7.4) in Greiner 384 PP plates (Greiner #784201). Intermediate compound plates contained 25µM library compounds in assay buffer containing 2.5% DMSO in columns 1-22, assay buffer containing 2.5% DMSO as neutral control in column 23 and 100µM Benzbromarone (Sigma #B5774) in assay buffer containing 2.5% DMSO in column 24 as ligand control (benchmark antagonist) and were stored in a stacker at RT. Simultaneous to compound dilution medium was aspirated from cell plates using a Biotek 405 microplate washer followed by washing the cells twice with 65 µl/well assay buffer. With the final aspiration of assay buffer the residual volume was adjusted to 15µl. 10µl compound solution were then added to the washed cell plates using a CyBio 384-well/25 µl pipetting head (Analytik Jena AG) resulting in a

final volume of 25µl assay buffer containing 10µM compound and 1% DMSO. Cell plates were incubated for 30 min at RT and 0% CO_2. After incubation cell plates were transferred to a FLIPR-Tetra and 25µl trigger solution (assay buffer containing 20 mM sodium iodide (Sigma #383112) and 4µM ionomycin (Sigma #I0634; stock solution 10mM in DMSO)) was added before reading iodide-quenching of eYFP fluorescence intensity. Final concentration of library compounds in columns 1-22 at read-out was 5µM in the presence of 10mM iodide, 2µM ionomycin and 0.5% DMSO. Neutral control column 23 received no ligand and the ligand control column received a final concentration 20µM benzbromarone in the presence of 10mM iodide, 2µM ionomycin, which corresponded to EC80 in this assay setup, and 0.5% DMSO. FLIPR-Tetra settings included excitation wavelength (470-495nm), emission wavelength (515-575nm), 7 reads before dispensing the trigger solution for baseline recording followed by 40 reads after trigger solution dispense. Data analysis was performed using Genedata Screener with aggregation rule "Max-Min/Max" (Min: baseline from 0 – 10 seconds prior to trigger solution dispense) and normalization based on neutral control (0% inhibition corresponding to 100% TMEM16A activity) and inhibitor control Benzbromarone (100% inhibition corresponding to 0% TMEM16A activity). HTS quality control parameters and statistics (S/B, Z-factor, RZ-factor, Z'-factor and RZ'-factor) were automatically calculated and recorded using Genedata Screener. For unbiased primary hit selection the POC cut-off (hit threshold) was calculated as Median+3xIQR+20% of all test wells. Confirmation Screening primary was run in triplicates (3 independent, consecutive runs) with confirmed hits defined as median (replicate POC values) > POC cut-off (POC cut-off primary screen). Compounds were selected for dose-response screening after database mining to eliminate frequent hitters and fluorescent primary hit compounds, which were detected by calculating baseline fluorescence intensity measured by

FLIPR-Tetra before addition of trigger solution for each compound well. Cut-off was set as Baseline FI <10x STDV of the neutral control. Non-fluorescent compounds were selected and dose response testing was performed with 22-step, 1:2 dilution following the eYFP assay format procedure described above. Threshold was set at IC50 <5µM.

The 22 dose response dilutions were also tested in Calcium flux assays using FLIPR Calcium 6 Assay Kit (Molecular Devices # R8190 and R8191) to eliminate compounds, which inhibit ionomycin-dependent increase of intracellular calcium concentration. HEK293T cells were propagated in Corning TC-treated flasks in propagation medium consisting of DMEM (PAN #P04-03550) containing 10% FBS (PAN #3302-P281402), 1x Pen/Strep (PAN #P06-07100), 1x L-glutamine (PAN #P04-80100), 10mM HEPES (PAN #P05-01100), 1x sodium-pyruvate (PAN #P04-43100). Prior to the assay 13,000 cells were plated per well in 30µl propagation medium in Corning Cellbind 384 well microtiter plates (Corning #3683) and cultivated for 24 hours. Cells were stained with labelling dye solution, which was assembled following a protocol provided by manufacturer followed by addition of 8mM probenecid (Sigma-Aldrich #P8761, 250mM stock solution in 1xHBSS (PAN #P04-49505) mixed with an equal volume of 1N NaOH and pH adjusted to 7.4). 25µl labeling dye were transferred per well using Agilent Bravo liquid handling platform followed by incubation for 2 hours at 37°C and 5% CO_2. Simultaneously, intermediate compound plates were prepared by transferring 0.64µl of compound solution from compound plates to 15µl assay buffer (1xHBSS (Life Technologies #14025050), 20 mM HEPES (PAN #P05-01100), adjusted to pH 7.4) in columns 1-22 of intermediate plates using a CyBio 384/25µl pipetting head (Analytik Jena AG) followed by storage in a stacker. In order to normalize the assay to identify compounds decreasing calcium signaling final assay concentration of 1µM ionomycin was tested as neutral control in column 23

and buffer only as blank control in column 24. When cell labelling was complete, 10µl of diluted compound were added per well using Agilent Bravo Platform and were incubated for 45 min at room temperature. Cell plates were then transferred to FLIPR-Tetra and 20µl trigger solution **(**assay buffer containing 4.25µM ionomycin (Sigma #I0634; stock solution 10mM in DMSO) was added to achieve a final Ionomycin concentration of 1µM, which corresponded to the EC80 in this assay setup, in the presence of 0.5% DMSO (final). FLIPR-Tetra settings included excitation wavelength (470-495nm), emission wavelength (515-575nm), baseline was recorded before dispensing the trigger solution followed by reading the ionomycin response. Data analysis was performed using Genedata Screener with aggregation rule "Max-Min/Max" (Min: baseline prior to trigger solution dispense) and normalization based on neutral control (0% inhibition) and blank control without ionomycin (100% inhibition). Dose response cut-off was set at IC50<10µM to eliminate compounds, which reduce ionomycin-triggered calcium signaling.

Development of the TMEM16A halide-sensitive YFP assay for routine tests of compound potency on target and medicinal chemistry support

Generation of HEK293T stable cell lines co-expressing TMEM16A and halide sensitive YFP.

In brief, the TMEM16A HEK293T eYFP (H149Q, I153L) stable cell line was generated by transfecting 10µg of linearized hTMEM16A(abc) DNA constructs into HEK293T eYFP (H149Q,I153L) stable cells. The transfected cells were cultured under 200 µg/ml of hygromycin B selection for 20 days and the stable pool was single cell seeded in 96 well plate and duplicated plate were made after single cell clones were formed. YFP function assay were performed on duplicated plate and clones producing higher changes in fluorescence from the YFP assay were chosen for further expansion to form a stable cell line.

TMEM16A eYFP FLIPR-Tetra assay for medchem and routine tests of compound activity.

HEK293T cells stably co-expressing hTMEM16A (abc) and the halide-sensitive YFP were cultured with DMEM/F-12, HEPES (Life Technologies, Catalog Number: 11330-032) plus 10% (heat inactive) FBS (Life Technologies, Catalog Number: 10082-147), 1X Pen Strep Glutamine (Gibco 10378-016), 0.5μg/ml of puromycin and 200μg/ml Hygromycin B. The day before the assay, 30μl/well of the cells suspension was seeded to achieve 15000 cells/well in 384 well plate (Corning® BioCoat™ Poly-D-Lysine 384 Well black / clear plate, Cat# 354663). Plates were incubated for 24 hours at 37^0C with 5% CO_2 . On the assay day, medium was removed and replaced with 20μl/well of assay buffer (Hank's Balanced Salt Solution with 10mM HEPES pH 7.4), 10μl/well of 40x diluted compounds was added to assay plate and it was incubated at room temperature for 30 min, after which baseline fluorescence was read in the FLIPR instrument for 10 seconds. Then, 5μl/well of a 3x trigger solution (24mM iodide, 3μM ionomycin in assay buffer) was added and the fluorescence kinetic trace was recorded for 2 minutes.

Q-Patch electrophysiology analysis of compound impact of TMEM16A currents.

HEK293 cells stably expressing the TMEM16A (acd) variant were purchased from SB Drug Discovery. The HEK293 TMEM16A (abc) stable cell line was from ChanTest and COLO-205 cells were purchased from ATCC. The same standard buffers and recording conditions listed below were used for QPatch studies on all three cell lines.

Recording Solutions: should be made weekly as below and can be stored at room temperature until use. Do not add ATP to internal solution until immediately before using on the QPatch (Sophion). The External buffer (in mM) was 140 NaCl, 4 KCl, 2 CaCl2, 1 MgCl2, 10

HEPES, 10 Glucose, pH7.4, while the Internal buffer (in mM) was 110 CsCl, 20 TEA-Cl, 5.374 CaCl2, 1.75 MgCl2, 10 EGTA, 10 HEPES, 4 Na2ATP, pH 7.2.

Once established in whole-cell configuration, cells are clamped to a holding potential (Vhold) of 0 mV on 48 well single hole patch plate. A standardized IV protocol is used to elicit ionic current through the TMEM16A chloride channel at 20 s intervals. Steady-state voltage pulses begin at -100 mV to +100 mV in +20 mV steps for a duration of 500 ms. After each pulse the voltage returns to -100 mV for 50 ms to obtain tail currents, and then returns to the holding potential of 0 mV until the beginning of the next sweep. Block of TMEM16A chloride current due to Test Article is measured at the +100 mV depolarization sweep of the third and final IV protocol run per concentration addition. This ensures a minimum of 60 s per concentration incubation before measuring current block. Currents are acquired at 10 kHz and filtered at 2 kHz, leak subtraction and Rseries are disabled. A 1 MΩ minimum resistance is set because cells are held in an open channel state and therefore resistance is low.

A cumulative concentration response is measured whereby each cell is exposed to five concentrations of test article with a dilution factor of 1:5 (e.g. 0.048, 0.24, 1.2, 6 and 30 µM). Cells are recorded for ~60 s per solution/compound addition. Initially, external solution is applied twice to allow currents to stabilize. Then vehicle (from the saline reservoir) is added twice to monitor any effect 0.3% DMSO might have on currents. This leads directly into the concentration runs by applying Concentration 1 (single addition) for 1 minute. Concentration 2 is then applied for the subsequent minute, etc. Recovery/washout is monitored for a final minute with a final external solution addition.

Peak outward current magnitude at 540ms through 550ms of the IV step is measured for each sweep at 10 s intervals. The final measurement at +100 mV is calculated for each

compound application. Each cell's current magnitude is then normalized to itself at the initial 0.3% vehicle control period prior to compound application. This step is to account for differences in current size for each cell. Normalized responses to test article are plotted against their concentrations to reveal a concentration-inhibition plot.

A Normalized Group Hill fit is then performed on the plotted results to yield a pooled IC50 value, reconstructed from a minimum of two cells/concentration. The Baseline Response as well as the Full Response are constrained to 1 and 0, respectively.

IonWorks Barracuda electrophysiology studies.

HEK293 cells stably expressing the human TMEM16A (abc) variant and CHO cells expressing the human CFTR gene were from ChanTest. The IonWorks Barracuda (IWB) procedure and data provided are from outsourced studies performed at ChanTest who were blinded as to the identity of the test articles or compounds provided by Amgen. As a control, benchmark inhibitors CFTRinh-172, GlyH-101 and benzbromarone were included amongst the blinded compounds submitted and performed as expected.

For IonWorks Barracuda studies on TMEM16A compounds, in brief eight test article concentrations were applied to naïve cells (n = 4, where n = the number of replicate wells/concentration) via steel needles of a 384-channel pipettor. Each application consists of addition of 20ul of 2X concentrated test article solution to the total 40ul final volume of the extracellular well of the Population Patch ClampTM (PPC) planar electrode. This addition is followed by mixing (1 times) of the PPC well content. Duration of exposure to each test article concentration was at least five minutes. The electrophysiology procedure used: (a) Intracellular solution containing 50 mM CsCl, 90 mM CsF, 5 mM MgCl2, 1 mM EGTA, 10 mM HEPES,

adjusted to pH 7.2 with CsOH; (b) Extracellular solution containing HEPES-Buffered Physiological Saline (HBPS): 137 mM NaCl, 4 mM KCl, 1.8 mM CaCl2, 1 mM MgCl2, 10 mM HEPES, 10 mM glucose, adjusted to pH 7.4 with NaOH; and (c) Ionomycin Stimulation of chloride currents where 10 μM ionomycin is added to all test solutions including vehicle and positive controls. The current was elicited by a 500-ms step pulse to 0 mV followed 1000-ms step pulse to -100 mV from holding potential, -30 mV, with stimulation frequency 0.05 Hz. The specific Recording Procedure is as follows: extracellular buffer is loaded into the PPC plate wells (11 μl per well). Cell suspension is then pipetted into the wells (9 μl per well) of the PPC planar electrode. After establishment of a whole-cell configuration via patch perforation, membrane currents are recorded using the on-board patch clamp amplifiers. Recordings (scans) were performed as follows: three scans before and fifteen scans during the five-minute interval after test article application. A full dose-response of benzbromarone was included on each plate as a positive control, while multiple replicates of DMSO were included as negative control. Final DMSO concentration for test and control articles was 0.3%.

For measuring compound effects on CFTR chloride currents, compounds were serially diluted in HEPES-buffered physiological saline to 2X final concentration allowing for an 8-point dose-response analysis. Test article concentrations were applied to naïve cells (n = 4, where n = the number of replicate wells/concentration) via steel needles, where each application will consist of addition of 20μl of 2X concentrated test article solution to a final 40μl volume in the extracellular well of the Population Patch ClampTM (PPC) planar electrode. After mixing (3 times), duration of exposure to compound is at least five minutes. Final solutions contain 0.3% DMSO. The electrophysiology procedure used: (a) Intracellular solution (mM): CsCl, 50; CsF 90; MgCl2, 5; EGTA, 1; HEPES, 10; adjusted to pH 7.2 with KOH, (b) Extracellular, HB-PS

Solution (composition in mM): NaCl, 137.0; KCl, 4.0; CaCl2, 1.8; MgCl2, 1; HEPES, 10; adjusted to pH 7.4 with NaOH; and (c) Stimulation, where CFTR current is activated with 20 μM forskolin added to all test solutions including vehicle and positive controls. The current is measured using a pulse pattern consisting of a voltage step to +60 mV, 100 ms duration; voltage ramp from +60 to -120 mV, 1000 ms; step to -120 mV, 200 ms; and step to 0 mV, 200 ms; from holding potential, –30 mV. Current amplitudes were measured at the voltage step to 0 mV. Recording Procedure was as follows: extracellular buffer is loaded into the PPC plate wells (11μl per well). Cell suspension was pipetted into the wells (9μl per well) of the PPC planar electrode. After establishment of a whole-cell configuration via patch perforation, membrane currents were recorded using the patch clamp amplifier in the IonWorks™ Barracuda system. Two recordings (scans) were then performed, one scan before and a second scan five minutes after test article application. Every plate included a full dose-response of CFTRinh-172 as a positive control. Data acquisition and analyses were performed using the IonWorks Barracuda™ system operation software (version 2.0.2). The decrease in current amplitude after test article application was used to calculate the percent block relative to control. Results for each test article concentration ($n \geq 2$) were averaged; the mean and standard deviation values were calculated, and used to generate dose-response curves. Inhibition effect was calculated as: % Inhibition = $(1 - I_{TA} / I_{Baseline}) \times 100\%$, where $I_{Baseline}$ and I_{TA} were the currents measured in control (before addition of a test article) and in the presence of a test article, respectively.

Histamine-induced depolarization of human bronchial smooth muscle cells.

Cultured human bronchial smooth muscle cells (BSMC) from Lonza were resuspended in Smooth Muscle Growth Medium-2 (SmGM-2; Lonza) at a concentration of 4×10^5 cells per ml.

One hundred microliters of cells per well were plated in a black wall clear bottom polystyrene 96-well tissue culture plate, and incubated in a 37°C humidified incubator with 5% CO_2 overnight. Cells were serum starved by removing the SmGM-2, and replaced with one hundred microliters per well of Smooth Muscle Cell Basal Medium 2 (SmBM-2), phenol red-free (PromoCell), and incubated in a 37°C humidified incubator with 5% CO_2 for 24 h. SmBM-2 was replaced with one hundred microliters of fresh SmBM-2. Compounds were dissolved in 100% DMSO and serially diluted ½ log in a polypropylene 96-well microtiter plate (drug plate). Columns 6 and 12 were reserved as controls (HI control and LO control respectively) and contained only DMSO. Serially diluted compounds were diluted in SmBM-2 to 10X the final concentration. Twenty-five microliters of 10X compound titrations, and one hundred microliters of Blue dye-loading buffer (FLIPR Membrane Potential Assay Kit; Molecular Devices) were added to the cells. Cells were pre-incubated at room temperature with compound for 0.5 h. Five micromolar (10X) histamine was prepared in SmBM-2. Using the FLIPR-Tetra (Molecular Devices), three measurements of the baseline fluorescence were taken over the span of one minute. Twenty-five microliters per well of 10X histamine were added to the first 11 columns of the plate containing the compound treated cells. Twenty-five microliters of SmBM-2 were added to column 12 for the LO control. Fifty-five fluorescence measurements were taken over the span of fourteen minutes. The area under the curve (AUC) from the fluorescence kinetic traces (normalized to baseline fluorescence) were calculated. The amount of fluorescence in the presence of compound compared with that in the presence of DMSO vehicle alone (HI control) was calculated using the formula: % control (POC) = (compd – average LO)/(average HI – average LO)*100.

While the method above using histamine represents the standard protocol we used to evaluate compound effects in blocking pro-contractile depolarization of human BSMCs, for some experiments provided as supplementary figures we employed the cholinergics methacholine or carbachol instead of histamine, or evaluated if the TMEM16A opener, Eact, could itself act like contractants to induce BSMC membrane depolarization.

Measuring antagonist effects on BSMC pro-contractile calcium flux.

Human BSMCs were obtained from Lonza, resuspended, cultured and serum starved for 24 hours as described in the histamine membrane potential assay earlier. Compounds and dilutions were prepared in same manner, except they were serially diluted in Assay Buffer (2mM CaCl2, 1mM MgCl2, 4.5mM KCl, 155mM NaCl, 5mM HEPES, 10mM glucose, pH7.4) to 4X the final concentration. A Calcium Indicator Working Solution (10 ml) was prepared by adding 1ml BD PBX Signal Enhancer (Cat# 51-9006254) and 10µl of BD Calcium Indicator (BD Cat# 850000 resuspended in 100% DMSO) to 9ml Assay Buffer. Following serum starvation of the BSMCs, culture media was aspirated off and 50µl of Calcium Indicator Working Solution was added to each well of microtiter plate. Twenty-five microliters of the 4X serially diluted compounds were then added and cells were incubated with compounds for 30 minutes at room temperature. Twenty-five microliters of a 4X histamine or methacholine solution (where 1X reflects EC_{80}-EC_{100} concentration from earlier validation of aliquot of cells from same donor) was then added and fluorescence changes were measured by a FLIPR-Tetra or internal FlashFluor instrument. In some experiments the TMEM16A opener, Eact, was used in place of histamine or methacholine.

Measuring bronchodilation of mouse tracheal rings by wire myograph.

Instrument and reagents.

A series of three Danish Myograph Technologies (DMT) 620M Multi Wire Myograph Systems instruments were typically used for each experiment, with each instrument containing four chambers and allowing tests on four tracheal rings. The instruments were interfaced with PowerLab 4/35 or PowerLab 8/35 data acquisition systems and a computer running DMT Device Enabler and LabChart Pro v8 (AD Instruments) for automatic recognition of devices and simultaneous recording of data. Carbachol (Cat# C4382) and isoproterenol (Cat# I2760) were from Sigma. Mouse IL-13 and mouse IL-1β were from R&D Systems. Histamine, theophylline and mouse TNFα were from Amgen.

Mice

Mice used for wire myograph studies were housed in groups at an AAALAC, International accredited facility. Animals were cared for in accordance with the *Guide for the Care and Use of Laboratory Animals*, 8th Edition. All research protocols were reviewed and approved by the Amgen Institutional Animal Care and Use Committee. Female C57 BL/6 (CRL, >12 weeks of age) were housed in individual ventilated caging (IVC) system on an irradiated corncob bedding (Envigo Teklad 7097). Lighting in animal holding rooms was maintained on 12:12 hr light:dark cycle, and the ambient temperature and humidity range was at 68 to 79°F and 30 to 70%, respectively. Animals had ad libitum access to irradiated pelleted feed[2] (Envigo Teklad Global Rodent Diet- soy protein free extruded 2020X) and reverse-osmosis (RO) chlorinated (0.3 to 0.5 ppm) water via an automatic watering system. Cages were changed biweekly inside an engineered cage changing station.

Standard wire myograph studies for measuring bronchodilation.

The trachea from C57 BL/6 mice was dissected and collected in PBS with Mg2+ and Ca2+. After further trimming, two 2mm sections (rings) per trachea were then placed in DMEM media containing PSG/HEPES/AA/NaPyr for 1 hour and used immediately or maintained overnight at 37°C in a humidified incubator with 5% CO2. Rings were then mounted into chambers of DMT wire myograph containing L-shaped mounting pins with 2-3 mN of force applied to secure rings on the pins and the rings were allowed to equilibrate for 25-30 min in a physiological saline buffer (PSS, 130 mM NaCl, 4.7 mM KCl, 1.2 mM MgS04, 14.9 mM NaHCO3, 1.2 mM KH2PO4, 0.026 mM EDTA, 1.6 mM CaCl2, 5.5 mM Dextrose). Throughout the experiment, rings were maintained at physiological temperature and gas conditions by heating buffer reservoir and chamber to 37°C and bubbling a 95% O_2, 5% CO_2 gas mixture into chamber.

After equilibration, a standard tissue Wake-Up procedure was applied by altering tension and then treatment with elevated potassium as follows: 3 mN tension was applied for 5-10 min, then another 2-3 mN tension to total of 5.5 mN and then to 7-8 mN for another 5 min; the tissue pre-tension was then set to 5 mN and allowed to equilibrate for 5-10 min followed by the removal of the PSS buffer and addition of KPSS (60 mM KCl, 74.7mM NaCl in PSS solution), with force changes monitored until they reached a plateau. The tissue was then washed four times with PSS over 5min and the KPSS treatment and washes repeated; the tissue was then allowed to sit in PSS for 10 min and the tension was set to 5 mN.

To qualify every tissue ring and determine its sensitivity to contractant and reference bronchodilator, 6 ml of PSS was added to each chamber and after 5 min ascending doses of the carbachol (CCh) contractant were added to determine the EC_{25}, EC_{50}, EC_{75} and EC_{95} for CCh for each ring (see ***Figure 3-figure supplement 1*** for example; raw traces and dose-response), where sufficient time (at least 5 min) was allowed for response to plateau after each dose. At the end of

the CCh dose-response study when no further increases in force were observed, the β-agonist and reference bronchodilator isoproterenol was added to 10 μM final concentration to monitor tissue relaxation. The tissue was then washed 3 times and then 3 times more with PSS for 5 min until tension returned to baseline.

Only tissue that passed the qualification tests above advanced to studies on test article compounds. Fresh PSS (6 ml) was then added to each tissue bath, tension was reset to 5 mN and the rings were treated with the calculated EC_{25}, EC_{50}, EC_{75} or EC_{95} concentration of CCh from GraphPad Prism analysis and allowed to incubate for at least 25 min and a plateau was achieved. For standard ascending dose-response studies to TMEM16A antagonists (***Figure 2*** and ***Table 1***), an EC_{75} or EC_{95} concentration of CCh was used to pre-contract tracheal rings. Ascending doses of the isoproterenol positive control, the vehicle negative controls or the test compound were then added to appropriate rings and incubated for 10 min or until plateau was achieved after each addition. At the end of the experiment when no further changes were observed to test article or positive control, theophylline was added to 2.2 mM final to fully relax airways. The dose-response curved and EC50 values for bronchodilation were derived from GraphPad Prism analysis of the data normalized to theophylline as 100% relaxation.

Bronchodilation of tracheal rings as function of differing levels of pre-contraction.

Standard procedures as listed above were used to prepare, mount and Wake-Up tracheal rings and the concentrations of carbachol providing EC_{25}, EC_{50}, EC_{75} or EC_{95} levels of contraction for each ring was determined as described above. Rings with differing levels of CCh pre-contraction were then treated with ascending doses of isoproterenol, benzbromarone, niclosamide or Compound 4 to determine the efficacy of bronchodilation, which was normalized to theophylline added at the end as control of 100% relaxation.

Effects of cytokines on compound efficacy in relaxing mouse tracheal rings.

Airway rings were treated overnight in 2 ml DMEM + PSG/HEPES/AA/NaPyr buffer alone or with the same solution supplemented with 100 ng/ml of mTNFα, mIL-13 and mIL-1β. Unlike like the typical Wake up protocol and ring qualifying tests, mouse tracheal rings were not exposed to KPSS and rings were not observed to relax with a β-agonist following discovery of CCh dose-responses. After several washes with PSS, EC_{75} concentrations of CCh were used to pre-contract rings for >30min alone or in the presence of cytokines. Ascending doses of isoproterenol, benzbromarone, or niclosamide were given to determine efficacy of bronchodilation normalized to theophylline as control of 100% relaxation.

Evaluating β-agonist short-term use-dependent desensitization.

Standard procedures were used to prepare and mount tissues. However, similar to the experiments assessing the effects of cytokines in relaxing tracheal rings, no KPSS or qualifying tests with isoproterenol to observe relaxation following discovery of CCh dose-responses. To assess use-dependent desensitization, EC_{50} concentrations of CCh were used to pre-contract rings followed by a dose-response with isoproterenol. Rings were then washed several times with PSS, pre-contracted again with EC_{50} CCh, and given another round of isoproterenol dose-response normalized to theophylline as control of 100% relaxation.

Assessing compound duration of action in bronchodilating.

Mouse airway rings were exposed to a typical Wake up procedure including the use of KPSS and discovery of EC_{75} CCh dose responses. However, no isoproterenol was used to observe tissue relaxation as part of the qualification procedure. With pre-contraction with EC_{75} CCh for >30min, rings were subjected to a compound dose-response, followed by a complete washout of

compound, and re-contracted with EC_{75} CCh. Traces were recorded for several hours thereafter and normalized to theophylline as control of 100% relaxation.

Measuring bronchodilation of human bronchial rings by wire myograph.

Outsourced bronchodilator studies performed at Biopta (Glasgow, United Kingdom).

Details of bronchodilator studies shown in ***Fig. 3F*** and ***Figure 3–figure supplement 6*** are provided below as part of the end assay report on Study CUR011 by Lee Christie (Biopta), key excerpts of which are provided explicitly and unaltered. Donors with any of the following conditions were excluded from the study: asthma, COPD, emphysema, lung cancer, Cystic Fibrosis, pulmonary fibrosis, pulmonary hypertension, pneumonia. Donors were also excluded if they had smoked in the past 12 months. Donors were also excluded if they had smoked in the past 12 months. Any macroscopically diseased/necrotic tissue was rejected. Furthermore, any tissues that did not respond to functional checks were rejected.

Human airway rings were set up under isometric conditions on a wire myograph in order to examine the influence of the test articles on bronchodilation. In order to assess tissue viability, the airways were challenged with carbachol (10 µM) and then isoprenaline (10 µM) to assess their constriction and relaxation responses, respectively. Airways that did not respond to these initial checks were not used.

Viable airways were pre-constricted with histamine (10 µM), then exposed to one of the following cumulative concentration response curves (CCRCs): positive control, vehicle (water, volume matched to positive control), test article, vehicle (DMSO concentration matched to test articles). At the end of each CCRC, theophylline (2.2 mM) was added to induce maximal relaxation of the tissue.

Specific methodology was as follows: **(a)** Quaternary branches of human airway rings were dissected free from surrounding parenchyma, cut into 2 mm rings and mounted in 5 mL organ baths containing physiological saline solution (composition: 119.0 mM NaCl, 4.7 mM KCl, 1.2 mM MgS04, 24.9 mM NaHCO3, 1.2 mM KH2PO4, 2.5 mM CaCl2, 11.1 mM glucose and 5 µM indomethacin), aerated with 95% O2/5% CO2, and warmed to 37ºC. The tissues were allowed to equilibrate for approximately 30 minutes, with washes approximately every 10 minutes, before being set to a tension of approximately 1.0 - 1.5 g and then allowed to equilibrate for a further 90 minutes with washes approximately every 15 minutes. Airways were re-tensioned to 1.0 – 1.5 g if the tension had dropped below 1.0 g during the first 30 minutes of equilibration. **(b)** Airways were exposed to carbachol (bath concentration 10 µM) in order to measure their contractile responses and then isoprenaline (10 µM) in order to assess their relaxation. Airways were washed out and allowed to return to baseline. **(c)** Airways were pre-constricted with histamine (10 µM) before conducting a CCRC to the test article, the positive control (isoprenaline), test article vehicle or positive control vehicle. The results for TMEM16A antagonist bronchodilation of two donors is provided in ***Figure 3–figure supplement 6***, where it should be noted there was no significant effect by any of the vehicles.

Bronchodilator studies that were performed internally at Amgen.

Bronchodilator studies using human bronchial rings (***Figure 3–figure supplements 7*** *and* ***8)*** used the same instruments and reagents described earlier for studies on mouse tracheal rings.

Non-transplantable human lungs were obtained through IIAM (Edison, NJ) from non-smoking donors who had been ventilated for <3 days with acceptable blood gases and used within 24 hours of cross-clamp time.

Human 4th order bronchial rings were isolated, sliced into 2mm long rings and then mounted individually in chambers of wire myographs containing 6 ml room temperature PSS per chamber. Chambers are aerated with 95% O_2/5% CO_2 throughout the experiment. Bronchial rings are allowed to equilibrate in PSS while chambers are warmed to 37°C. Tension on the airway rings was gradually increased until reaching a steady state passive tension of 9.8 mN. The rings were then equilibrated for additional 40-60 minutes, changing buffer every 15-20 minutes. Tension was adjusted if it dropped below 9.8 mN. Airway rings were "woken up" by exposing to pre-warmed, aerated KPSS and allowing rings to reach plauteau of constriction, followed by washing rings 4 times with PSS. This procedure was repeated 2 additional times.

Airway contraction response was then assessed by treating with increasing doses of the contractant, carbachol (10 nM to 10 μM), waiting for response plateaus (at least 5 minutes between additions). Airways are then relaxed by addition of 10 μM isoproterenol. Airways that demonstrated expected contraction and relaxation were used to evaluate test compounds after a washout and re-equilibration period.

Airway rings were contracted with EC_{75} of carbachol and then exposed to one of the following CCRCs: vehicle (DMSO concentration matched to test article), isoproterenol (positive control), test compound. At the end of each CCRC, rings were fully relaxed by addition of 2.2 mM theophylline. One hundred percent contraction was calculated by subtracting the stable tension remaining in the airway ring after theophylline addition from the tension achieved after addition of EC_{75} carbachol while 100% relaxation is the net tension remaining after theophylline addition. Dose response curves and EC_{50} values for bronchodilation were determined in GraphPad Prism.

Evaluating TMEM16A expression and splice variants produced in airway smooth muscle cells and the bronchial epithelium.

RNA sequencing

The RNA-Seq Amgen lung cell dataset containing primary human bronchial epithelial cells and airway smooth muscle cells (**Figure 5-figure supplement 1**) has been described earlier, as has the method for RNA sequencing (***Aisenberg et al.***, ***2016***), with modifications and additional details provided below. Similar RNA sequencing and data analysis methods were applied to generate the new RNA-Seq dataset described here for untreated or IL-13 treated mature bronchial epithelial ALI cultures, the results of which are shown in **Figure 5-figure supplement 2** and **3**.

Data were analyzed using the Array Studio (Omicsoft, NC) platform, as previously described (***Aisenberg et al.***, ***2016***), but using v9.0 of the Oshell software and the GENCODE (***Harrow et al.***, ***2012***) gene model (release 24; Comprehensive version was used for alignment, and Basic version was used for quantification). FPKM values were normalized using a modified version of upper-quartile normalization (***Mortazavi et al.***, ***2008; Robinson et al.***, ***2010***) in which the 70th percentile FPKM among genes was fixed at a value of 10 (excluding those genes belonging to families with high homology or with maximal transcript length <500 bp). Data from the Cancer Cell Line Encyclopedia (***Barretina et al.***, ***2012***) were processed by OmicSoft using the same analysis pipeline and normalized using the same methods.

Generating human bronchial epithelial ALI cultures and effects of Th2 cytokines.

To determine the effects of IL-13 on TMEM16A versus Muc5AC mRNA expression over time in the human bronchial epithelium and evaluate TMEM16A alternative splicing, normal and COPD human bronchial epithelial cells from Lonza were grown on 6.5mm permeable supports (Corning Transwell 3470) submerged in apical and basolateral growth media (BEGM, Lonza,

CC-3170), until confluent at ~5 days. Once confluent, apical media was removed, and basolateral growth media was replaced with ALI maintenance media (PneumaCult, STEMCELL Technologies #05001) to initiate the air-liquid interface (ALI). Cultures were then maintained at ALI for ~21 days, with basolateral maintenance media being replenished on Monday-Wednesday-Friday schedule, to generate fully differentiated human bronchial epithelial cells. Cultures were then left untreated or treated with 20 ng/ml IL-13 for 1, 3, 5 or 7 days. For each time point, RNA was prepared from the ALI cultures for the NextGen RNA sequencing following the Qiagen RNeasy Mini kit (cat # 74104) protocol. Each ALI culture was solubilized with 350 μl of Qiagen lysis buffer RLT on the apical transwell and immediately spun through a Qiashredder (Qiagen # 79654) at 15,000 rpm for 2 minutes. The samples were either stored at -80°C and processed at a later date or immediately prepared following the Qiagen RNeasy Mini kit protocol including Part 2 which contains the Qiagen RNase-Free DNase set (Cat # 79254) treatment. Total RNA was eluted in 45 μl of RNase free water supplied from the kit and quantified on a Nanodrop ND-1000 spectrophotometer.

TMEM16A protein expression was determined by immunohistochemistry of untreated or IL-4 or IL-13 treated human bronchial epithelial ALI cultures. Fully differentiated human bronchial epithelial ALI cultures were generated using methods similar to those described above, except cultures were expanded on permeable supports for 3 days and maintained at ALI for 31 days prior to treatment. At 31 days post-airlift, cultures were left untreated or treated with either 20 ng/ml IL-4 or 20 ng/ml IL-13 for 1, 2, 3, or 5 days. For each timepoint, Transwells were fixed both apically and basolaterally with 2% paraformaldehyde for 2 hours at room temperature, then washed with 70% ethanol. Permeable membranes containing the ALI cultures were then

cut away from the plastic insert using a scalpel and processed for immunohistochemistry as described below.

TMEM16A expression in tissue isolated from naïve or asthmatic cynomolgus monkeys.

Tissue from naïve or asthmatic cynomolgus monkeys was obtained from Charles River Laboratories. Naïve adult cynos were never challenged with *Ascaris suum* aerosol, were from the standard CRL colony and were negative by intradermal screening for *A. suum*. Adult cynos exhibiting sensitivity to *A. suum* antigen and characterized as asthmatic, presumably due to early exposure and allergy to *A. suum* or similar parasite, were maintained in a separate colony and confirmed over time as reproducible sensitivity to an *A. suum* aerosol challenge. Naïve, unchallenged asthmatic (>2 weeks), asthmatic acute challenged (4 hours post aerosol A. suum) and asthmatic subacute challenged (24 hours post *A. suum* aerosol) cynos were euthanized and lung vasculature infused with cold HypoThermosol biopreservation media. Lungs and trachea were shipped on ice packs overnight and necropsy was immediately performed on arrival to prepare specimens for immunohistochemistry and bronchodilation studies.

Immunohistochemistry

The routinely formalin-fixed, paraffin embedded tissue blocks were sectioned at a 4 µm thickness and processed for IHC. Paraffin was removed from the tissue sections with xylene and the sections were rehydrated with graded ethanol and immersed in distilled water. Antigen retrieval was performed using Diva Decloaker pretreatment reagent (Biocare Medical, Concord, CA) in a Biocare Decloaking Chamber (Biocare Medical, Concord, CA) set to reach 125ºC for 30 seconds, then 90ºC for 10 seconds. Tissue sections were processed at room temperature in a Lab Vision 720 automated staining instrument (Thermo Scientific, Waltham, MA). Endogenous peroxidase was blocked using Hydrogen Peroxide Block (cat# TA-125-HP, Thermo Scientific,

Waltham, MA) for 10 minutes. Protein Block (cat# X0909, Dako North America) was applied to the tissue sections for 10 minutes. Tissue sections were incubated with anti-human TMEM16A (cat# Ab53212, Abcam, San Francisco, CA). Envision+ System HRP labelled Polymer (cat# K4003, Dako North America) was used to detect the primary antibody. Sections were incubated with DAB plus chromogen substrate (cat#K3468) for 5 minutes.

Effects of TMEM16A opener Eact on Muc5AC and leukotriene production from bronchial epithelial air-liquid interface cultures.

Normal, asthma and COPD human bronchial epithelial (HBE) cells were from Lonza (Walkersville, MD). Cells were grown on 0.4 μM transparent PET transwell membranes insert (BD biosciences, San Diego). S-ALI air-liquid interface media (Lonza) was changed every other day until the cells reached confluence, at which time the apical medium was removed to establish an air liquid interface cultures. The basolateral medium was changed every other day. All experimentation was carried out on day 14-18 after ALI establishment. At this point, mature secretory cells are present in these differentiating cultures and the cells respond with maximal proliferation to IL-13 (10 ng/ml) (Peprotech, Rocky Hill, NJ, USA).

Human ALI cultures from a normal donor were treated with Eact, Eact vehicle and 10 ng/ml IL13 in basolateral medium for 48 hrs. After 48hr, 100 μl of basolateral medium were collected for determining leukotriene B4 and C4 secretion using ELISA kits from Enzo Life Sciences, Inc. and LSBio LifeSpan Biosciences Inc., respectively, and by following manufacture's protocols. There was a n of 3 replicate ALI cultures per condition.

The determine the effects of Eact on mucin secretion, mature human bronchial epithelial ALI cultures established from normal, asthma and COPD patients (2 donors, each) were treated

with vehicle or 5 μM Eact in basal media for 72 hours. To collect mucus, the apical side of ALI cultures (n = 2 ALIs per donor) was washed two times with 0.5 ml of 10 mM DTT (37°C for 15 min, each) and the washes were combined. Levels of Muc5AC protein in apical washes was then determined using a Muc5AC ELISA kit (Cosmo Bio USA, Carlsbad, CA) and following the manufacture's protocol.

Acknowledgements

The authors wish to thank the Amgen Protein Technology group for TMEM16A expression constructs, the scientific team at Sophion and ChanTest (CRL) for help in developing the QPatch and IonWorks Barracuda electrophysiology assays or counterscreens against CFTR, scientists at Biopta (ReproCELL) for bronchodilation studies, and past members of the Airway Smooth Muscle Working Group, Asthma, COPD and IPF Teams at Amgen who contributed to building a foundation in the respiratory efforts which enabled these studies, including Heather Thomas, Ken Schooley, Ryan Brown, Deb Hopkins, Anna Pirrone, Leanne Peiser, Cindy Willis, Daniela Metz and Heather Arnett.

Additional information

Funding

The authors are current or past Amgen employees who may own shares in the company. The studies were funded by Amgen Inc., but the corporate funders had no role in study design, data collection, or the decision to submit the work for publication.

Author Contributions

A.H., K.L. and K.W. developed and conducted the high-throughput screen and performed follow-up experiments to identify validated hits. P.W. and D.P. performed medchem support in determining compound potency in eYFP assay. B.L., K.H., J.M. and J.KS. developed TMEM16A electrophysiology assays, performed experiments and/or analyzed data. K.G. and X.X. developed and analyzed compounds for effects on ASM membrane potential or calcium flux. K.M., R.E., D.M. and A.L. developed and characterized compounds for bronchodilation of mouse, cynomolgus monkey or human tissue. K.M. ran routine bronchodilation studies to support medchem and performed studies evaluating compound ability to resist use- and inflammatory-desensitization. E.T., K.H., S.E., O.H., K.M., B.B., J.W., and M.F. conducted experiments evaluating TMEM16A expression and splice variants. J.K.S., D.S., M.C., T.B., A.B., J.J., J.P. and M.W. were involved in conception or enablement. J.C. and L.L. synthesized compounds and analyzed data. J.K.S. initiated the project, supervised the program and wrote the first

draft of the manuscript. All authors discussed and commented on the manuscript.

Author ORCIDs

Andreas Hochheimer, https://orcid.org/0000-0002-1572-9334

John K. Sullivan, https://orcid.org/0000-0001-9840-852X

Present Address

Katja Labitzke, Clariant Produkte (Deutschland) GmbH , Planegg, Germany.

Longbin Liu, CHDI Management, CHDI Foundation, Los Angeles, CA, USA.

Anh Leith, Dept. Genome Sciences, University of Washington, Seattle, WA, USA.

Esther Trueblood, Seattle Genetics, Bothell, WA, USA.

Teresa L. Born, Sartorius Stedim BioOutsource, Cambridge, MA, USA.

Alison Budelsky, Immunology Research, Lilly Research Laboratories, San Diego, CA, USA.

Dirk Smith, Insight Bioconsulting, Bainbridge Island, WA, USA

Kerstin Weikl, Assay.Works GmbH, Regensburg, Germany.

Andreas Hochheimer, ISAR Bioscience GmbH, Planegg, Germany.

John K. Sullivan, PolestarBio LLC, Newbury Park, CA, USA.

Ethics

Animal experimentation and tissue: All animal procedures and tissue collections were conducted in an Association for Assessment and Accreditation of Laboratory Animal Care accredited facility in accordance with the requirements and guidelines of the US National Research Council and in compliance with the protocols approved by the Institutional Animal Care and Use Committee of the following institutions: Amgen Inc., Thousand Oaks, CA; Charles River, Shrewsbury, MA.

All human lung specimens were collected under Institutional Review Board approval with appropriate informed consent. In all cases, materials obtained were surplus to standard clinical practice. Patient identity and PHI/identifying information were redacted from tissues and clinical data.

References

Ahmed, K., Shaw, H. V., Koval, A., & Katanaev, V. L. (2016). A Second WNT for Old Drugs: Drug Repositioning against WNT-Dependent Cancers. *Cancers (Basel), 8*(7). doi:10.3390/cancers8070066

Aisenberg, W. H., Huang, J., Zhu, W., Rajkumar, P., Cruz, R., Santhanam, L., Natarajan, N., Yong, H. M., De Santiago, B., Oh, J. J., Yoon, A. R., Panettieri, R. A., Homann, O., Sullivan, J. K., Liggett, S. B., Pluznick, J. L., & An, S. S. (2016). Defining an olfactory receptor function in airway smooth muscle cells. *Sci Rep, 6*, 38231. doi:10.1038/srep38231

Barretina, J., Caponigro, G., Stransky, N., Venkatesan, K., Margolin, A. A., Kim, S., Wilson, C. J., Lehar, J., Kryukov, G. V., Sonkin, D., Reddy, A., Liu, M., Murray, L., Berger, M. F., Monahan, J. E., Morais, P., Meltzer, J., Korejwa, A., Jane-Valbuena, J., Mapa, F. A., Thibault, J., Bric-Furlong, E., Raman, P., Shipway, A., Engels, I. H., Cheng, J., Yu, G. K., Yu, J., Aspesi, P., Jr., de Silva, M., Jagtap, K., Jones, M. D., Wang, L., Hatton, C., Palescandolo, E., Gupta, S., Mahan, S., Sougnez, C., Onofrio, R. C., Liefeld, T., MacConaill, L., Winckler, W., Reich, M., Li, N., Mesirov, J. P., Gabriel, S. B., Getz, G., Ardlie, K., Chan, V., Myer, V. E., Weber, B. L., Porter, J., Warmuth, M., Finan, P., Harris, J. L., Meyerson, M., Golub, T. R., Morrissey, M. P., Sellers, W. R., Schlegel, R., & Garraway, L. A. (2012). The Cancer Cell Line Encyclopedia enables predictive modelling of anticancer drug sensitivity. *Nature, 483*(7391), 603-607. doi:10.1038/nature11003

Benedetto, R., Ousingsawat, J., Wanitchakool, P., Zhang, Y., Holtzman, M. J., Amaral, M., Rock, J. R., Schreiber, R., & Kunzelmann, K. (2017). Epithelial Chloride Transport by CFTR Requires TMEM16A. *Sci Rep, 7*(1), 12397. doi:10.1038/s41598-017-10910-0

Bian, S., Bai, J. P., Chapin, H., Le Moellic, C., Dong, H., Caplan, M., Sigworth, F. J., & Navaratnam, D. S. (2011). Interactions between beta-catenin and the HSlo potassium channel regulates HSlo surface expression. *PLoS One, 6*(12), e28264. doi:10.1371/journal.pone.0028264

Bill, A., Gutierrez, A., Kulkarni, S., Kemp, C., Bonenfant, D., Voshol, H., Duvvuri, U., & Gaither, L. A. (2015). ANO1/TMEM16A interacts with EGFR and correlates with sensitivity to EGFR-targeting therapy in head and neck cancer. *Oncotarget, 6*(11), 9173-9188. doi:10.18632/oncotarget.3277

Britschgi, A., Bill, A., Brinkhaus, H., Rothwell, C., Clay, I., Duss, S., Rebhan, M., Raman, P., Guy, C. T., Wetzel, K., George, E., Popa, M. O., Lilley, S., Choudhury, H., Gosling, M., Wang, L., Fitzgerald, S., Borawski, J., Baffoe, J., Labow, M., Gaither, L. A., & Bentires-Alj, M. (2013). Calcium-activated chloride channel ANO1 promotes breast cancer progression by activating EGFR and CAMK signaling. *Proc Natl Acad Sci U S A, 110*(11), E1026-1034. doi:10.1073/pnas.1217072110

Buchholz, B., Faria, D., Schley, G., Schreiber, R., Eckardt, K. U., & Kunzelmann, K. (2014). Anoctamin 1 induces calcium-activated chloride secretion and proliferation of renal cyst-forming epithelial cells. *Kidney Int, 85*(5), 1058-1067. doi:10.1038/ki.2013.418

Caputo, A., Caci, E., Ferrera, L., Pedemonte, N., Barsanti, C., Sondo, E., Pfeffer, U., Ravazzolo, R., Zegarra-Moran, O., & Galietta, L. J. (2008). TMEM16A, a membrane protein associated with calcium-dependent chloride channel activity. *Science, 322*(5901), 590-594. doi:10.1126/science.1163518

Chen, W., Mook, R. A., Jr., Premont, R. T., & Wang, J. (2017). Niclosamide: Beyond an antihelminthic drug. *Cell Signal*. doi:10.1016/j.cellsig.2017.04.001

Cho, H., Yang, Y. D., Lee, J., Lee, B., Kim, T., Jang, Y., Back, S. K., Na, H. S., Harfe, B. D., Wang, F., Raouf, R., Wood, J. N., & Oh, U. (2012). The calcium-activated chloride channel anoctamin 1 acts as a heat sensor in nociceptive neurons. *Nat Neurosci, 15*(7), 1015-1021. doi:10.1038/nn.3111

Dang, S., Feng, S., Tien, J., Peters, C. J., Bulkley, D., Lolicato, M., Zhao, J., Zuberbuhler, K., Ye, W., Qi, L., Chen, T., Craik, C. S., Nung Jan, Y., Minor, D. L., Jr., Cheng, Y., & Yeh Jan, L. (2017). Cryo-EM structures of the TMEM16A calcium-activated chloride channel. *Nature*. doi:10.1038/nature25024

Danielsson, J., Perez-Zoghbi, J., Bernstein, K., Barajas, M. B., Zhang, Y., Kumar, S., Sharma, P. K., Gallos, G., & Emala, C. W. (2015). Antagonists of the TMEM16A calcium-activated chloride channel modulate airway smooth muscle tone and intracellular calcium. *Anesthesiology, 123*(3), 569-581. doi:10.1097/ALN.0000000000000769

Danielsson, J., Yim, P., Rinderspacher, A., Fu, X. W., Zhang, Y., Landry, D. W., & Emala, C. W. (2014). Chloride channel blockade relaxes airway smooth muscle and potentiates relaxation by beta-agonists. *Am J Physiol Lung Cell Mol Physiol, 307*(3), L273-282. doi:10.1152/ajplung.00351.2013

De La Fuente, R., Namkung, W., Mills, A., & Verkman, A. S. (2008). Small-molecule screen identifies inhibitors of a human intestinal calcium-activated chloride channel. *Mol Pharmacol, 73*(3), 758-768. doi:10.1124/mol.107.043208

Duvvuri, U., Shiwarski, D. J., Xiao, D., Bertrand, C., Huang, X., Edinger, R. S., Rock, J. R., Harfe, B. D., Henson, B. J., Kunzelmann, K., Schreiber, R., Seethala, R. S., Egloff, A. M., Chen, X., Lui, V. W., Grandis, J. R., & Gollin, S. M. (2012). TMEM16A induces MAPK and contributes directly to tumorigenesis and cancer progression. *Cancer Res, 72*(13), 3270-3281. doi:10.1158/0008-5472.CAN-12-0475-T

Forrest, A. S., Joyce, T. C., Huebner, M. L., Ayon, R. J., Wiwchar, M., Joyce, J., Freitas, N., Davis, A. J., Ye, L., Duan, D. D., Singer, C. A., Valencik, M. L., Greenwood, I. A., & Leblanc, N. (2012). Increased TMEM16A-encoded calcium-activated chloride channel activity is associated with pulmonary hypertension. *Am J Physiol Cell Physiol, 303*(12), C1229-1243. doi:10.1152/ajpcell.00044.2012

Gallos, G., Remy, K. E., Danielsson, J., Funayama, H., Fu, X. W., Chang, H. Y., Yim, P., Xu, D., & Emala, C. W., Sr. (2013). Functional expression of the TMEM16 family of calcium-activated chloride channels in airway smooth muscle. *Am J Physiol Lung Cell Mol Physiol, 305*(9), L625-634. doi:10.1152/ajplung.00068.2013

Gorrieri, G., Scudieri, P., Caci, E., Schiavon, M., Tomati, V., Sirci, F., Napolitano, F., Carrella, D., Gianotti, A., Musante, I., Favia, M., Casavola, V., Guerra, L., Rea, F., Ravazzolo, R., Di Bernardo, D., & Galietta, L. J. (2016). Goblet Cell Hyperplasia Requires High Bicarbonate Transport To Support Mucin Release. *Sci Rep, 6*, 36016. doi:10.1038/srep36016

Hakonarson, H., Herrick, D. J., Serrano, P. G., & Grunstein, M. M. (1996). Mechanism of cytokine-induced modulation of beta-adrenoceptor responsiveness in airway smooth muscle. *J Clin Invest, 97*(11), 2593-2600. doi:10.1172/JCI118708

Harrow, J., Frankish, A., Gonzalez, J. M., Tapanari, E., Diekhans, M., Kokocinski, F., Aken, B. L., Barrell, D., Zadissa, A., Searle, S., Barnes, I., Bignell, A., Boychenko, V., Hunt, T., Kay, M., Mukherjee, G., Rajan, J., Despacio-Reyes, G., Saunders, G., Steward, C., Harte, R., Lin, M., Howald, C., Tanzer, A., Derrien, T., Chrast, J., Walters, N., Balasubramanian, S., Pei, B., Tress, M., Rodriguez, J. M., Ezkurdia, I., van Baren, J., Brent, M., Haussler, D., Kellis, M., Valencia, A., Reymond, A., Gerstein, M., Guigo, R., & Hubbard, T. J. (2012). GENCODE: the reference human genome annotation for The ENCODE Project. *Genome Res, 22*(9), 1760-1774. doi:10.1101/gr.135350.111

Heinze, C., Seniuk, A., Sokolov, M. V., Huebner, A. K., Klementowicz, A. E., Szijarto, I. A., Schleifenbaum, J., Vitzthum, H., Gollasch, M., Ehmke, H., Schroeder, B. C., & Hubner, C. A. (2014). Disruption of vascular Ca2+-activated chloride currents lowers blood pressure. *J Clin Invest, 124*(2), 675-686. doi:10.1172/JCI70025

Huang, F., Zhang, H., Wu, M., Yang, H., Kudo, M., Peters, C. J., Woodruff, P. G., Solberg, O. D., Donne, M. L., Huang, X., Sheppard, D., Fahy, J. V., Wolters, P. J., Hogan, B. L., Finkbeiner, W. E., Li, M., Jan, Y. N., Jan, L. Y., & Rock, J. R. (2012). Calcium-activated chloride channel TMEM16A modulates mucin secretion and airway smooth muscle contraction. *Proc Natl Acad Sci U S A, 109*(40), 16354-16359. doi:10.1073/pnas.1214596109

Hwang, S. J., Basma, N., Sanders, K. M., & Ward, S. M. (2016). Effects of new-generation inhibitors of the calcium-activated chloride channel anoctamin 1 on slow waves in the gastrointestinal tract. *Br J Pharmacol, 173*(8), 1339-1349. doi:10.1111/bph.13431

Janssen, L. J., & Sims, S. M. (1995). Ca(2+)-dependent Cl- current in canine tracheal smooth muscle cells. *Am J Physiol, 269*(1 Pt 1), C163-169.

Jin, X., Shah, S., Liu, Y., Zhang, H., Lees, M., Fu, Z., Lippiat, J. D., Beech, D. J., Sivaprasadarao, A., Baldwin, S. A., Zhang, H., & Gamper, N. (2013). Activation of the Cl- channel ANO1 by localized calcium signals in nociceptive sensory neurons requires coupling with the IP3 receptor. *Sci Signal, 6*(290), ra73. doi:10.1126/scisignal.2004184

Large, W. A., & Wang, Q. (1996). Characteristics and physiological role of the Ca(2+)-activated Cl- conductance in smooth muscle. *Am J Physiol, 271*(2 Pt 1), C435-454.

Lee, B., Cho, H., Jung, J., Yang, Y. D., Yang, D. J., & Oh, U. (2014). Anoctamin 1 contributes to inflammatory and nerve-injury induced hypersensitivity. *Mol Pain, 10*, 5. doi:10.1186/1744-8069-10-5

Lemoine, H., & Overlack, C. (1992). Highly potent beta-2 sympathomimetics convert to less potent partial agonists as relaxants of guinea pig tracheae maximally contracted by carbachol. Comparison of relaxation with receptor binding and adenylate cyclase stimulation. *J Pharmacol Exp Ther, 261*(1), 258-270.

Li, Y., Li, P. K., Roberts, M. J., Arend, R. C., Samant, R. S., & Buchsbaum, D. J. (2014). Multi-targeted therapy of cancer by niclosamide: A new application for an old drug. *Cancer Lett, 349*(1), 8-14. doi:10.1016/j.canlet.2014.04.003

Lin, J., Jiang, Y., Li, L., Liu, Y., Tang, H., & Jiang, D. (2015). TMEM16A mediates the hypersecretion of mucus induced by Interleukin-13. *Exp Cell Res, 334*(2), 260-269. doi:10.1016/j.yexcr.2015.02.026

Liu, S., Feng, J., Luo, J., Yang, P., Brett, T. J., & Hu, H. (2016). Eact, a small molecule activator of TMEM16A, activates TRPV1 and elicits pain- and itch-related behaviours. *Br J Pharmacol, 173*(7), 1208-1218. doi:10.1111/bph.13420

Liu, W., Lu, M., Liu, B., Huang, Y., & Wang, K. (2012). Inhibition of Ca(2+)-activated Cl(-) channel ANO1/TMEM16A expression suppresses tumor growth and invasiveness in human prostate carcinoma. *Cancer Lett, 326*(1), 41-51. doi:10.1016/j.canlet.2012.07.015

Liu, Y., Zhang, H., Huang, D., Qi, J., Xu, J., Gao, H., Du, X., Gamper, N., & Zhang, H. (2015). Characterization of the effects of Cl(-) channel modulators on TMEM16A and bestrophin-1 Ca(2)(+) activated Cl(-) channels. *Pflugers Arch, 467*(7), 1417-1430. doi:10.1007/s00424-014-1572-5

Lu, W., Lin, C., Roberts, M. J., Waud, W. R., Piazza, G. A., & Li, Y. (2011). Niclosamide suppresses cancer cell growth by inducing Wnt co-receptor LRP6 degradation and inhibiting the Wnt/beta-catenin pathway. *PLoS One, 6*(12), e29290. doi:10.1371/journal.pone.0029290

Macielag, M. J., Demers, J. P., Fraga-Spano, S. A., Hlasta, D. J., Johnson, S. G., Kanojia, R. M., Russell, R. K., Sui, Z., Weidner-Wells, M. A., Werblood, H., Foleno, B. D., Goldschmidt, R. M., Loeloff, M. J., Webb, G. C., & Barrett, J. F. (1998). Substituted salicylanilides as inhibitors of two-component regulatory systems in bacteria. *J Med Chem, 41*(16), 2939-2945. doi:10.1021/jm9803572

McGarvey, L. P., Butler, C. A., Stokesberry, S., Polley, L., McQuaid, S., Abdullah, H., Ashraf, S., McGahon, M. K., Curtis, T. M., Arron, J., Choy, D., Warke, T. J., Bradding, P., Ennis, M., Zholos, A., Costello, R. W., & Heaney, L. G. (2014). Increased expression of bronchial epithelial transient receptor potential vanilloid 1 channels in patients with severe asthma. *J Allergy Clin Immunol, 133*(3), 704-712.e704. doi:10.1016/j.jaci.2013.09.016

Mook, R. A., Jr., Wang, J., Ren, X. R., Chen, M., Spasojevic, I., Barak, L. S., Lyerly, H. K., & Chen, W. (2015). Structure-activity studies of Wnt/beta-catenin inhibition in the Niclosamide chemotype: Identification of derivatives with improved drug exposure. *Bioorg Med Chem, 23*(17), 5829-5838. doi:10.1016/j.bmc.2015.07.001

Moore, P. E., Lahiri, T., Laporte, J. D., Church, T., Panettieri, R. A., Jr., & Shore, S. A. (2001). Selected contribution: synergism between TNF-alpha and IL-1 beta in airway smooth muscle cells: implications for beta-adrenergic responsiveness. *J Appl Physiol (1985), 91*(3), 1467-1474.

Moore, W. C., Bleecker, E. R., Curran-Everett, D., Erzurum, S. C., Ameredes, B. T., Bacharier, L., Calhoun, W. J., Castro, M., Chung, K. F., Clark, M. P., Dweik, R. A., Fitzpatrick, A. M., Gaston, B., Hew, M., Hussain, I., Jarjour, N. N., Israel, E., Levy, B. D., Murphy, J. R., Peters, S. P., Teague, W. G., Meyers, D. A., Busse, W. W., Wenzel, S. E., & National Heart, L. B. I. s. S. A. R. P. (2007). Characterization of the severe asthma phenotype by the National Heart, Lung, and Blood

Institute's Severe Asthma Research Program. *J Allergy Clin Immunol, 119*(2), 405-413. doi:10.1016/j.jaci.2006.11.639

Moore, W. C., Meyers, D. A., Wenzel, S. E., Teague, W. G., Li, H., Li, X., D'Agostino, R., Jr., Castro, M., Curran-Everett, D., Fitzpatrick, A. M., Gaston, B., Jarjour, N. N., Sorkness, R., Calhoun, W. J., Chung, K. F., Comhair, S. A., Dweik, R. A., Israel, E., Peters, S. P., Busse, W. W., Erzurum, S. C., Bleecker, E. R., National Heart, L., & Blood Institute's Severe Asthma Research, P. (2010). Identification of asthma phenotypes using cluster analysis in the Severe Asthma Research Program. *Am J Respir Crit Care Med, 181*(4), 315-323. doi:10.1164/rccm.200906-0896OC

Mortazavi, A., Williams, B. A., McCue, K., Schaeffer, L., & Wold, B. (2008). Mapping and quantifying mammalian transcriptomes by RNA-Seq. *Nat Methods, 5*(7), 621-628. doi:10.1038/nmeth.1226

Nakano, T., Inoue, H., Fukuyama, S., Matsumoto, K., Matsumura, M., Tsuda, M., Matsumoto, T., Aizawa, H., & Nakanishi, Y. (2006). Niflumic acid suppresses interleukin-13-induced asthma phenotypes. *Am J Respir Crit Care Med, 173*(11), 1216-1221. doi:10.1164/rccm.200410-1420OC

Namkung, W., Phuan, P. W., & Verkman, A. S. (2011a). TMEM16A inhibitors reveal TMEM16A as a minor component of calcium-activated chloride channel conductance in airway and intestinal epithelial cells. *J Biol Chem, 286*(3), 2365-2374. doi:10.1074/jbc.M110.175109

Namkung, W., Thiagarajah, J. R., Phuan, P. W., & Verkman, A. S. (2010). Inhibition of Ca2+-activated Cl- channels by gallotannins as a possible molecular basis for health benefits of red wine and green tea. *FASEB J, 24*(11), 4178-4186. doi:10.1096/fj.10-160648

Namkung, W., Yao, Z., Finkbeiner, W. E., & Verkman, A. S. (2011b). Small-molecule activators of TMEM16A, a calcium-activated chloride channel, stimulate epithelial chloride secretion and intestinal contraction. *FASEB J, 25*(11), 4048-4062. doi:10.1096/fj.11-191627

Ni, Y. L., Kuan, A. S., & Chen, T. Y. (2014). Activation and inhibition of TMEM16A calcium-activated chloride channels. *PLoS One, 9*(1), e86734. doi:10.1371/journal.pone.0086734

Oh, S. J., Hwang, S. J., Jung, J., Yu, K., Kim, J., Choi, J. Y., Hartzell, H. C., Roh, E. J., & Lee, C. J. (2013). MONNA, a potent and selective blocker for transmembrane protein with unknown function 16/anoctamin-1. *Mol Pharmacol, 84*(5), 726-735. doi:10.1124/mol.113.087502

Osada, T., Chen, M., Yang, X. Y., Spasojevic, I., Vandeusen, J. B., Hsu, D., Clary, B. M., Clay, T. M., Chen, W., Morse, M. A., & Lyerly, H. K. (2011). Antihelminth compound niclosamide downregulates Wnt signaling and elicits antitumor responses in tumors with activating APC mutations. *Cancer Res, 71*(12), 4172-4182. doi:10.1158/0008-5472.CAN-10-3978

Ousingsawat, J., Martins, J. R., Schreiber, R., Rock, J. R., Harfe, B. D., & Kunzelmann, K. (2009). Loss of TMEM16A causes a defect in epithelial Ca2+-dependent chloride transport. *J Biol Chem, 284*(42), 28698-28703. doi:10.1074/jbc.M109.012120

Ousingsawat, J., Mirza, M., Tian, Y., Roussa, E., Schreiber, R., Cook, D. I., & Kunzelmann, K. (2011). Rotavirus toxin NSP4 induces diarrhea by activation of TMEM16A and inhibition of Na+ absorption. *Pflugers Arch, 461*(5), 579-589. doi:10.1007/s00424-011-0947-0

Paulino, C., Kalienkova, V., Lam, A. K. M., Neldner, Y., & Dutzler, R. (2017a). Activation mechanism of the calcium-activated chloride channel TMEM16A revealed by cryo-EM. *Nature*. doi:10.1038/nature24652

Paulino, C., Neldner, Y., Lam, A. K., Kalienkova, V., Brunner, J. D., Schenck, S., & Dutzler, R. (2017b). Structural basis for anion conduction in the calcium-activated chloride channel TMEM16A. *Elife, 6*. doi:10.7554/eLife.26232

Perez-Cornejo, P., Gokhale, A., Duran, C., Cui, Y., Xiao, Q., Hartzell, H. C., & Faundez, V. (2012). Anoctamin 1 (Tmem16A) Ca2+-activated chloride channel stoichiometrically interacts with an ezrin-radixin-moesin network. *Proc Natl Acad Sci U S A, 109*(26), 10376-10381. doi:10.1073/pnas.1200174109

Peters, C. J., Yu, H., Tien, J., Jan, Y. N., Li, M., & Jan, L. Y. (2015). Four basic residues critical for the ion selectivity and pore blocker sensitivity of TMEM16A calcium-activated chloride channels. *Proc Natl Acad Sci U S A, 112*(11), 3547-3552. doi:10.1073/pnas.1502291112

Pineda-Farias, J. B., Barragan-Iglesias, P., Loeza-Alcocer, E., Torres-Lopez, J. E., Rocha-Gonzalez, H. I., Perez-Severiano, F., Delgado-Lezama, R., & Granados-Soto, V. (2015). Role of anoctamin-1 and bestrophin-1 in spinal nerve ligation-induced neuropathic pain in rats. *Mol Pain, 11*, 41. doi:10.1186/s12990-015-0042-1

Piper, A. S., Greenwood, I. A., & Large, W. A. (2002). Dual effect of blocking agents on Ca2+-activated Cl(-) currents in rabbit pulmonary artery smooth muscle cells. *J Physiol, 539*(Pt 1), 119-131.

Qin, Y., Jiang, Y., Sheikh, A. S., Shen, S., Liu, J., & Jiang, D. (2016). Interleukin-13 stimulates MUC5AC expression via a STAT6-TMEM16A-ERK1/2 pathway in human airway epithelial cells. *Int Immunopharmacol, 40*, 106-114. doi:10.1016/j.intimp.2016.08.033

Rapetti-Mauss, R., Bustos, V., Thomas, W., McBryan, J., Harvey, H., Lajczak, N., Madden, S. F., Pellissier, B., Borgese, F., Soriani, O., & Harvey, B. J. (2017). Bidirectional KCNQ1:beta-catenin interaction drives colorectal cancer cell differentiation. *Proc Natl Acad Sci U S A*. doi:10.1073/pnas.1702913114

Robinett, K. S., Koziol-White, C. J., Akoluk, A., An, S. S., Panettieri, R. A., Jr., & Liggett, S. B. (2014). Bitter taste receptor function in asthmatic and nonasthmatic human airway smooth muscle cells. *Am J Respir Cell Mol Biol, 50*(4), 678-683. doi:10.1165/rcmb.2013-0439RC

Robinson, M. D., & Oshlack, A. (2010). A scaling normalization method for differential expression analysis of RNA-seq data. *Genome Biol, 11*(3), R25. doi:10.1186/gb-2010-11-3-r25

Rossignol, J. F. (2014). Nitazoxanide: a first-in-class broad-spectrum antiviral agent. *Antiviral Res, 110*, 94-103. doi:10.1016/j.antiviral.2014.07.014

Rossignol, J. F., Abu-Zekry, M., Hussein, A., & Santoro, M. G. (2006). Effect of nitazoxanide for treatment of severe rotavirus diarrhoea: randomised double-blind placebo-controlled trial. *Lancet, 368*(9530), 124-129. doi:10.1016/S0140-6736(06)68852-1

Schreiber, R., Faria, D., Skryabin, B. V., Wanitchakool, P., Rock, J. R., & Kunzelmann, K. (2015). Anoctamins support calcium-dependent chloride secretion by facilitating calcium signaling in adult mouse intestine. *Pflugers Arch, 467*(6), 1203-1213. doi:10.1007/s00424-014-1559-2

Schroeder, B. C., Cheng, T., Jan, Y. N., & Jan, L. Y. (2008). Expression cloning of TMEM16A as a calcium-activated chloride channel subunit. *Cell, 134*(6), 1019-1029. doi:10.1016/j.cell.2008.09.003

Scudieri, P., Caci, E., Bruno, S., Ferrera, L., Schiavon, M., Sondo, E., Tomati, V., Gianotti, A., Zegarra-Moran, O., Pedemonte, N., Rea, F., Ravazzolo, R., & Galietta, L. J. (2012). Association of TMEM16A chloride channel overexpression with airway goblet cell metaplasia. *J Physiol, 590*(23), 6141-6155. doi:10.1113/jphysiol.2012.240838

Senkowski, W., Zhang, X., Olofsson, M. H., Isacson, R., Hoglund, U., Gustafsson, M., Nygren, P., Linder, S., Larsson, R., & Fryknas, M. (2015). Three-Dimensional Cell Culture-Based Screening Identifies the Anthelmintic Drug Nitazoxanide as a Candidate for Treatment of Colorectal Cancer. *Mol Cancer Ther, 14*(6), 1504-1516. doi:10.1158/1535-7163.MCT-14-0792

Shore, S. A., Laporte, J., Hall, I. P., Hardy, E., & Panettieri, R. A., Jr. (1997). Effect of IL-1 beta on responses of cultured human airway smooth muscle cells to bronchodilator agonists. *Am J Respir Cell Mol Biol, 16*(6), 702-712. doi:10.1165/ajrcmb.16.6.9191472

Sondo, E., Caci, E., & Galietta, L. J. (2014). The TMEM16A chloride channel as an alternative therapeutic target in cystic fibrosis. *Int J Biochem Cell Biol, 52*, 73-76. doi:10.1016/j.biocel.2014.03.022

Takayama, Y., Uta, D., Furue, H., & Tominaga, M. (2015). Pain-enhancing mechanism through interaction between TRPV1 and anoctamin 1 in sensory neurons. *Proc Natl Acad Sci U S A, 112*(16), 5213-5218. doi:10.1073/pnas.1421507112

Thiagarajah, J. R., Donowitz, M., & Verkman, A. S. (2015). Secretory diarrhoea: mechanisms and emerging therapies. *Nat Rev Gastroenterol Hepatol, 12*(8), 446-457. doi:10.1038/nrgastro.2015.111

Trian, T., Burgess, J. K., Niimi, K., Moir, L. M., Ge, Q., Berger, P., Liggett, S. B., Black, J. L., & Oliver, B. G. (2011). beta2-Agonist induced cAMP is decreased in asthmatic airway smooth muscle due to increased PDE4D. *PLoS One, 6*(5), e20000. doi:10.1371/journal.pone.0020000

Wang, H., Zou, L., Ma, K., Yu, J., Wu, H., Wei, M., & Xiao, Q. (2017). Cell-specific mechanisms of TMEM16A Ca2+-activated chloride channel in cancer. *Mol Cancer, 16*(1), 152. doi:10.1186/s12943-017-0720-x

Wang, Q., Leo, M. D., Narayanan, D., Kuruvilla, K. P., & Jaggar, J. H. (2016). Local coupling of TRPC6 to ANO1/TMEM16A channels in smooth muscle cells amplifies vasoconstriction in cerebral arteries. *Am J Physiol Cell Physiol, 310*(11), C1001-1009. doi:10.1152/ajpcell.00092.2016

Wang, Y. X., & Kotlikoff, M. I. (1997). Inactivation of calcium-activated chloride channels in smooth muscle by calcium/calmodulin-dependent protein kinase. *Proc Natl Acad Sci U S A, 94*(26), 14918-14923.

Wellman, G. C., & Nelson, M. T. (2003). Signaling between SR and plasmalemma in smooth muscle: sparks and the activation of Ca2+-sensitive ion channels. *Cell Calcium, 34*(3), 211-229.

WHO. (2015). The Selection and Use of Essential Medicines. *World Health Organ Tech Rep Ser*(994), vii-xv, 1-546.

Yang, Y. D., Cho, H., Koo, J. Y., Tak, M. H., Cho, Y., Shim, W. S., Park, S. P., Lee, J., Lee, B., Kim, B. M., Raouf, R., Shin, Y. K., & Oh, U. (2008). TMEM16A confers receptor-activated calcium-dependent chloride conductance. *Nature, 455*(7217), 1210-1215. doi:10.1038/nature07313

Yim, P. D., Gallos, G., Perez-Zoghbi, J. F., Trice, J., Zhang, Y., Siviski, M., Sonett, J., & Emala, C. W., Sr. (2013). Chloride channel blockers promote relaxation of TEA-induced contraction in airway smooth muscle. *J Smooth Muscle Res, 49*, 112-124.

Yocum, G. T., Chen, J., Choi, C. H., Townsend, E. A., Zhang, Y., Xu, D., Fu, X. W., Sanderson, M. J., & Emala, C. W. (2017). Role of transient receptor potential vanilloid 1 in the modulation of airway smooth muscle tone and calcium handling. *Am J Physiol Lung Cell Mol Physiol, 312*(6), L812-l821. doi:10.1152/ajplung.00064.2017

Zhang, C. H., Li, Y., Zhao, W., Lifshitz, L. M., Li, H., Harfe, B. D., Zhu, M. S., & ZhuGe, R. (2013). The transmembrane protein 16A Ca(2+)-activated Cl- channel in airway smooth muscle contributes to airway hyperresponsiveness. *Am J Respir Crit Care Med, 187*(4), 374-381. doi:10.1164/rccm.201207-1303OC

Zhang, Y., Wang, X., Wang, H., Jiao, J., Li, Y., Fan, E., Zhang, L., & Bachert, C. (2015). TMEM16A-Mediated Mucin Secretion in IL-13-Induced Nasal Epithelial Cells From Chronic Rhinosinusitis Patients. *Allergy Asthma Immunol Res, 7*(4), 367-375. doi:10.4168/aair.2015.7.4.367

Zhuge, R., Bao, R., Fogarty, K. E., & Lifshitz, L. M. (2010). Ca2+ sparks act as potent regulators of excitation-contraction coupling in airway smooth muscle. *J Biol Chem, 285*(3), 2203-2210. doi:10.1074/jbc.M109.067546

HTS	Small molecule hits	Cell line	Assay modality	Test cmpd. incubation/ stimulation	Hit cut-off	S/B	Avg. RZ/RZ'
Small molecule library	581,849						
Primary (n=1, 5µM final)	1,445	HEK293T:eYFP:TMEM16A(abc)	FI eYFP	30 min, 10µM@RT/ 10mM Iodide, 2µM ionomycin (final)	POC <72.6%	6.5	0.83 / 0.83
Confirmation (n=3, 5µM final)	673	HEK293T:eYFP:TMEM16A(abc)	FI eYFP	same as above	POC <72.6%	6.5	0.76 / 0.80
Validation molecule autofluorescence (n=1, 5µM final)	491	HEK293T:eYFP:TMEM16A(abc)	FI	30 min, 10µM@RT	Baseline FI <10x STDV of neutral control	n.a.	n.a.
Validation dose response intracellular $[Ca^{2+}]\downarrow$ 22-step, 1:2 dilution	328	HEK293T	FI Calcium 6	45 min, 10µM@RT/ 1µM ionomycin (final)	IC50 >10µM	29.5	0.74 / 0.81
Dose response 22-step, 1:2 dilution	145	HEK293T:eYFP:TMEM16A(abc)	FI eYFP	30 min [2x]@RT/ 10mM Iodide, 2µM ionomycin (final)	IC50 <5µM	6.2	0.76 / 0.79
Quality control	130		Mass spec.	n.a.	50% purity correct mass	n.a.	n.a.

Figure 1_Supplementary Figure 1. High-throughput-screening for TMEM16A antagonists and hit triaging.

Figure 1_Figure Supplement 1. High-throughput-screening for TMEM16A antagonists and hit triaging. High-throughput-screening of a small molecule library for TMEM16A antagonists using the halide-sensitive YFP (eYFP) assay was conducted in a fully automated and scheduled setup. The eYFP assay allows identification of TMEM16A inhibitors by measuring TMEM16A-dependent quenching of eYFP fluorescence intensity (FI). Cells were incubated with the test compound before the assay was started by addition of trigger solution containing Ionomycin and iodide ions. Ionomycin triggers the Ca2+-dependent activation of TMEM16A, which allows iodide ions to enter the cell and quench eYFP fluorescence intensity. Assay results were normalized based on the benchmark TMEM16A inhibitor benzbromarone (100% inhibition corresponding to 0% TMEM16A activity) and neutral control (0% inhibition corresponding to 100% TMEM16A activity) and reported as percent-of-control (POC). Hit cut-off is a statistical value that was calculated based on the results of all test wells. Compounds providing >27.4% inhibition corresponding to <72.6% POC TMEM16A activity were called hits. Statistical quality control parameters such RZ-factor and RZ'-factor and signal/background ratio (S/B) were determined throughout the HTS campaign. During primary screening the entire library was tested at a single concentration and yielded 1,445 primary hits. Confirmation screening tested all primary hits again in three independent, consecutive runs and delivered 673 confirmed hits. Auto-fluorescent compounds were eliminated based on the baseline fluorescence intensity recorded prior to addition of trigger solution and resulted in 491 non-fluorescent hits. These hits were next tested in dose response assays at 22 concentrations in calcium flux assays. This eliminated false-positive TMEM16A antagonists that inhibited Ionomycin-dependent increase of intracellular calcium concentration. Dose response testing of the remaining hits revealed 145 hits with an IC50<5 M and finally 130 validated hits, which passed quality control by mass spec analysis.

Further details are provided in the materials and methods section.

A. RZ'-factor and signal distribution per plate over entire HTS campaign

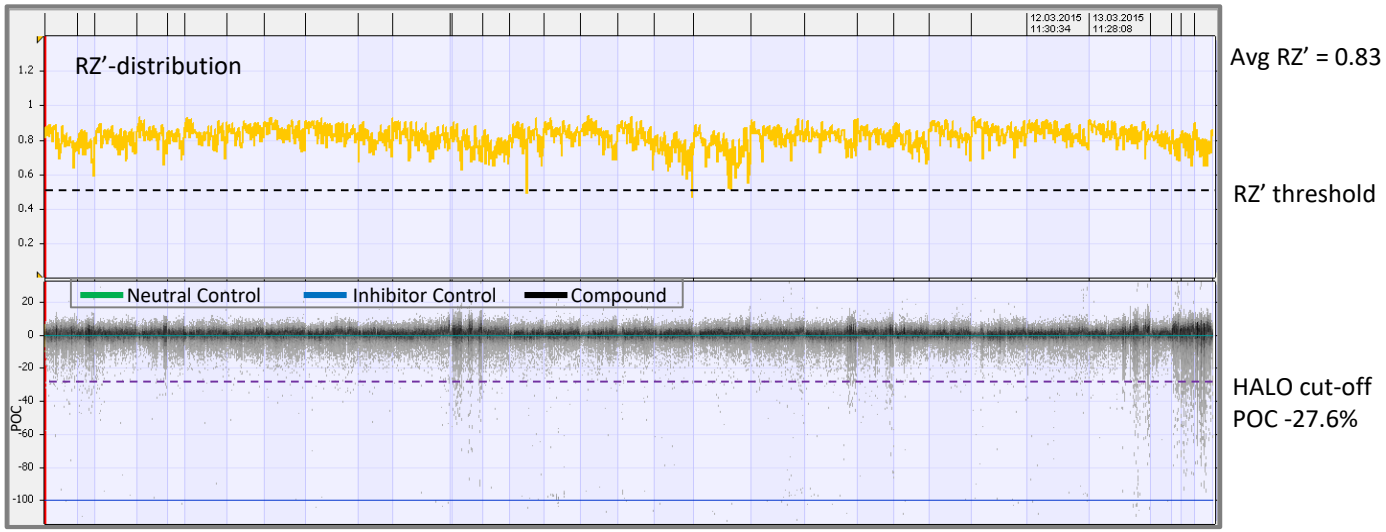

B. Average HTS quality control metrics

Avg	S/B	Z' Factor	RZ' Factor	Z Factor	RZ Factor
HTS	6.5	0.76	0.83	0.74	0.83

Figure 1_Supplementary Figure 2. Signal distribution and quality control metrics of the TMEM16A HTS campaign.
Data analysis of the entire HTS campaign was performed using Genedata Screener. (**A.**) RZ'-factor and signal distribution per plate over entire HTS campaign. RZ'-factor was calculated per plate and is plotted per plate over the entire HTS campaign (top panel). Average RZ' was 0.83 and RZ' threshold was set at 0.5. Normalization of library compound activities was based on neutral control (0% inhibition) and on TMEM16A inhibitor control Benzbromarone (-100% inhibition) are are plotted as percent-of-control (POC)(bottom panel). Unbiased hit threshold is given as HALO (Hit Assessment and Lead Optimization) cut-off, which was calculated as Median+3xIQR+20% of all test wells. (**B.**) Average HTS quality control metrics. Statistical quality control parameters such Z-factor, Z'-factor, RZ-factor, RZ'-factor and signal/background ratio (S/B) were determined throughout the HTS campaign and are summarized as average values.

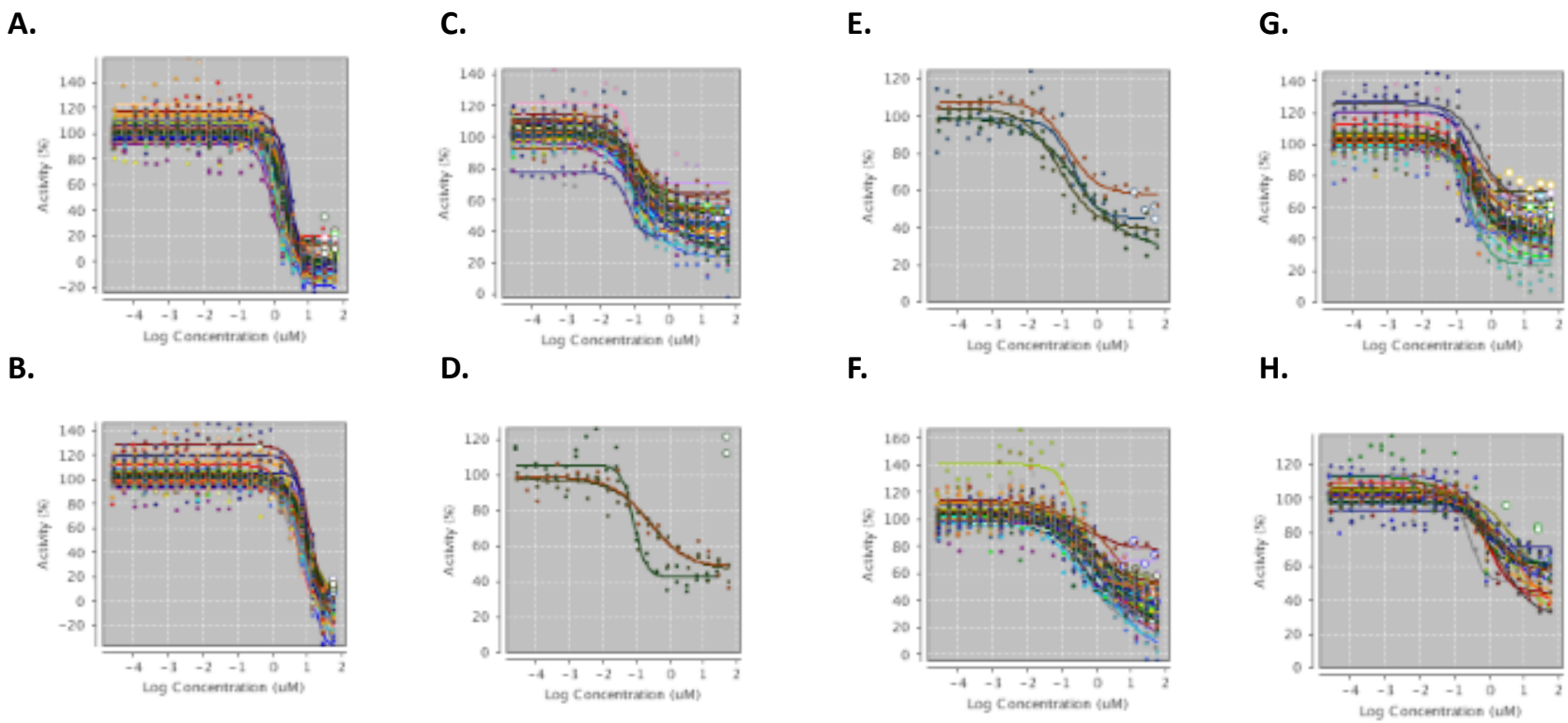

Figure 1_Supplementary Figure 3. Composite dose-response data of compound impact in blocking ionomycin-induced TMEM16A (abc) eYFP quenching, where iodide was used as the permeant anion. Shown are the results of separate experiments run on differing days. Benzbromarone (**A**) and CaCCinh-A01 (**B**) fully blocked the iodide eYFP response, with IC_{50} (μM) of 1.5081 ± .504 (n=58) and 8.125 ± 2.72 (n=58), while niclosamide (**C**), Cpds 2-5 (**D-G**) and the benchmark TMEM16A antagonist 1PBC (**H**) showed potent but partial block of the ionomycin-induced eYFP response with IC_{50} (μM) values of 0.13208 ± 0.0671 (n=42), 0.19643 ± 0.105 (n=3), 0.184 ± 0.0891 (n=4), 0.95369 ± 0.648 (n=54), 0.36967 ± 0.131 (n=42) and 1.5233 ± 1.36 (n=17), respectively. Activity (%) is the same as Percent of Control (POC), where 100% is no block of the ionomycin-induced iodide quenching of the TMEM16A eYFP response, while 0% is full inhibition of the TMEM16A halide sensitive YFP response.

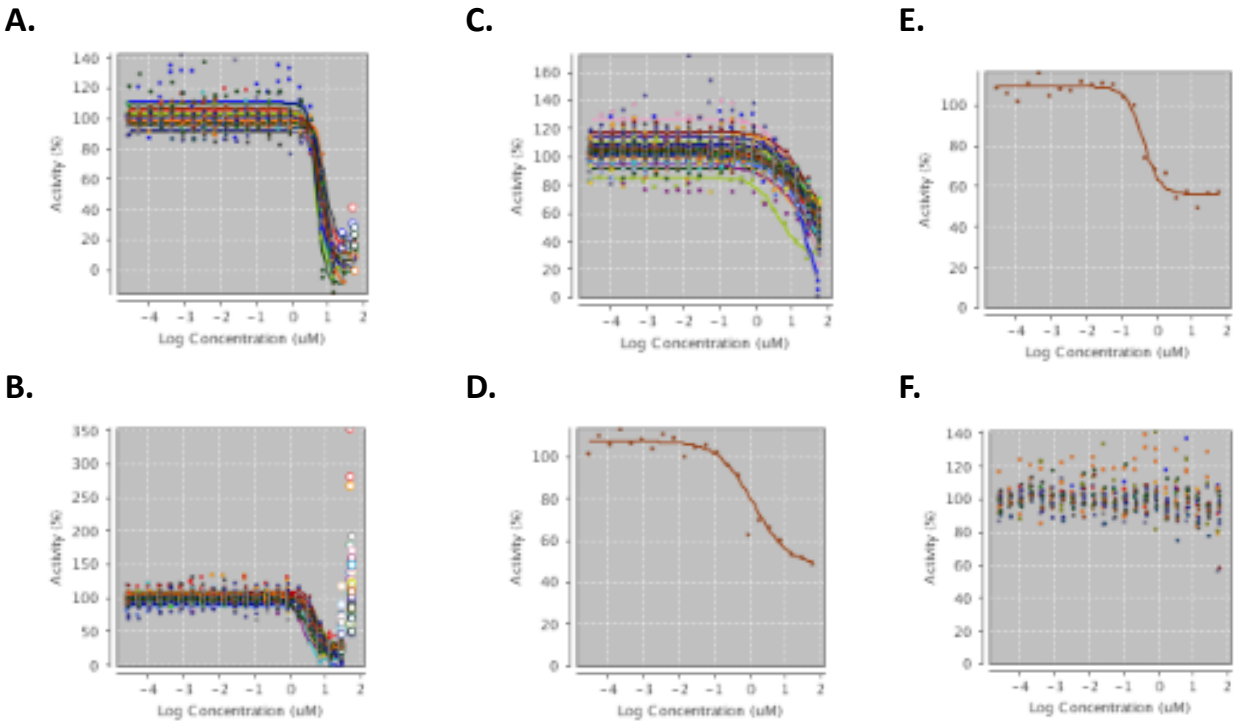

Figure 1_Supplementary Figure 4. Composite dose-response data of compound impact in blocking ionomycin-induced TMEM16A (abc) eYFP quenching, where iodide was used as the permeant anion. Shown are the results of separate experiments run on differing days with maximum concentration being 55.6 μM. MONNA (**A**) and dichlorophen (**B**) fully blocked the iodide eYFP response, with IC_{50} (μM) of 6.2947 ± 1.47 (n=19) and 4.3647 ± 1.21 (n=58), while niflumic acid (**C**) showed weak activity and IC_{50} (μM) of 26.57 ± 11.8 (n=55). Nitazoxanide (**D**) and its metabolic product tizoxanide (**E**) showed potent, but partial inhibition with IC_{50} values (μM) of 1.23 (n=1, t=1) and 0.398 (n=1). The benchmark TMEM16A antagonist, T16Ainh-A01 (**F**), was inactive (IC_{50} > 55.6 μM, n= 16) in blocking the ionomycin-induced eYFP response. We were also unable to show activity of this compound by QPatch electrophysiology using HEK293/TMEM16A cells and elevated intracellular calcium (Table 1), while all the other compounds were confirmed active in this ephys assay. The loss of dichlorophen activity at the highest doses is most likely due to poor compound solubility at these higher doses. Activity (%) is the same as Percent of Control (POC), where 100% is no block of the ionomycin-induced iodide quenching of the TMEM16A eYFP response, while 0% is full inhibition of the TMEM16A halide sensitive YFP response.

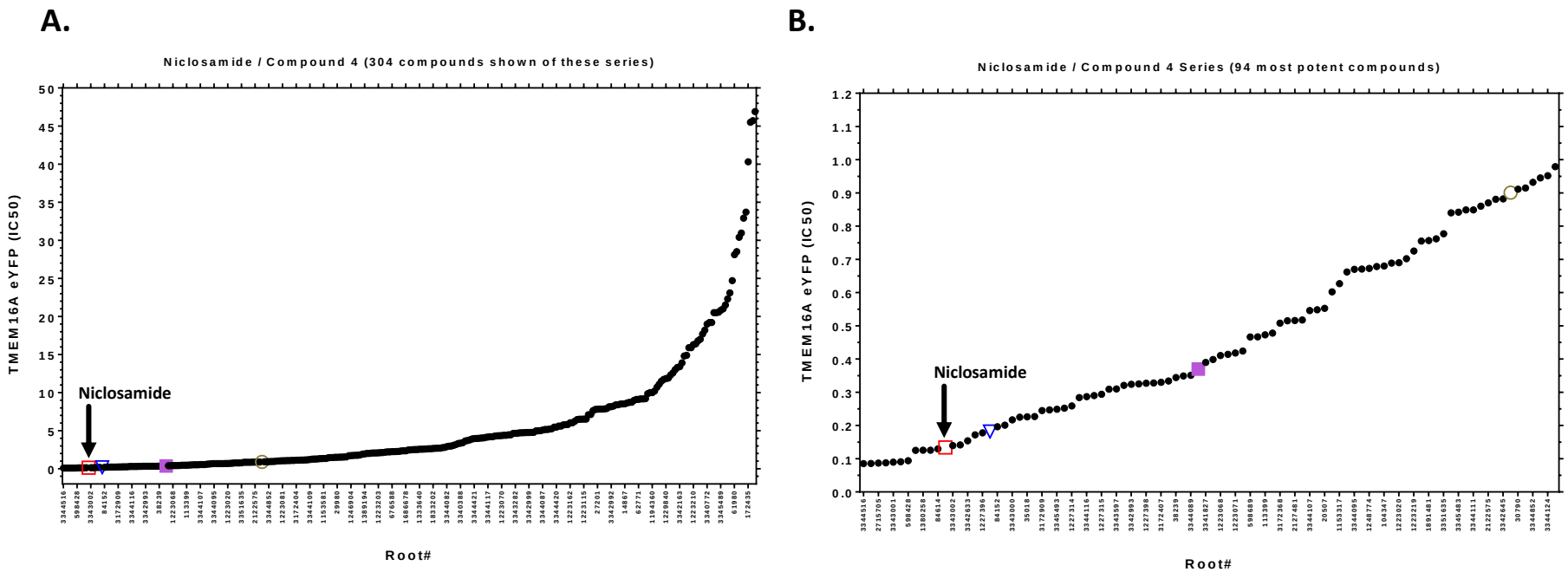

Figure 1_Supplementary Figure 5. Distribution of potency of Niclosamide related compounds in the TMEM16A halide-sensitive YFP assay. A total of 304 distinct compounds from the niclosamide and Cpd 4 series had IC_{50} < 50 μM (**A**) , with the 94 most potent compounds provided in (**B**). An additional 78 compounds aren't displayed as they were considered inactive having an IC_{50} > 50 μM. The compound identification number (root#) is listed on x-axis versus the potency (IC_{50}, μM) on y-axis. It should be noted due to the large number of compounds shown, the x-axis only provides a subset of the root identification numbers that are plotted. The location of niclosamide (Cpd 1) (red, open square), Cpd 2 (blue, open triangle), Cpd 3 (84152 label on x-axis), Cpd 4 (brown, open circle) and Cpd 5 (purple, solid square) are shown in the plots.

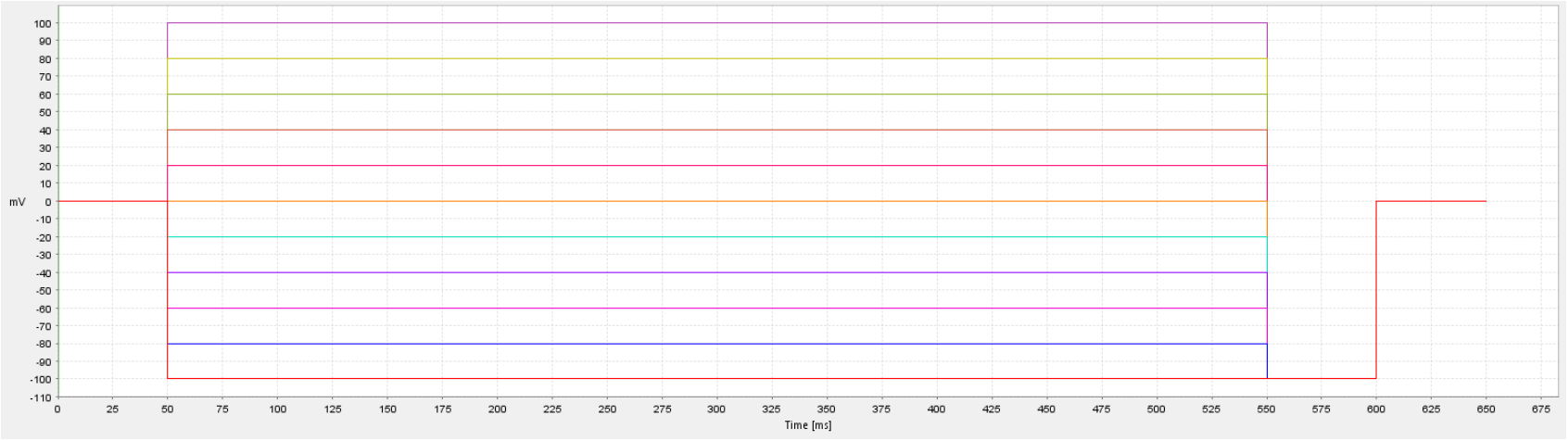

Figure 1_Supplementary Figure 6. Voltage protocol for measuring impact of compounds on TMEM16A (acd) in HEK293 cells by QPatch electrophysiology. A holding potential at 0 mV was used on 48 well single hole patch plates. A standardized current-voltage (IV) protocol was as follows: 500 ms +20 mV steps from -100 mV to +100 mV with a step to -100 mV after each pulse for 50 ms to obtain tail currents. Further details on recording conditions are provided in the Material and Methods section.

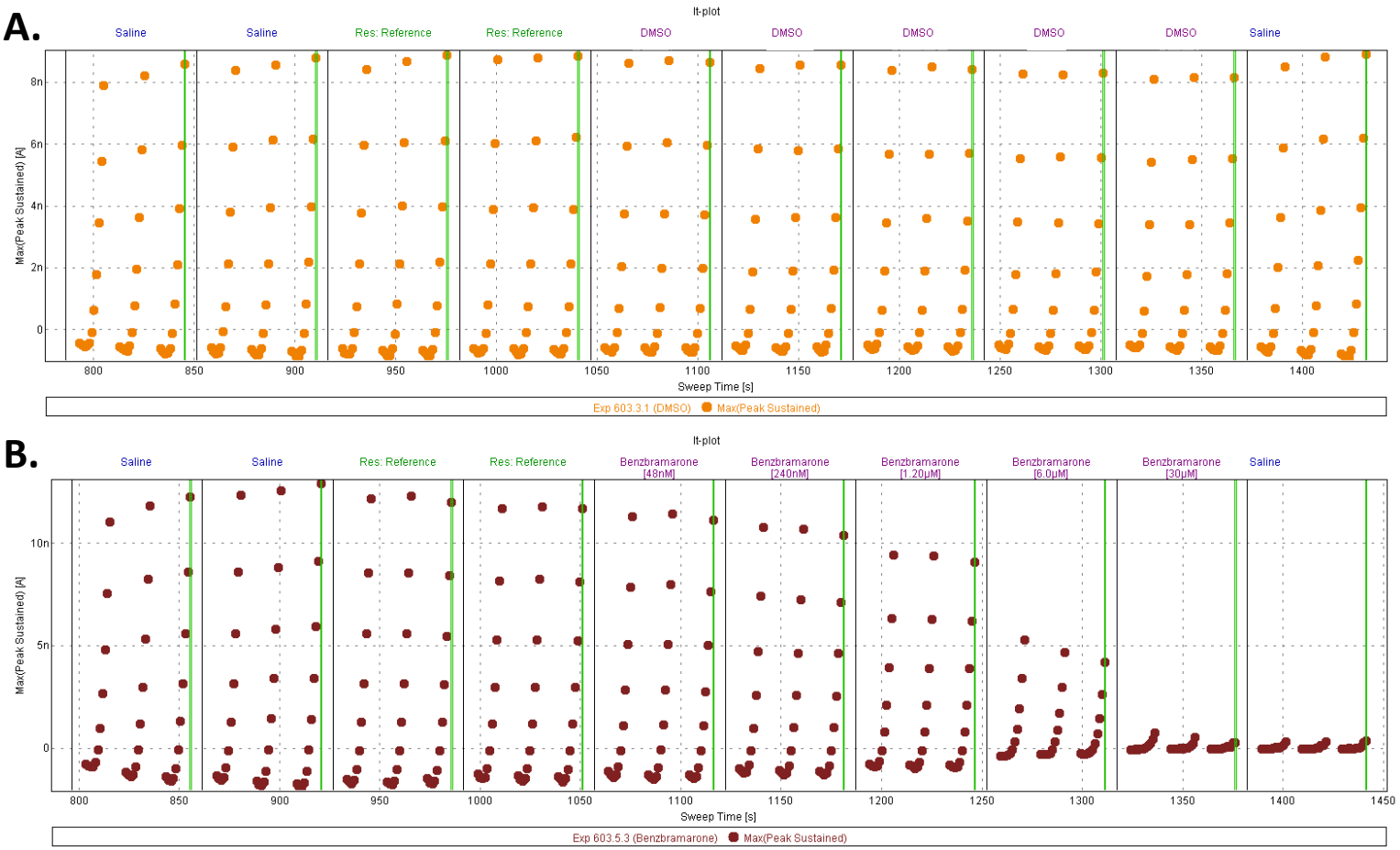

Figure 1_Supplementary Figure 7. Representative TMEM16A (acd) raw traces showing current (nA) versus time (second) plots using the QPatch ephys protocol described in Figure 1_Supplementary Figure 6. For each treatment (saline, reference – vehicle control, DMSO or compound) three I/V protocols were run from -100 to +100 mV (20 mV steps). The current is stable over the 1450s time frame shown, unaffected by repeat additions of the 0.3% DMSO vehicle (**A**), but suppressed by increasing concentrations of benzbromarone (**B**).

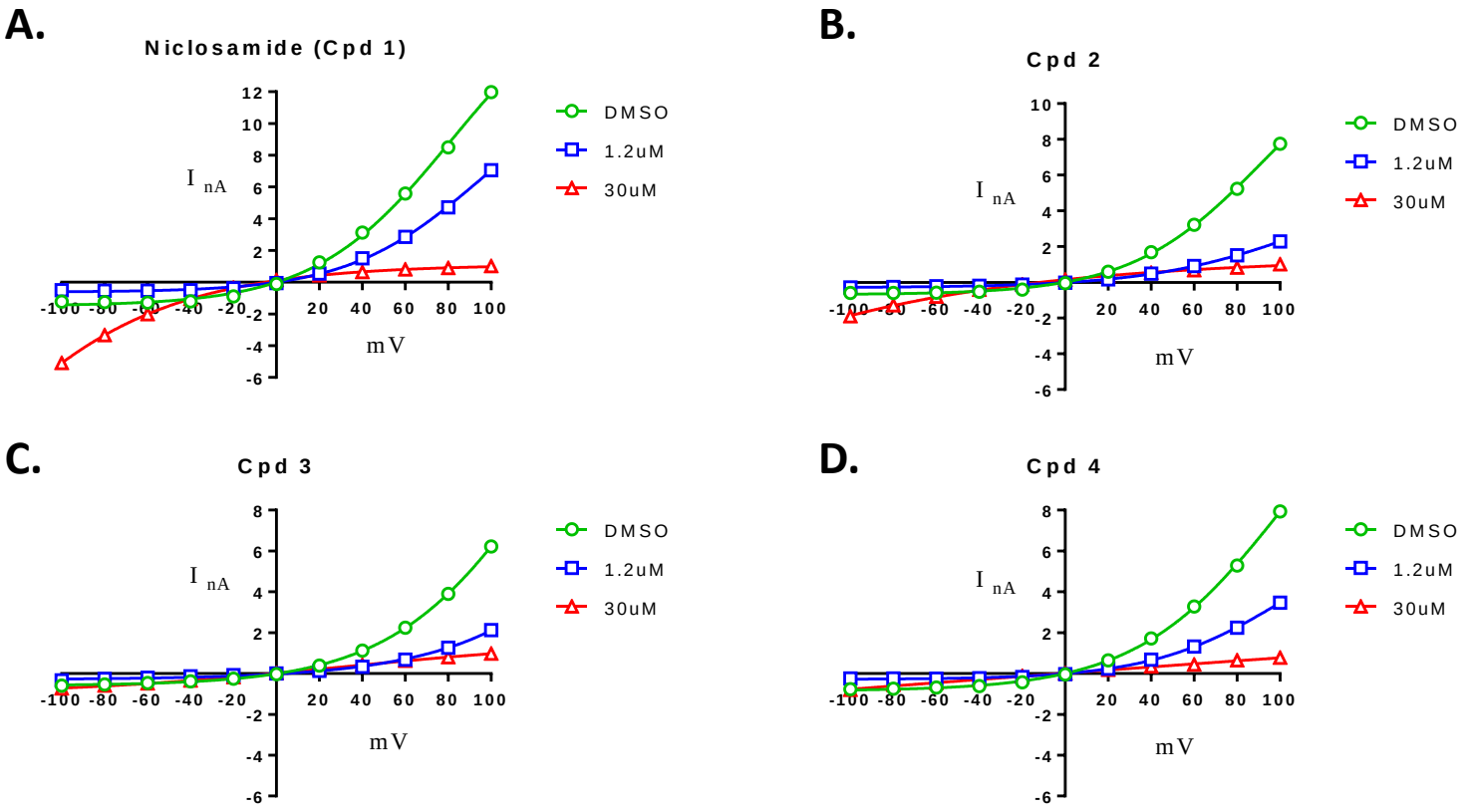

Figure 1_Supplementary Figure 8. HEK293 / TMEM16A (acd) QPatch electrophysiology assay using 170 nM free $[Ca^{2+}]_i$. Representative I/V traces of Niclosamide (Cpd 1) and related compounds, Cpds 2-4, are shown in panels **A-D**, respectively.

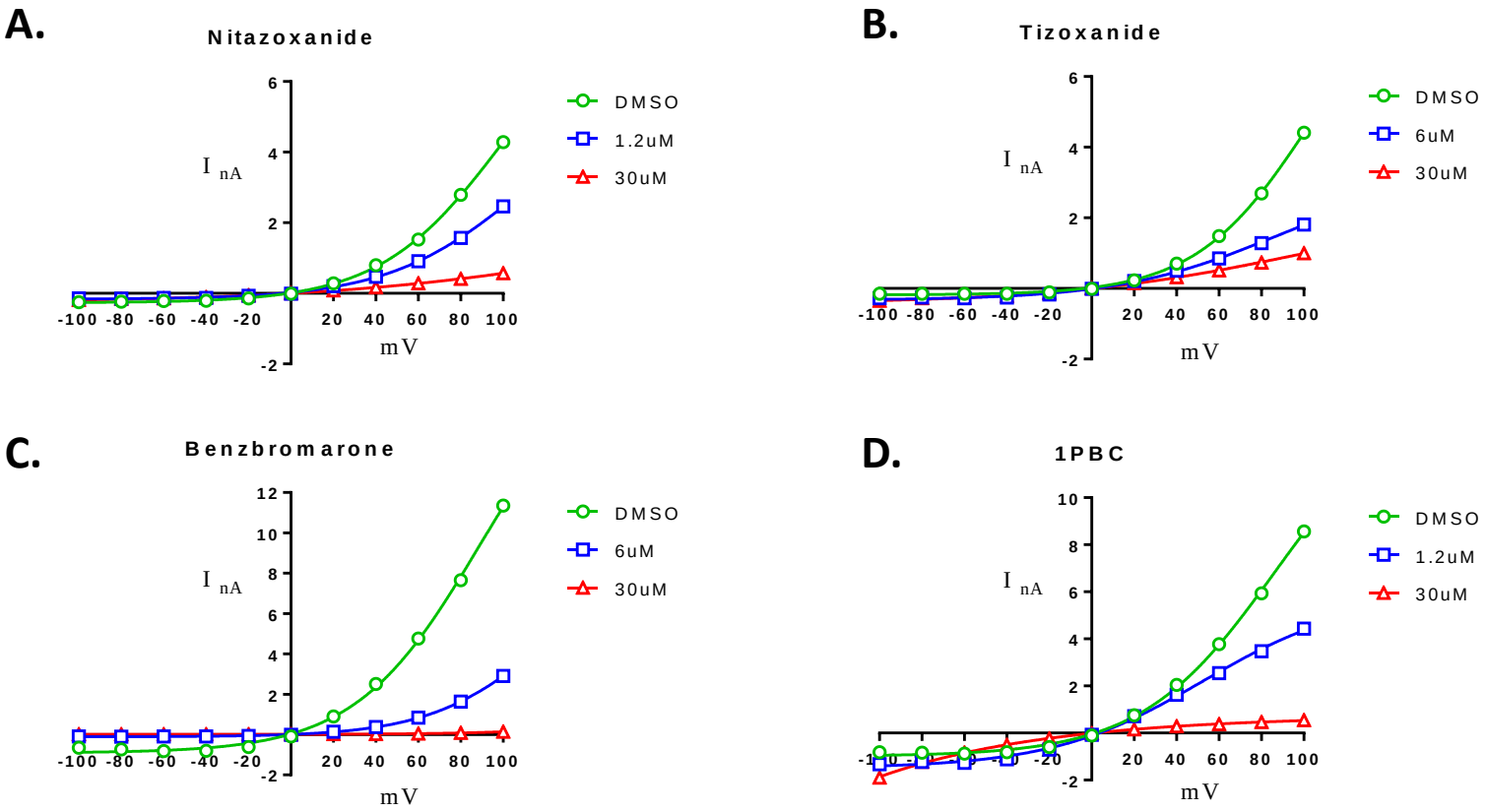

Figure 1_Supplementary Figure 9. HEK293 / TMEM16A (acd) QPatch assay using 170 nM free $[Ca^{2+}]_i$. Representative I/V traces of nitazoxanide (**A**), tizoxanide (**B**) and the TMEM16A benchmark antagonists benzbromarone (**C**) and 1PBC (**D**) are shown.

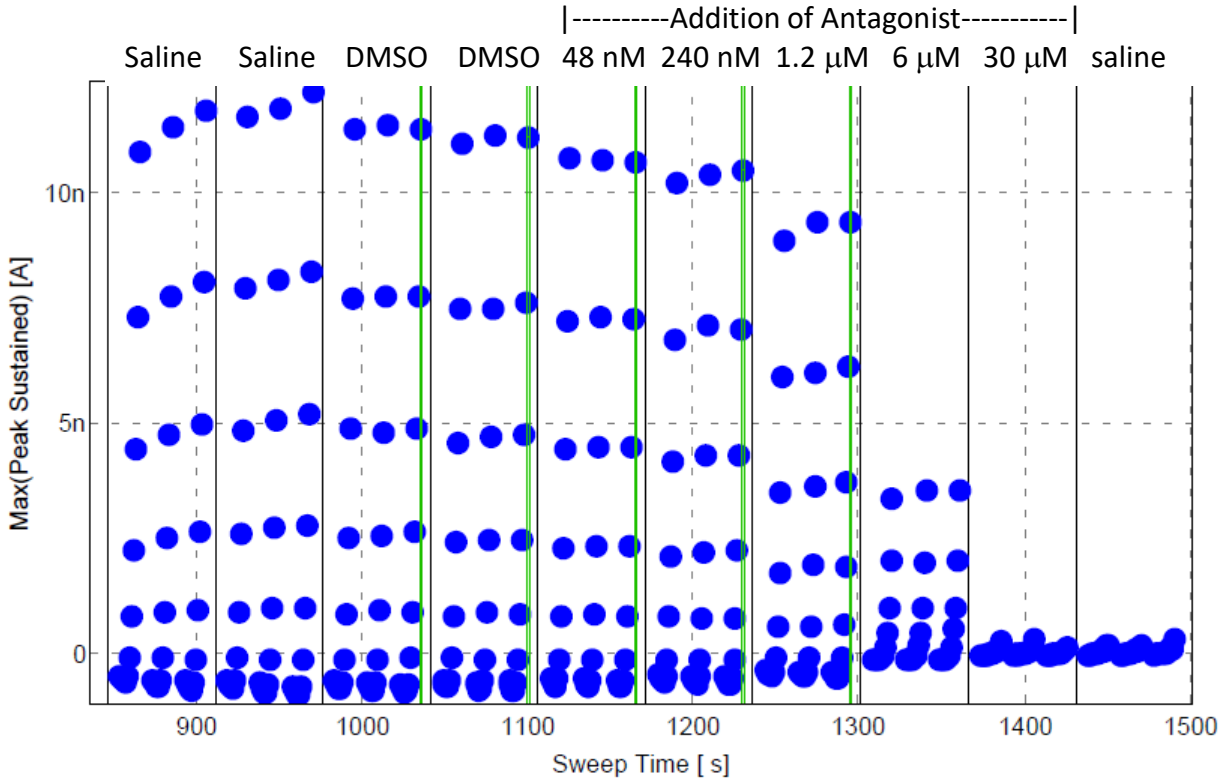

Figure 2_Supplementary Figure 1. Impact of benzbromarone on TMEM16A (acd) calcium-activated chloride currents as measured by QPatch electrophysiology. Shown is a representative recording of the impact of progressive (5-fold) increases of benzbromarone on the TMEM16A current-voltage response.

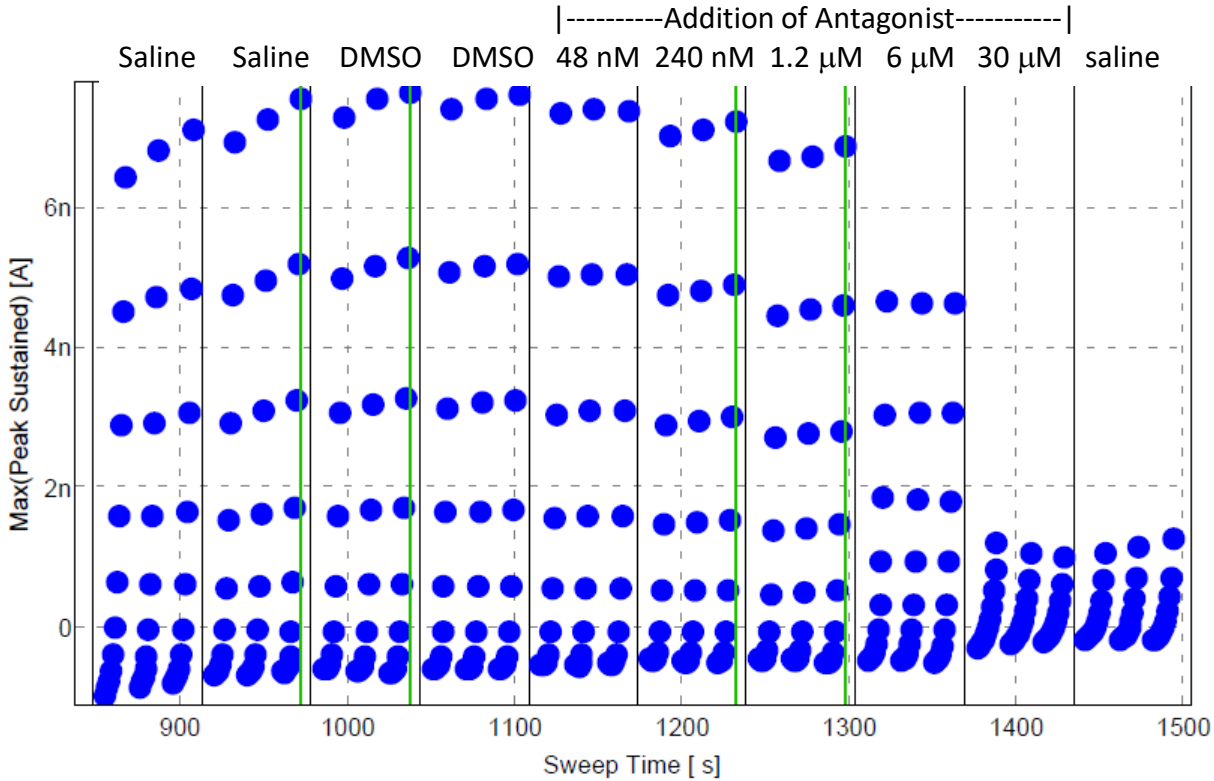

Figure 2_Supplementary Figure 2. Impact of CaCCinh-A01 on TMEM16A (acd) calcium-activated chloride currents as measured by QPatch electrophysiology. Shown is a representative recording of the impact of progressive (5-fold) increases of CaCCinh-A01 on the TMEM16A current-voltage response.

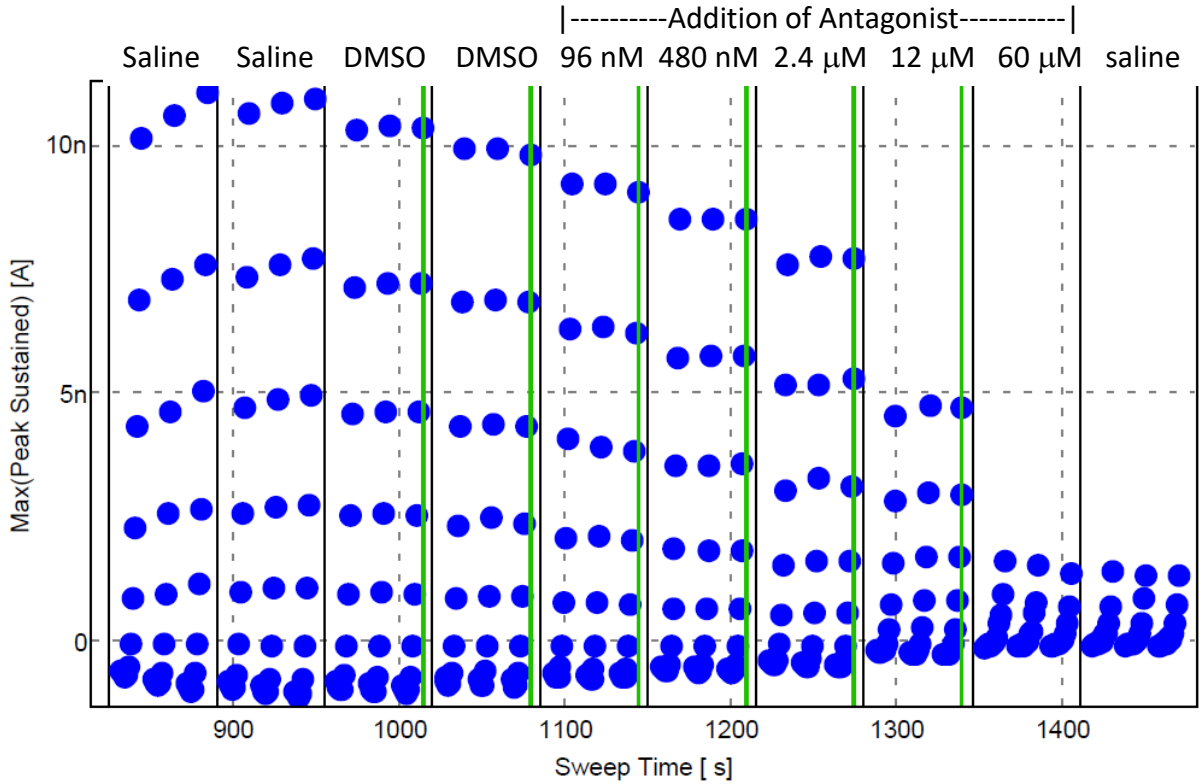

Figure 2_Supplementary Figure 3. Impact of MONNA on TMEM16A (acd) calcium-activated chloride currents as measured by QPatch electrophysiology. Shown is a representative recording of the impact of progressive (5-fold) increases of MONNA on the TMEM16A current-voltage response.

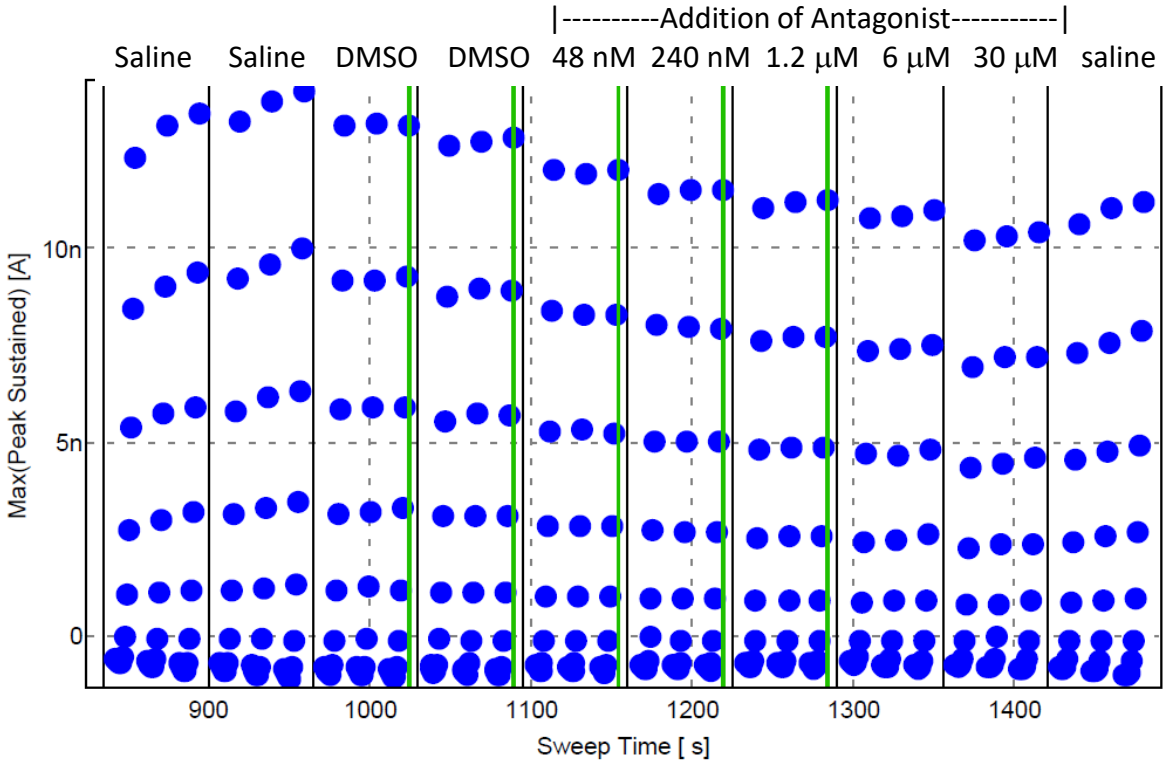

Figure 2_Supplementary Figure 4. Impact of T16Ainh-A01 on TMEM16A (acd) calcium-activated chloride currents as measured by QPatch electrophysiology. Shown is a representative recording of the impact of progressive (5-fold) increases of T16Ainh-A01 on the TMEM16A current-voltage response.

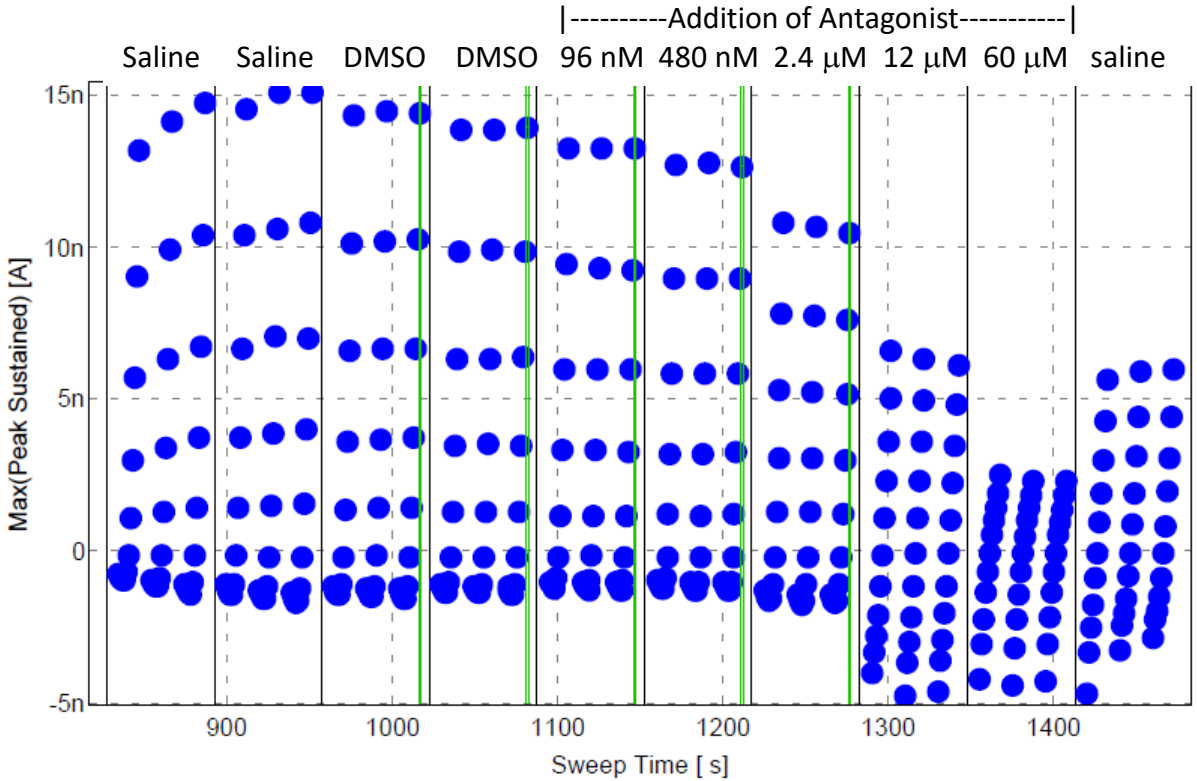

Figure 2_Supplementary Figure 5. Impact of niflumic acid on TMEM16A (acd) calcium-activated chloride currents as measured by QPatch electrophysiology. Shown is a representative recording of the impact of progressive (5-fold) increases of niflumic acid on the TMEM16A current-voltage response.

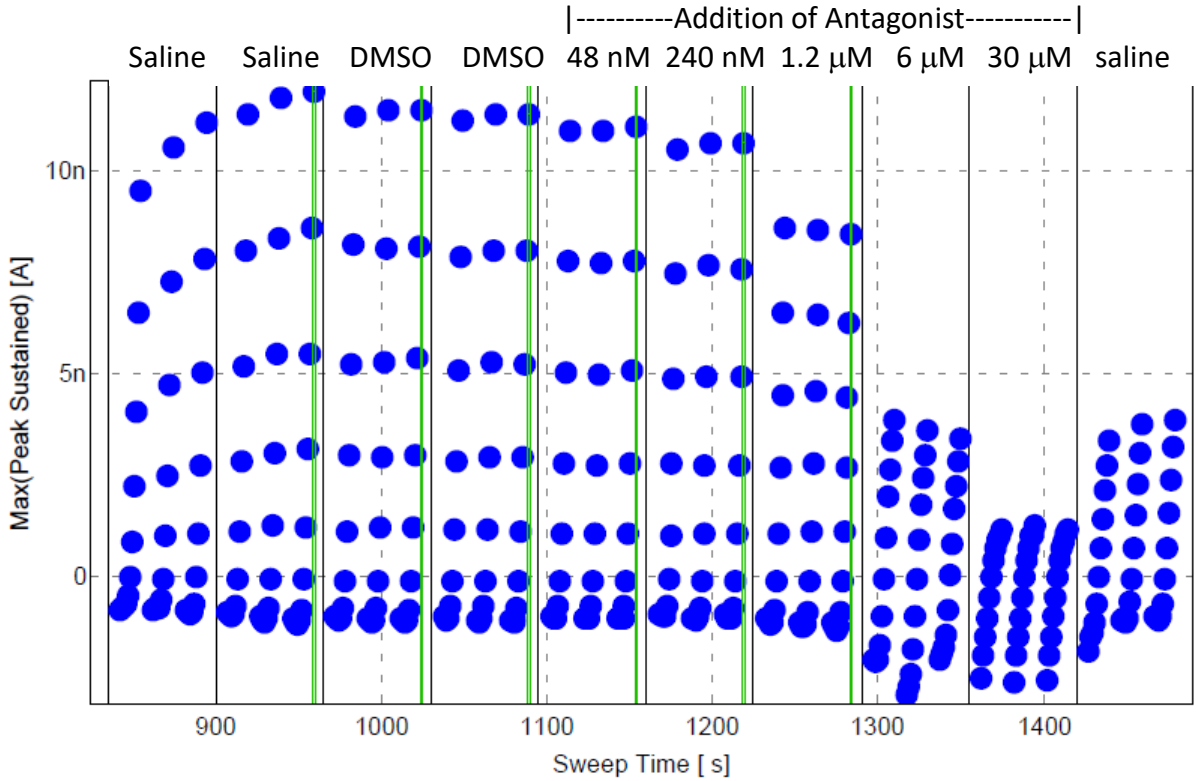

Figure 2_Supplementary Figure 6. Impact of 1PBC on TMEM16A (acd) calcium-activated chloride currents as measured by QPatch electrophysiology. Shown is a representative recording of the impact of progressive (5-fold) increases of 1PBC on the TMEM16A current-voltage response.

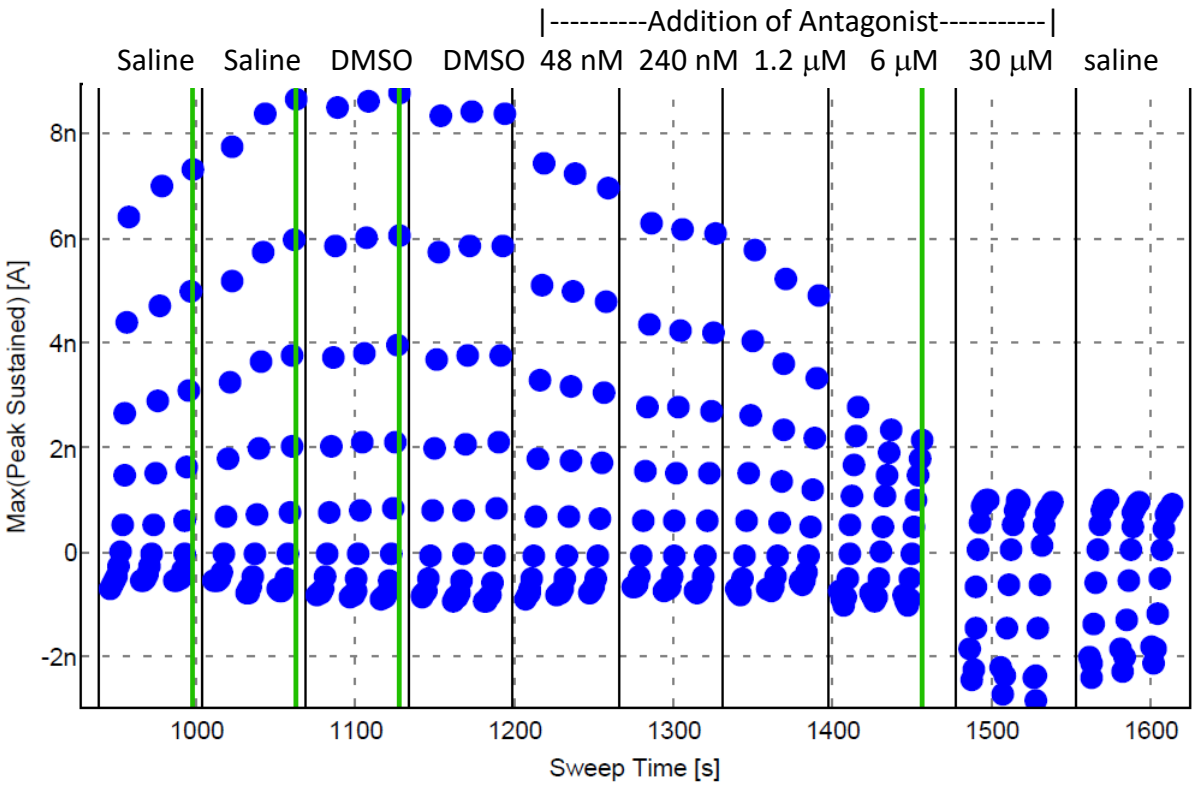

Figure 2_Supplementary Figure 7. Impact of niclosamide on TMEM16A (acd) calcium-activated chloride currents as measured by QPatch electrophysiology. Shown is a representative recording of the impact of progressive (5-fold) increases of niclosamide on the TMEM16A current-voltage response.

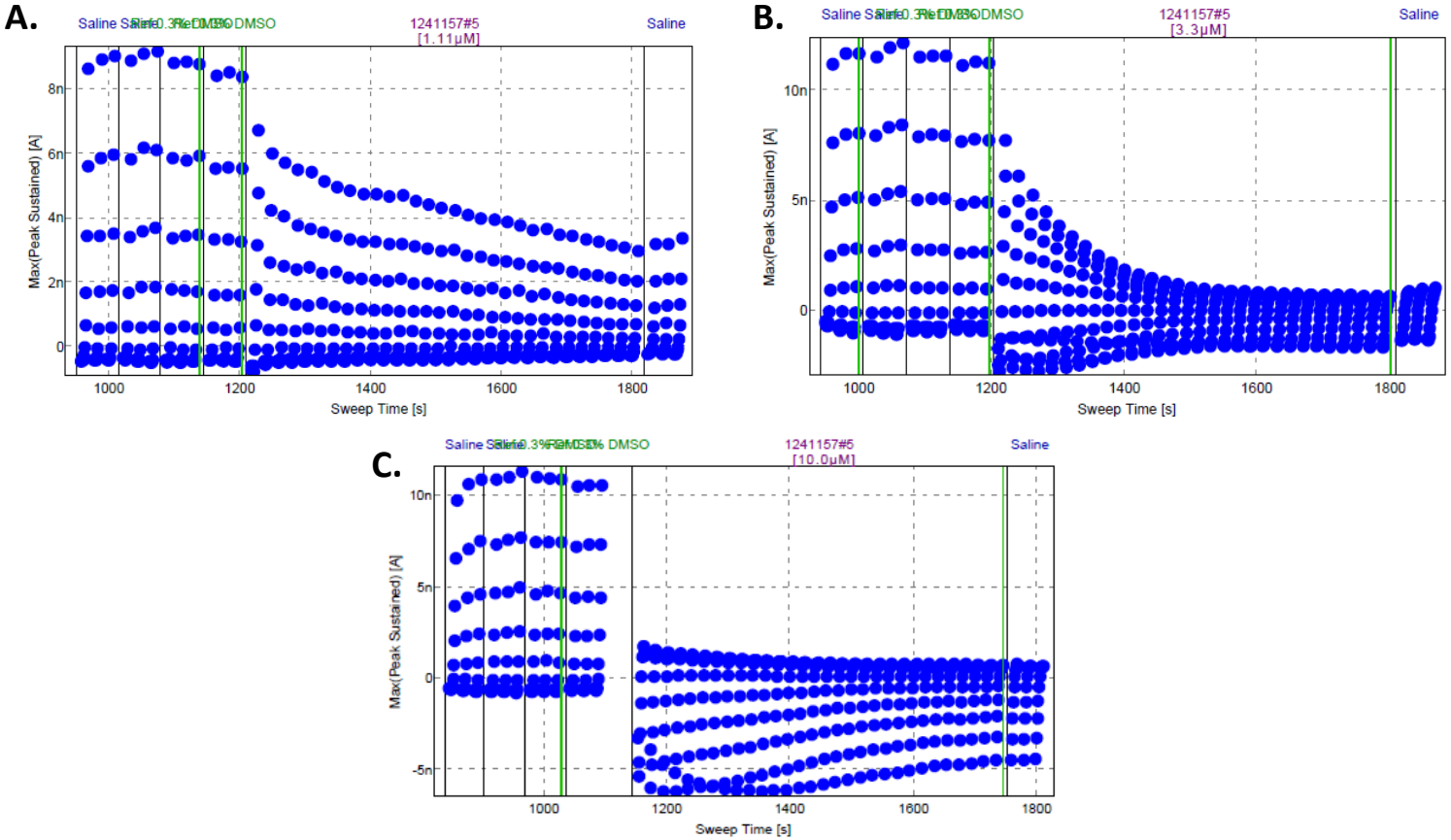

Figure 2_Supplementary Figure 8. Effect of longer incubation times of niclosamide (Cpd 1, 1241157) on TMEM16A (acd) calcium-activated chloride currents at differing membrane potentials as measured by whole cell patch clamp electrophysiology. Shown is representative QPatch recordings over time after addition of 1.1 µM (**A**), 3.3 µM (**B**) and 10.0 µM (**C**) of compound. Using a Vhold of 0 mV, niclosamide decreased the outward currents, but caused a paradoxical increase of the inward currents.

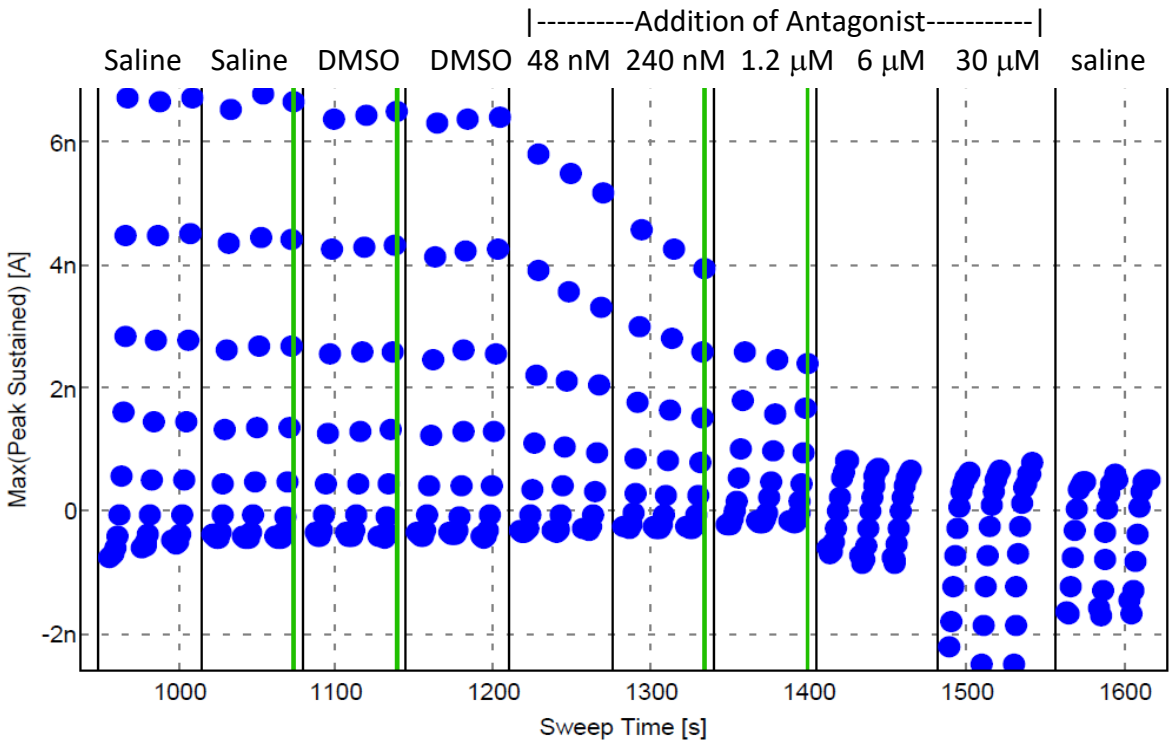

Figure 2_Supplementary Figure 9. Impact of Compound 2 on TMEM16A (acd) calcium-activated chloride currents as measured by QPatch electrophysiology. Shown is a representative recording of the impact of progressive (5-fold) increases of Compound 2 on the TMEM16A current-voltage response.

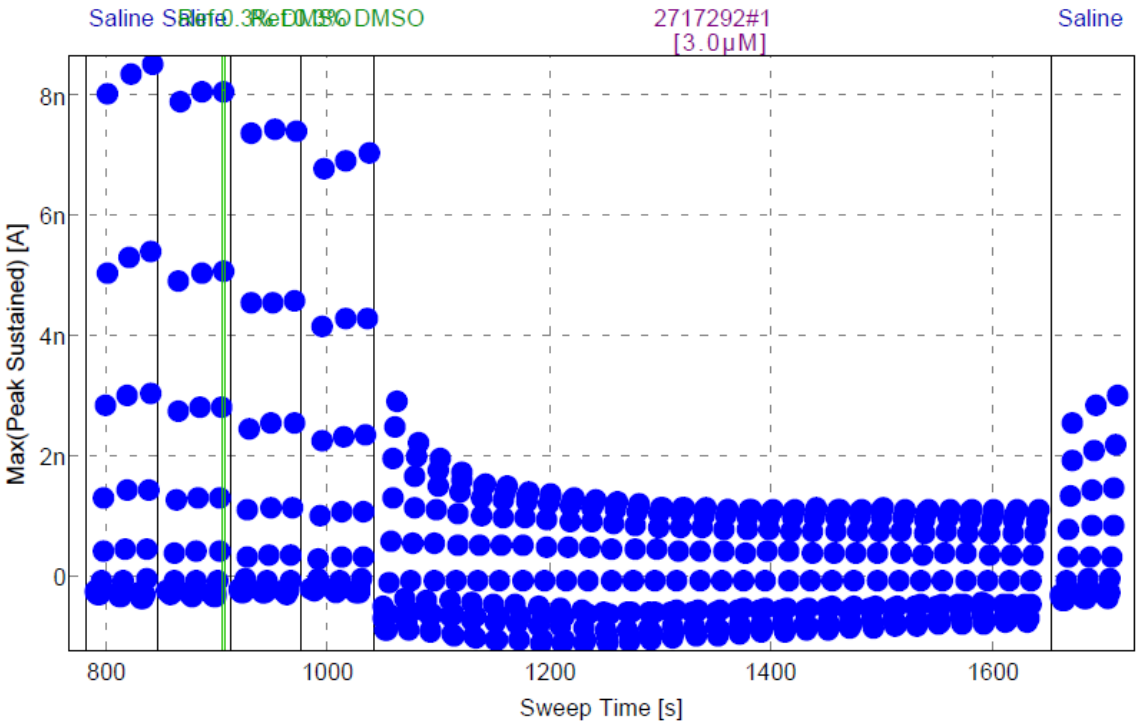

Figure 2_Supplementary Figure 10. Effect of longer incubation times of Compound 2 (Cpd 2, 2717292) on TMEM16A (acd) calcium-activated chloride currents at different membrane potentials as measured by whole cell patch clamp electrophysiology. Shown is representative QPatch recordings over time after addition of 3.0 µM compound. Using a Vhold of 0 mV, Cpd 2 shows robust block of outward currents and a slight stimulation of inward currents.

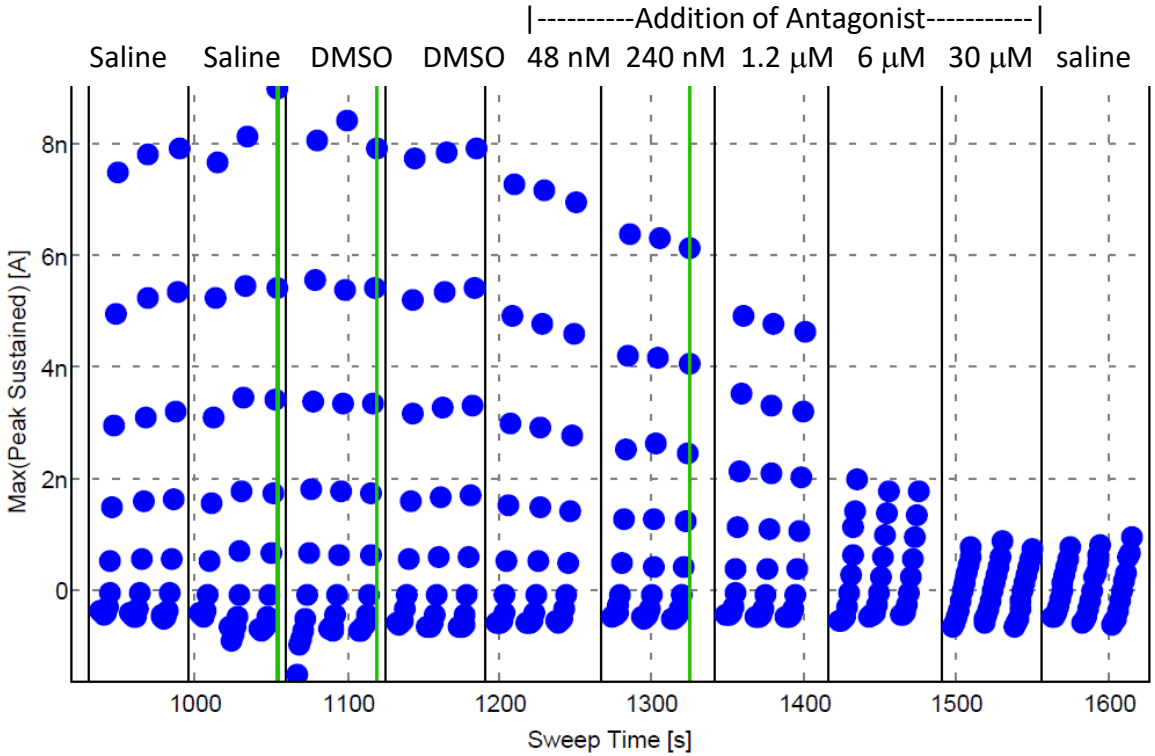

Figure 2_Supplementary Figure 11. Impact of Compound 4 on TMEM16A (acd) calcium-activated chloride currents as measured by QPatch electrophysiology. Shown is a representative recording of the impact of progressive (5-fold) increases of Compound 4 on the TMEM16A current-voltage response.

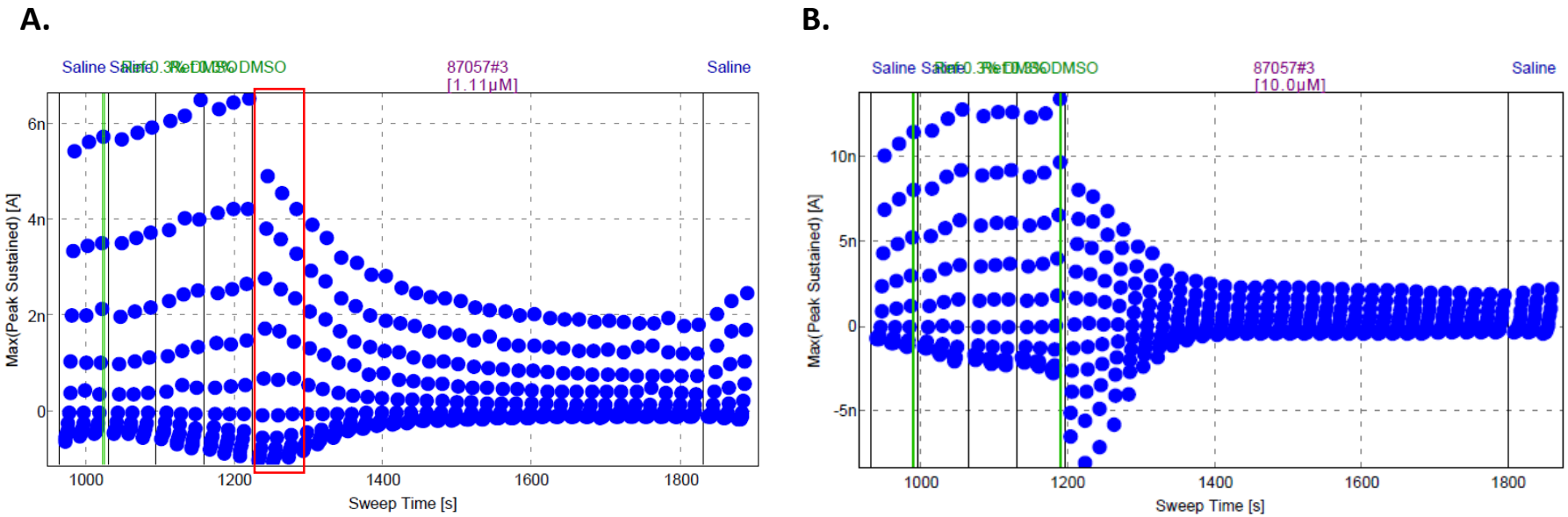

Figure 2_Supplementary Figure 12. Effect of longer incubation times and repeated pulses on Compound 4 (Cpd 4, 87057) block of TMEM16A (acd) calcium-activated chloride currents as measured by whole cell patch clamp electrophysiology. Shown are representative QPatch recordings over time after addition of 1.1 µM (**A**) or 10 µM Cpd 4 (**B**). The red rectangle of panel (**A**) is the typical time frame allowed for each compound dose of our standard cumulative concentration response protocol, which suggests our standard QPatch protocol may not allow enough time for some compounds to block and may underestimate potency. The kinetics of Cpd 4 at 10 µM reveal a progressive and stable inhibition of the outward current, but transient stimulation of the inward current which resolves over time (**B**).

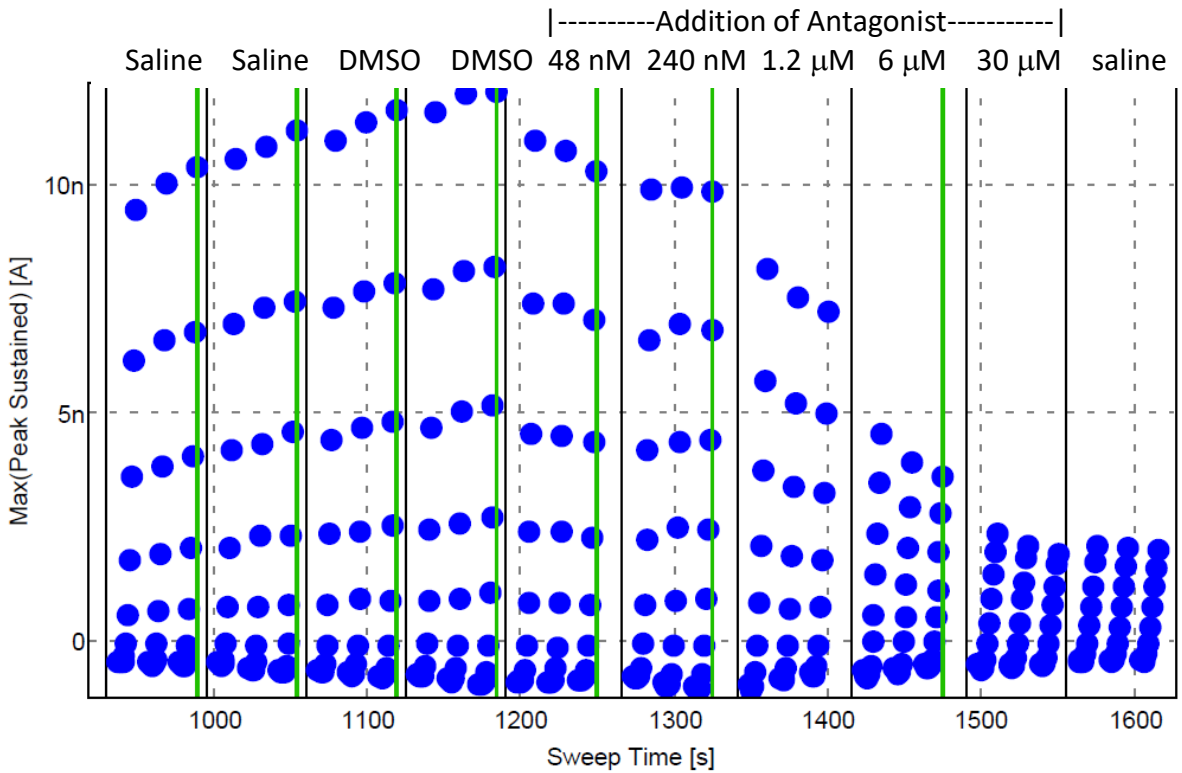

Figure 2_Supplementary Figure 13. Impact of Compound 3 on TMEM16A (acd) calcium-activated chloride currents as measured by QPatch electrophysiology. Shown is a representative recording of the impact of progressive (5-fold) increases of Compound 3 on the TMEM16A current-voltage response.

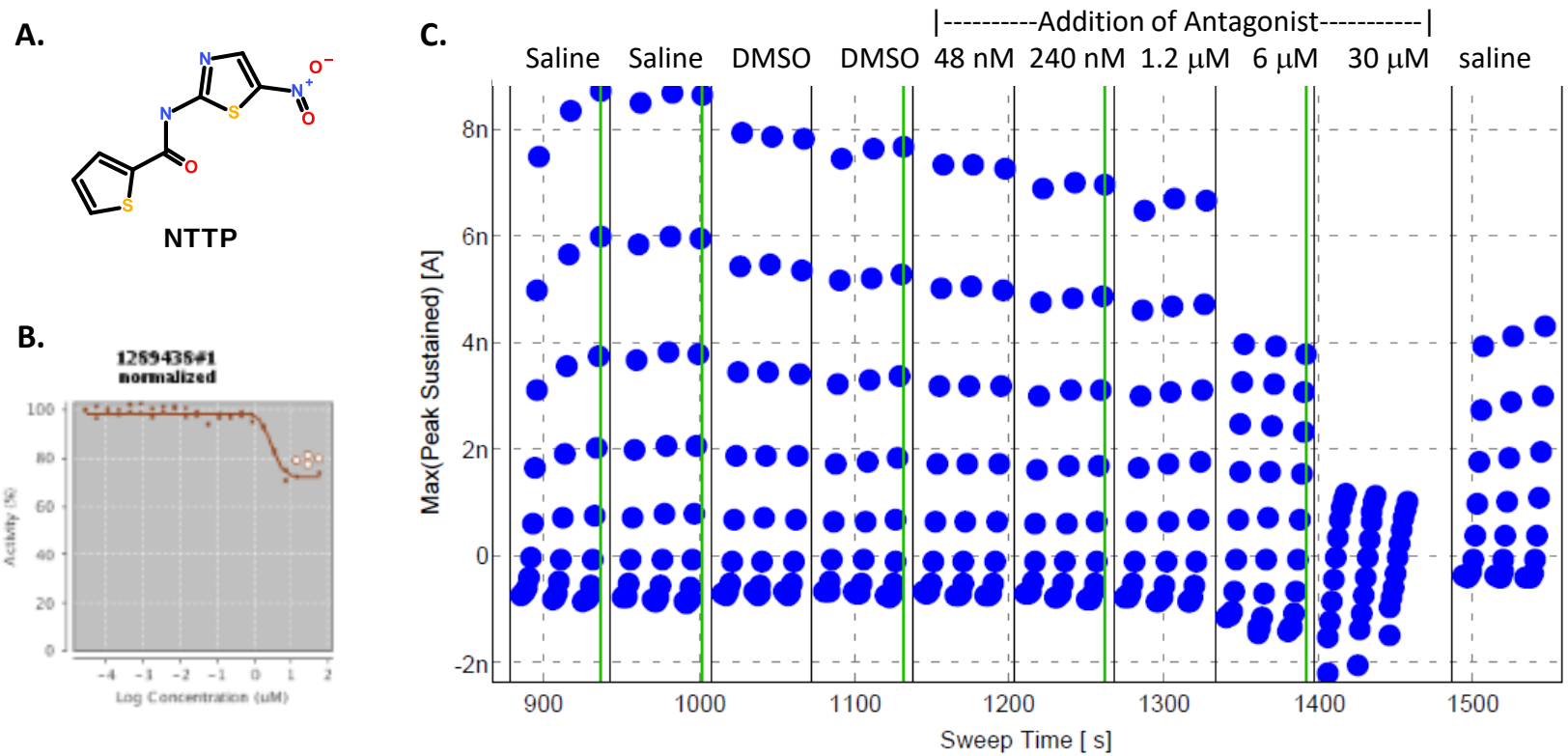

Figure 2_Supplementary Figure 14. Impact of NTTP (1289438) on TMEM16A iodide eYFP response and chloride currents. Panel (**A**) provides the structure of NTTP. Dose response results from the TMEM16A (abc) eYFP assay (**B**) indicates NTTP provides potent (IC_{50} = 2.84 µM) but partial block of the ionomycin-induced eYFP quenching using iodide as the permeant anion and NTTP concentrations up to 55.6 µM. In contrast, Panel (**C**) shows in a representative QPatch electrophysiology recording NTTP provides near complete block of the calcium-activated chloride current (IC_{50} = 4.69 µM; n=4). These findings are consistent with those by ***Peters et al. (2015)*** in the supplementary section of their online article.

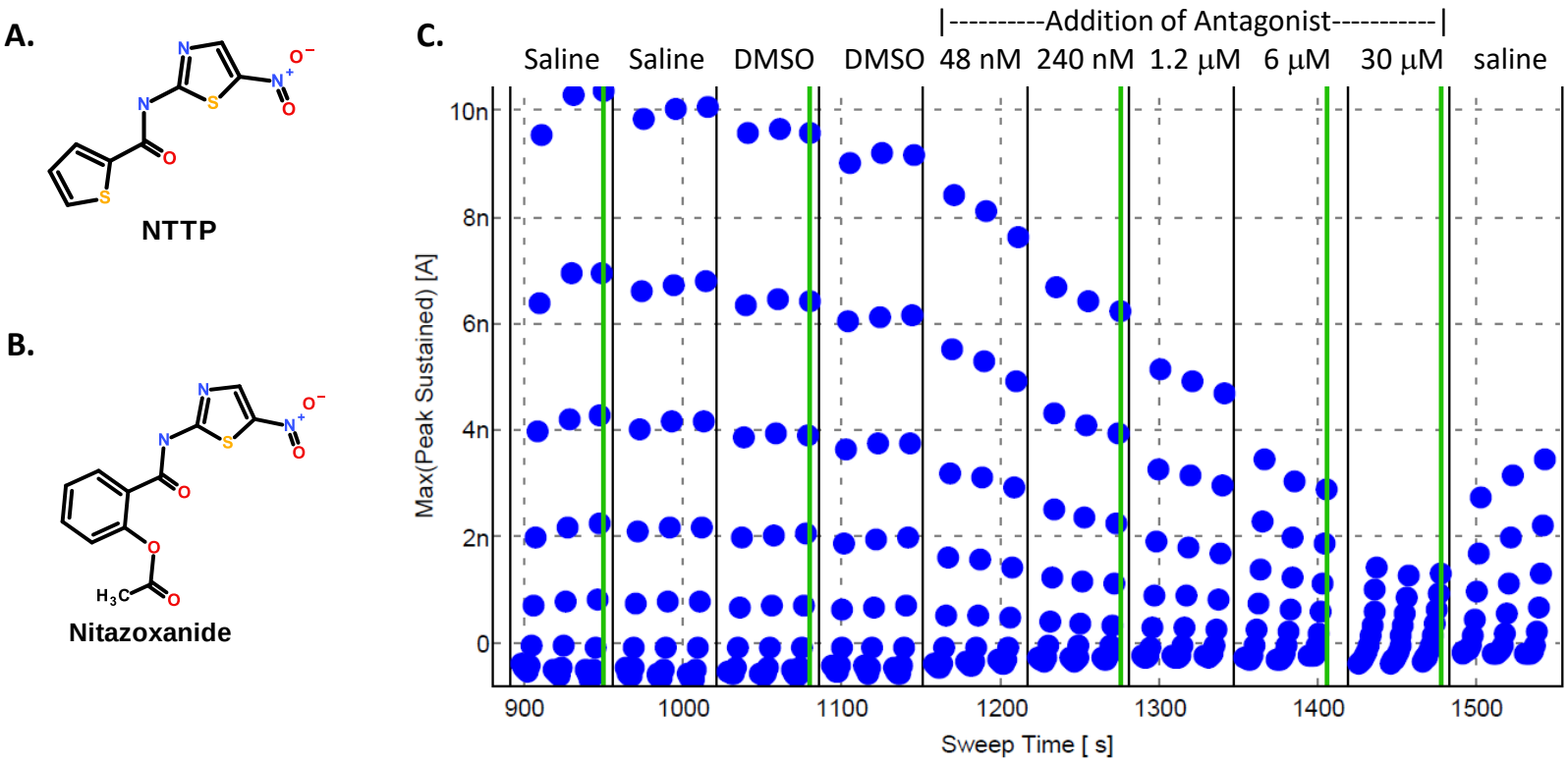

Figure 2_Supplementary Figure 15. The approved drug nitazoxanide is a TMEM16A antagonist that is structurally similar to NTTP. The structures of NTTP and nitazoxanide are provided in Panels (**A**) and (**B**), respectively. Panel (**C**) shows representative results from our QPatch electrophysiology studies evaluating nitazoxanide inhibition of the TMEM16A (acd) calcium-activated chloride current in HEK293 cells after applying progressive (5-fold) increases in drug. The average nitazoxanide IC_{50} from three separate QPatch recordings was 1.26 μM.

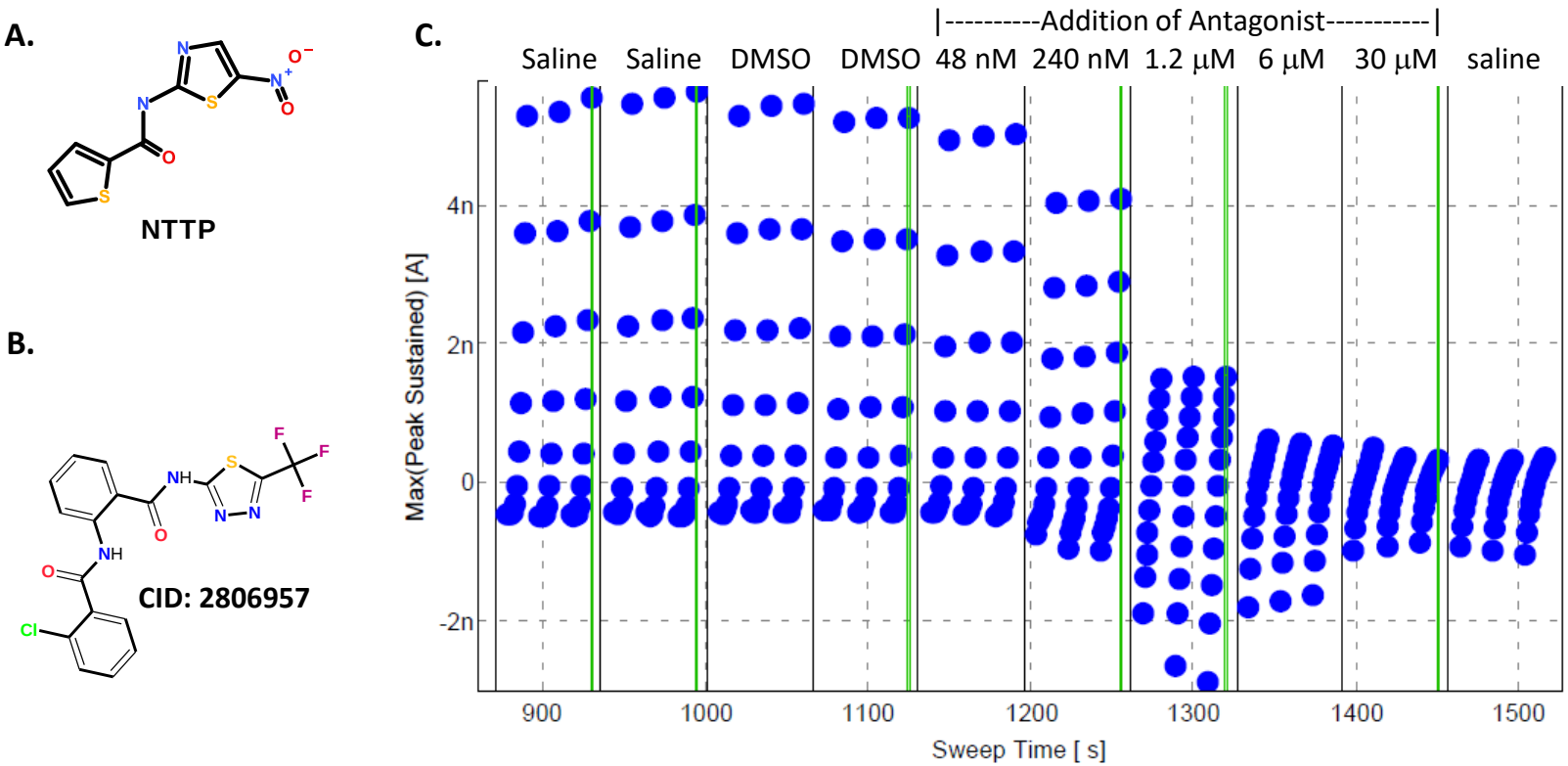

Figure 2_Supplementary Figure 16. Impact of NTTP-related compound, CID# 2806957 on TMEM16A (acd) calcium-activated chloride currents as measured by QPatch electrophysiology. Panel (**A**) provides the structure of NTTP, while Panel (**B**) provides the structure of CID# 2806957. A representative recording of progressive (5-fold) increases in concentration of CID# 2806957 on the TMEM16A current-voltage response is shown in Panel (**C**). This compound provided and average IC_{50} of 0.67 µM (n=3) for blocking the TMEM16A outward current.

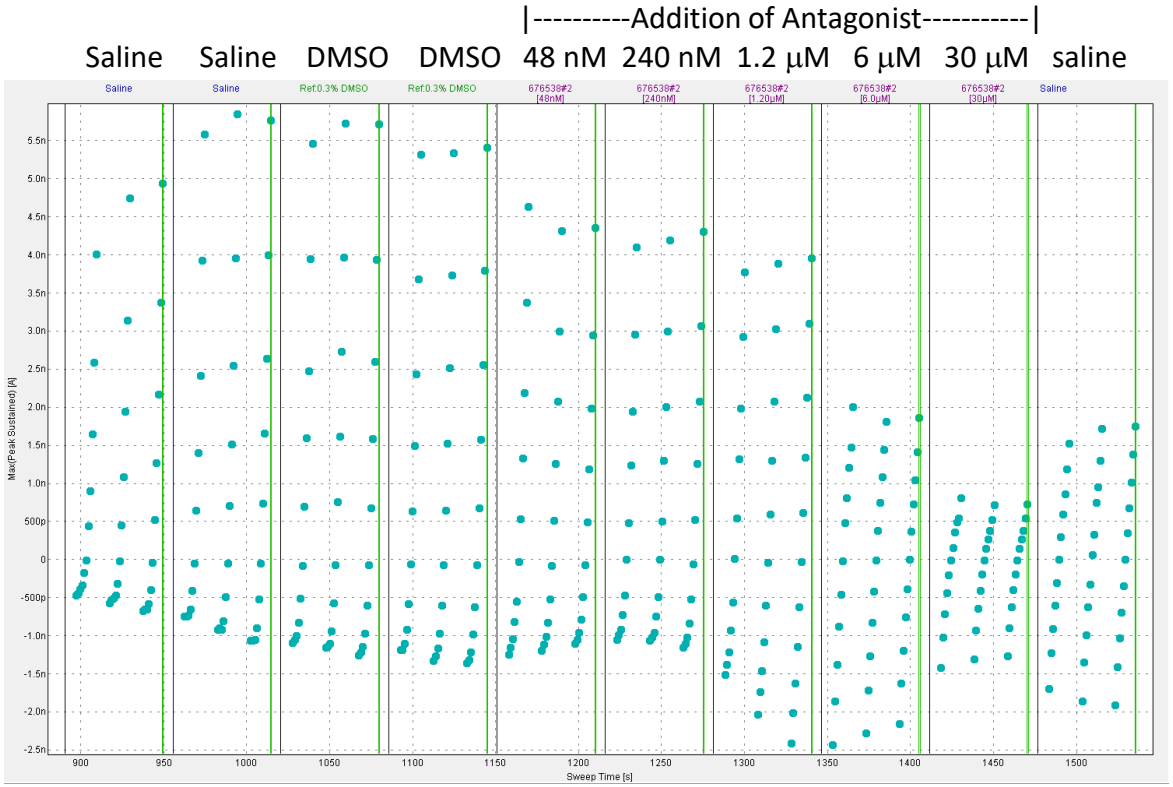

Figure 2_Supplementary Figure 17. Impact of the TMEM16A antagonist 1PBC on COLO-205 calcium-activated chloride currents as measured by QPatch electrophysiology. Shown is raw data from COLO-205 cells measuring the effect of 1PBC on the TMEM16A outward and inward currents .

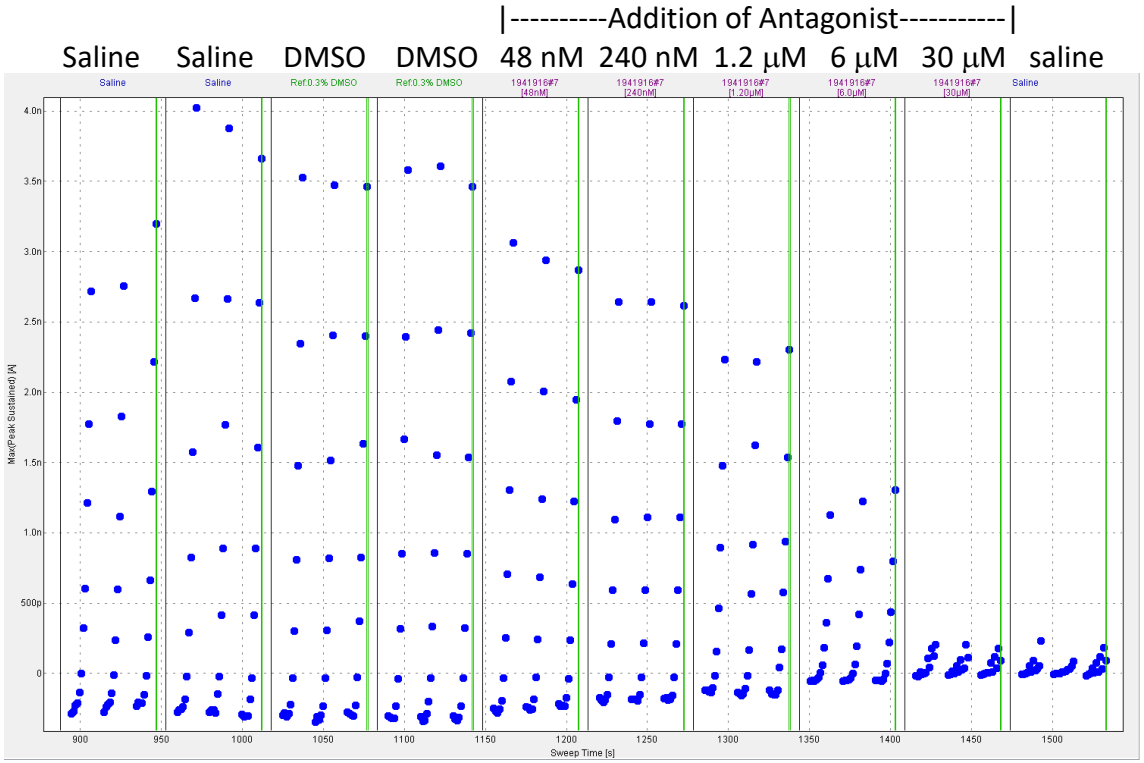

Figure 2_Supplementary Figure 18. Impact of the TMEM16A antagonist benzbromarone on COLO-205 native calcium-activated chloride currents. Shown is raw data from a QPatch recording measuring concentration dependent effects on the TMEM16A current-voltage response.

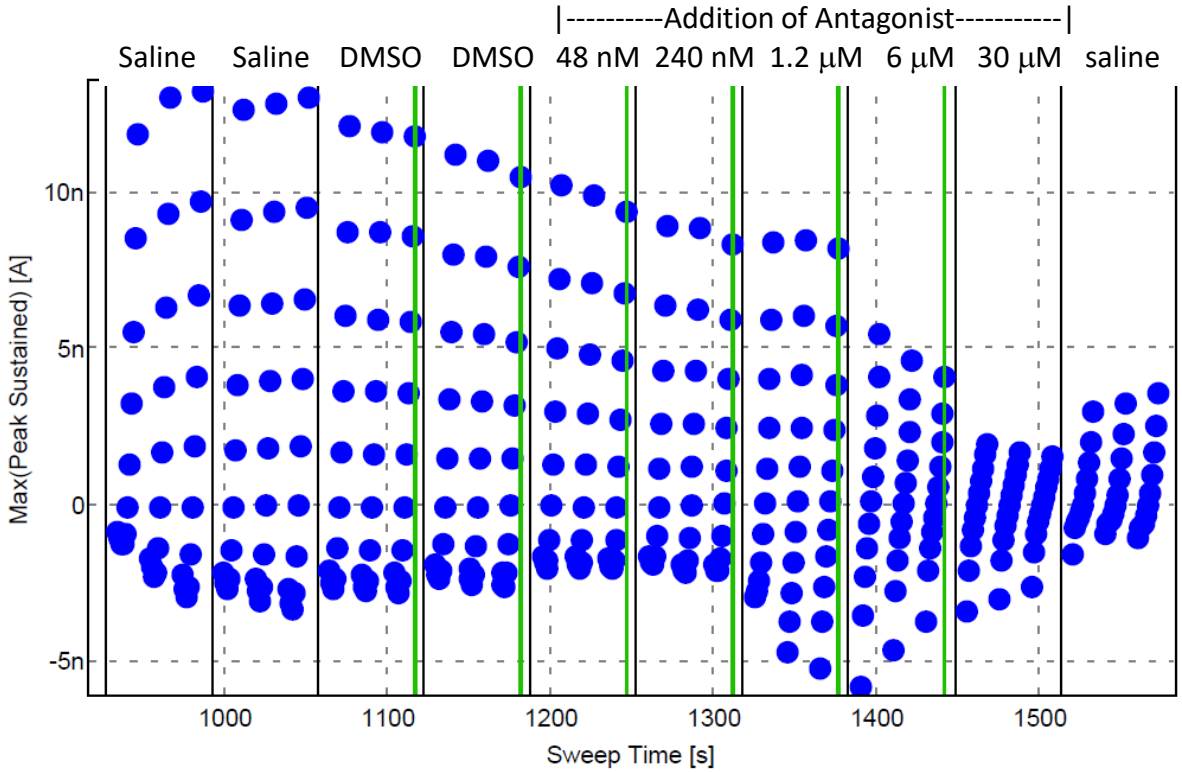

Figure 2_Supplementary Figure 19. QPatch electrophysiology study of impact 1PBC on TMEM16A (abc) splice variant expressed in HEK293 cells. Shown is raw data from a recording measuring the effect of 1PBC on the TMEM16A (abc) outward and inward currents.

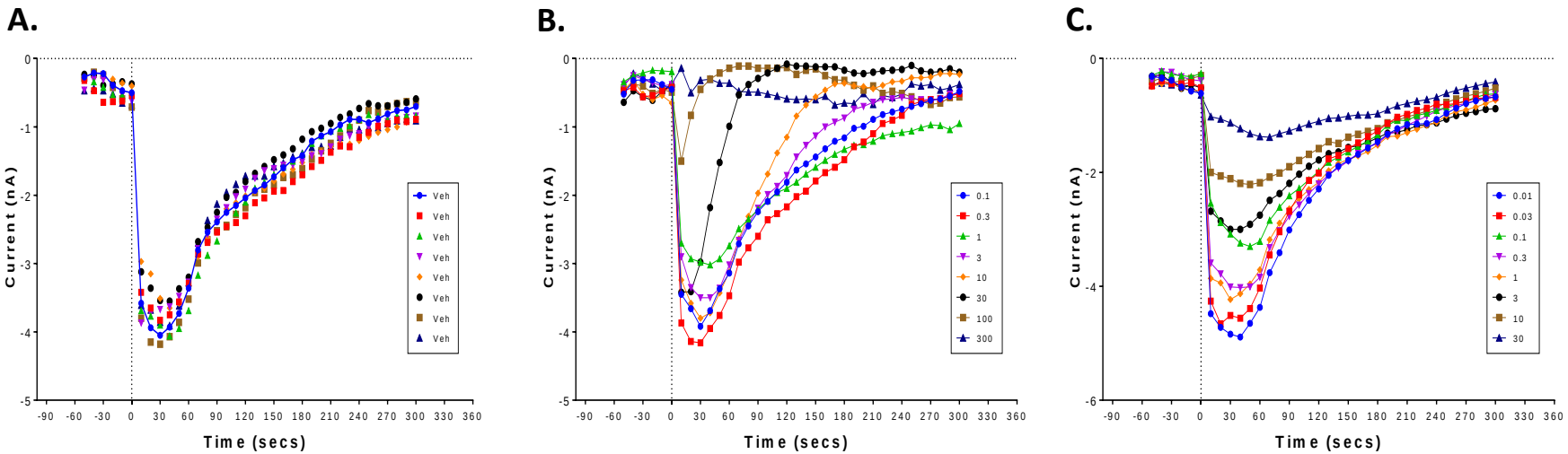

Figure 2_Supplementary Figure 20. Niflumic acid and benzbromarone inhibit the ionomycin-induced TMEM16A (abc) inward current at -100 mV as measured by IonWorks Barracuda perforated patch clamp electrophysiology studies. The inward current over time is shown following the co-addition (time 0) of ionomycin (10 μM) with the DMSO vehicle control (**A**), or various concentration of the antagonists benzbromarone (**B**) or niflumic acid (**C**). Benzbromarone (0.1 – 300 μM) and niflumic acid (0.01 – 30 μM) caused a concentration dependent inhibition of the inward current. From these ephys studies, it's apparent the cloned TMEM16A current in HEK293 cells shows rapid inactivation. Using similar perforated patch clamp methods to what are described here, ***Wang and Kotlikoff (1997)*** similarly find endogenous calcium-activated chloride currents recorded from tracheal smooth muscle cells exhibit rapid inactivation following ionomycin or caffeine addition.

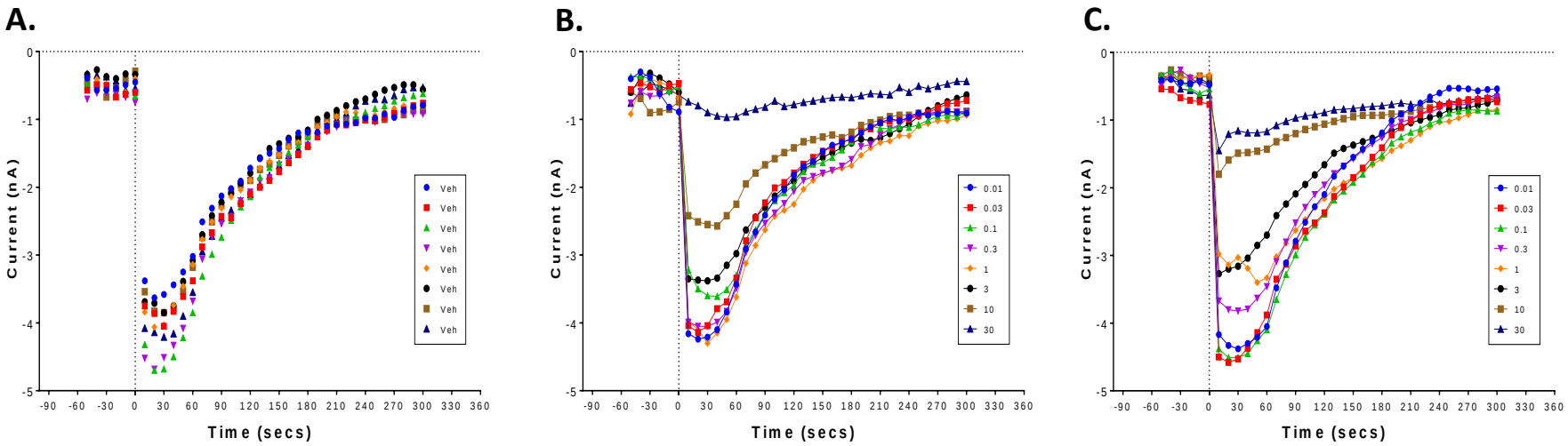

Figure 2_Supplementary Figure 21. 1PBC and Compound 4 inhibit the ionomycin-induced TMEM16A (abc) inward current at -100 mV as measured by IonWorks Barracuda perforated patch clamp electrophysiology studies. The inward current following addition of 10 μM ionomycin (time 0) is shown for the DMSO vehicle control (**A**), 1PBC (**B**) and Compound 4 (**C**). Vehicle control or differing concentrations of the antagonists 1PBC or Compound 4 ranging from 0.01 – 30 μM were added at the same time as the ionomycin stimulus.

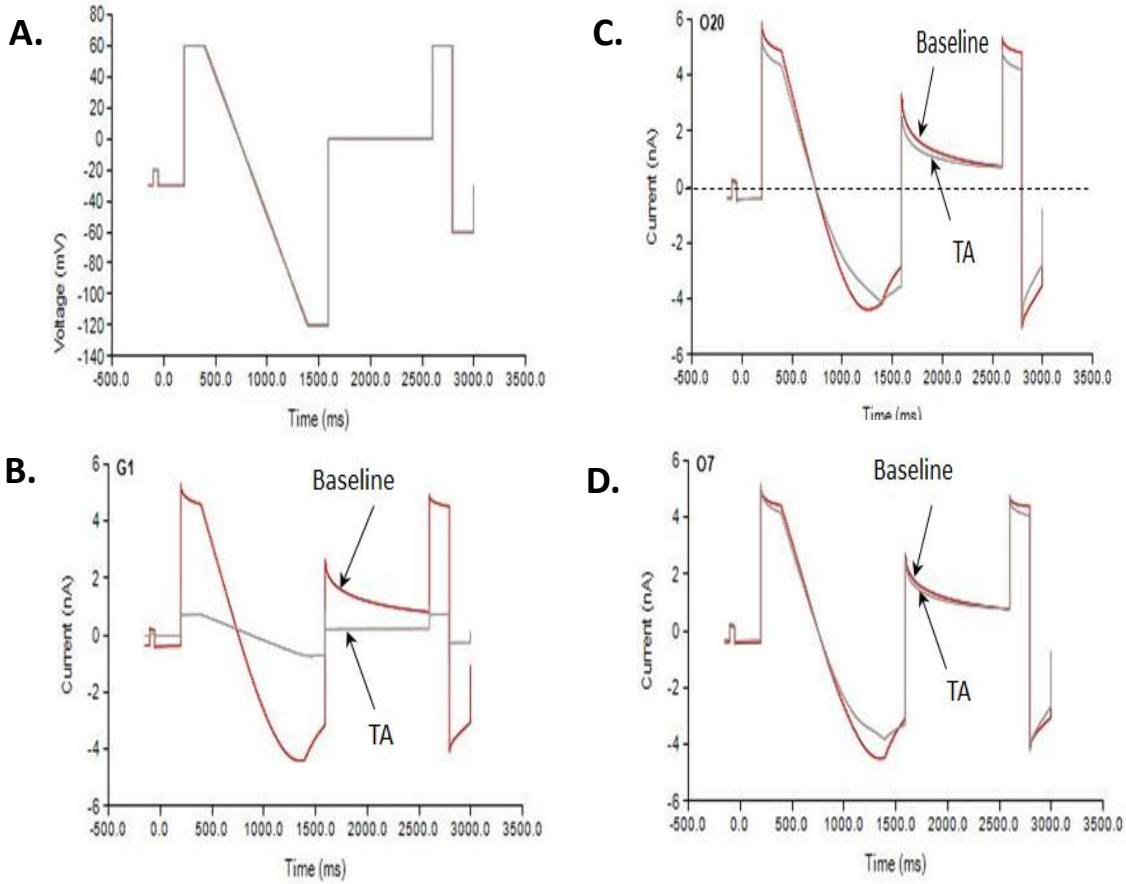

Figure 2_Supplementary Figure 22. Niclosamide and Compound 4 do not impact the CFTR chloride current in IonWorks Barracuda electrophysiology studies. Panel (**A**) provides the voltage protocol for the CFTR recordings. Red traces (**A-D**) show the baseline current, while grey traces show the current following addition of the Test Article (TA) or compound. While 10 μM of the benchmark inhibitor, CFTRinh-172, fully inhibited the cAMP-activated chloride current (**B**), there were no significant effects on the CFTR chloride current following addition of 10 μM niclosamide (**C**) or 10 μM Compound 4 (**D**).

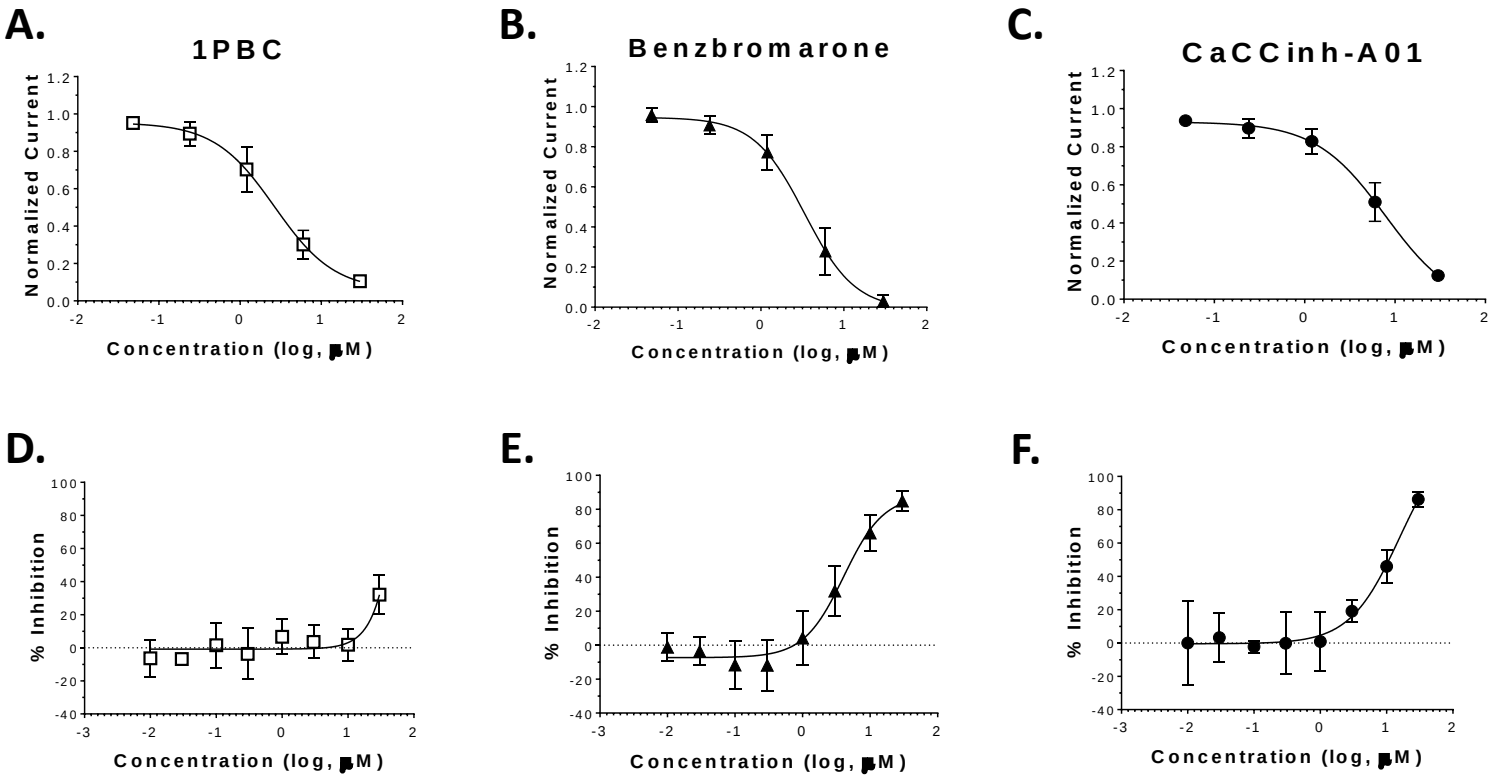

Figure 2_Supplementary Figure 23. Selectivity of benchmark TMEM16A antagonists in inhibiting TMEM16A (**A-C**) versus CFTR (**D-F**) chloride currents. The dose-response results in panels **A-C** are from QPatch electrophysiology studies using HEK293 / TMEM16A (acd) cells and 170 nM free intracellular calcium, while panels **D-F** show the results from IonWorks Barracuda studies using CHO / CFTR cells activated with 20 μM forskolin. Data shown are the mean and standard deviation of 6-7 recordings (**A-C**) or 3-4 recordings (**D-F**).

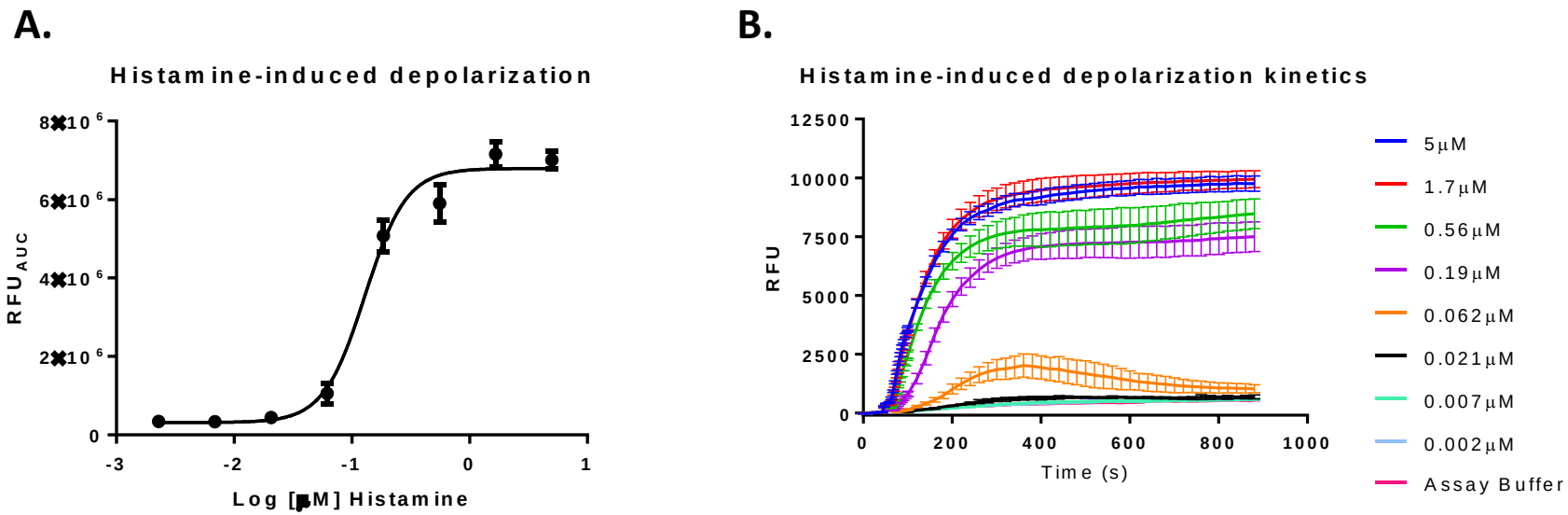

Figure 2_Supplementary Figure 24. Representative histamine dose-response study in the FLIPR membrane potential assay using cultured primary human airway smooth muscle cells to determine the sensitivity to contractile agents. Histamine induced a dose-dependent increase in fluorescence (**A**) corresponding to ASM depolarization, a response which was sustained as shown in the kinetic traces provided in panel (**B**). Routine experiments with TMEM16A antagonists involved pre-incubation of cells with compound for ~30 minutes and then treatment with an EC_{90} concentration of histamine.

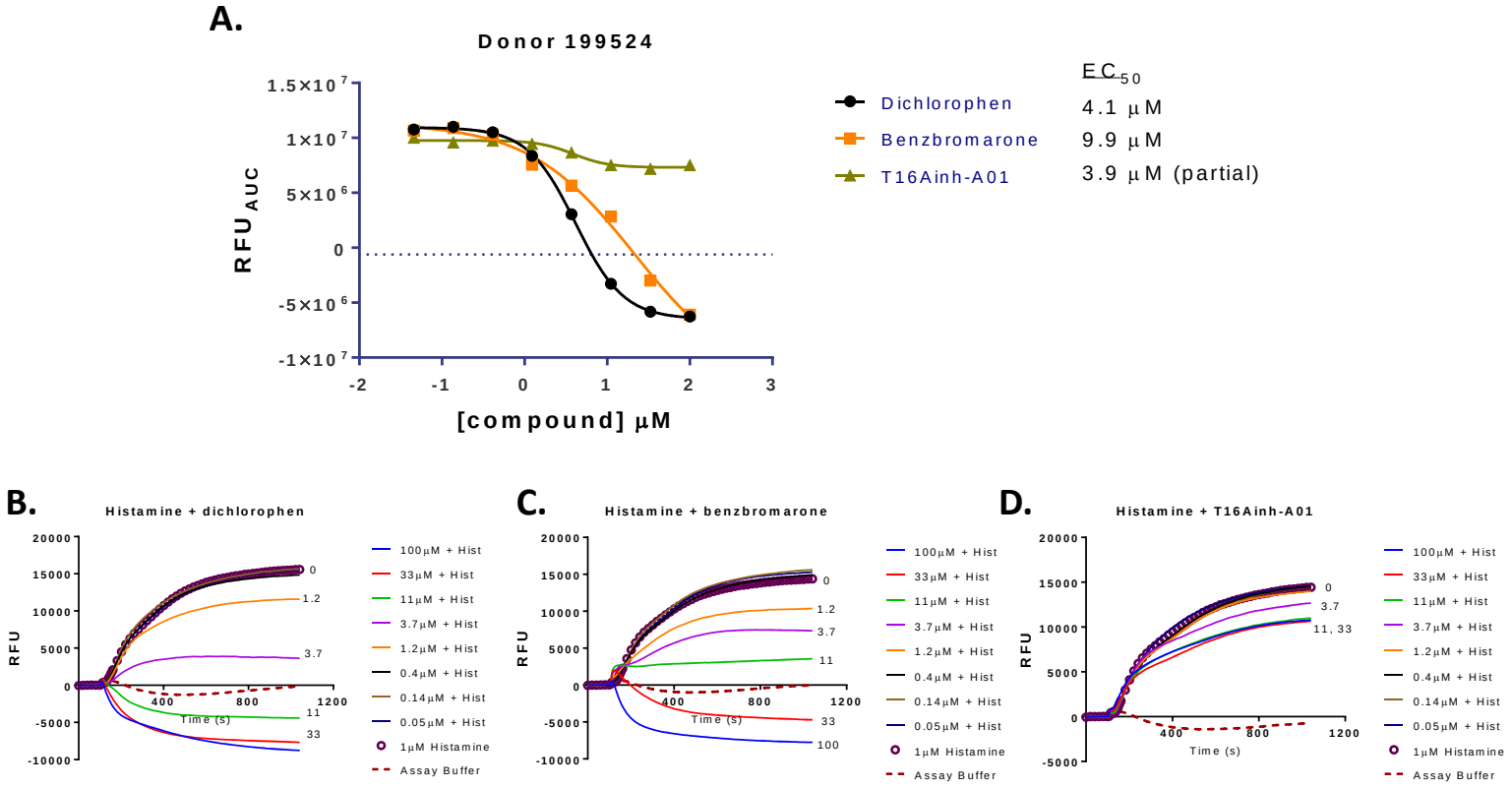

Figure 2_Supplementary Figure 25. The TMEM16A antagonists dichlorophen and benzbromarone fully inhibit the histamine-induced depolarization of primary human airway smooth muscle cells (donor 199524), while T16Ainh-A01 shows just partial effects. Panels (**B-D**) show raw fluorescence data from the membrane potential assay of buffer alone, buffer plus histamine and the combination of various µM concentrations of dichlorophen (**B**), benzbromarone (**C**) and T16Ainh-A01 (**D**) with histamine. Panel (**A**) plots the dose-dependent changes in area under the curve (AUC) of TMEM16A antagonists. Dichlorophen and benzbromarone fully reversed histamine depolarization and induced some hyperpolarization. RFU = relative fluorescence units.

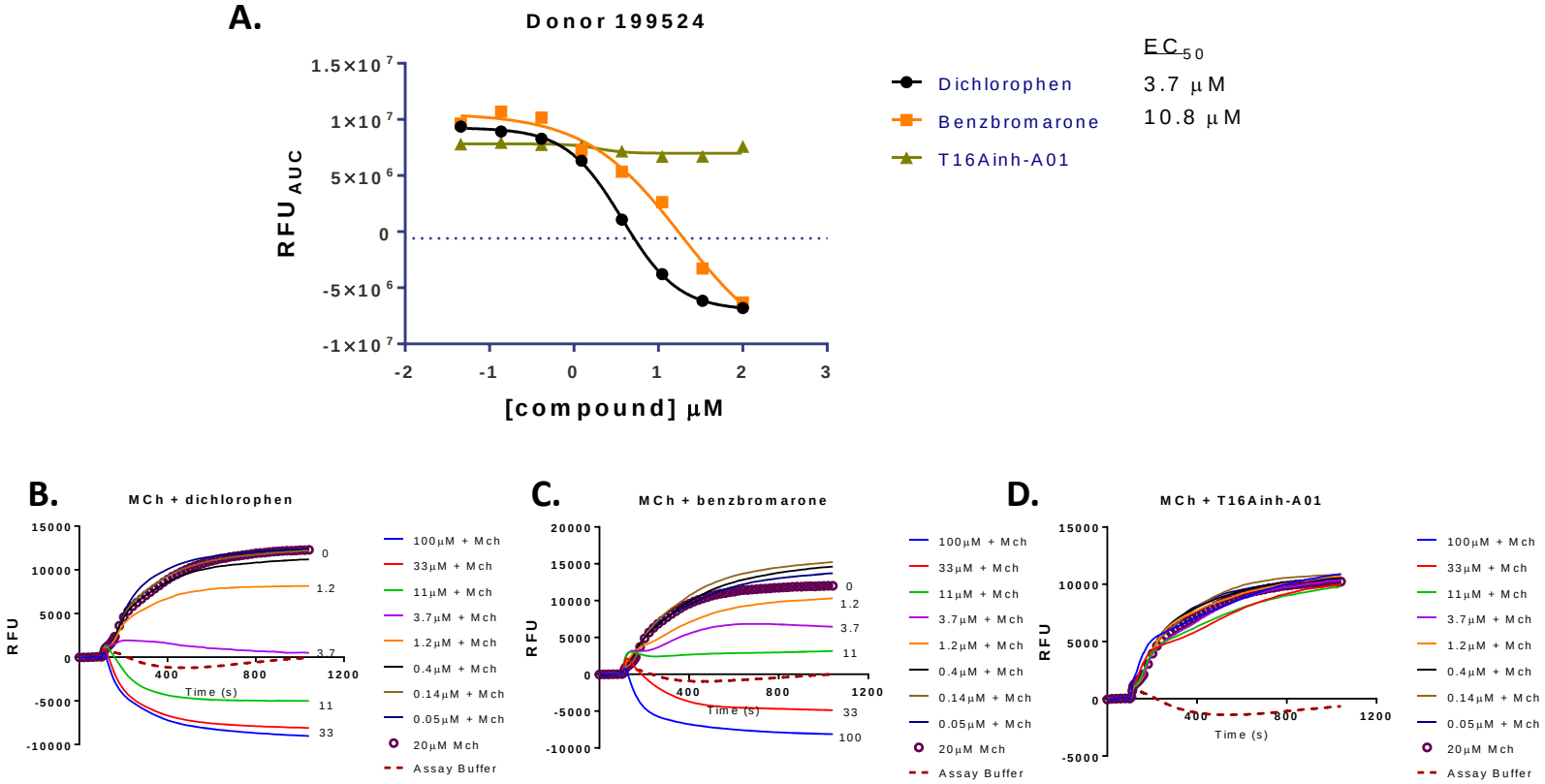

Figure 2_Supplementary Figure 26. The TMEM16A antagonists dichlorophen and benzbromarone fully inhibit the methacholine (Mch)-induced depolarization of primary human airway smooth muscle cells (donor 199524), while T16Ainh-A01 showed little effect. Panels (**B-D**) show raw fluorescence data from the membrane potential assay of buffer alone, buffer plus methacholine and the combination of various µM concentrations of dichlorophen (**B**), benzbromarone (**C**) and T16Ainh-A01 (**D**) with methacholine. Panel (**A**) plots the dose-dependent changes in area under the curve (AUC) of TMEM16A antagonists. Dichlorophen and benzbromarone fully reversed methacholine depolarization and induced some hyperpolarization. RFU = relative fluorescence units.

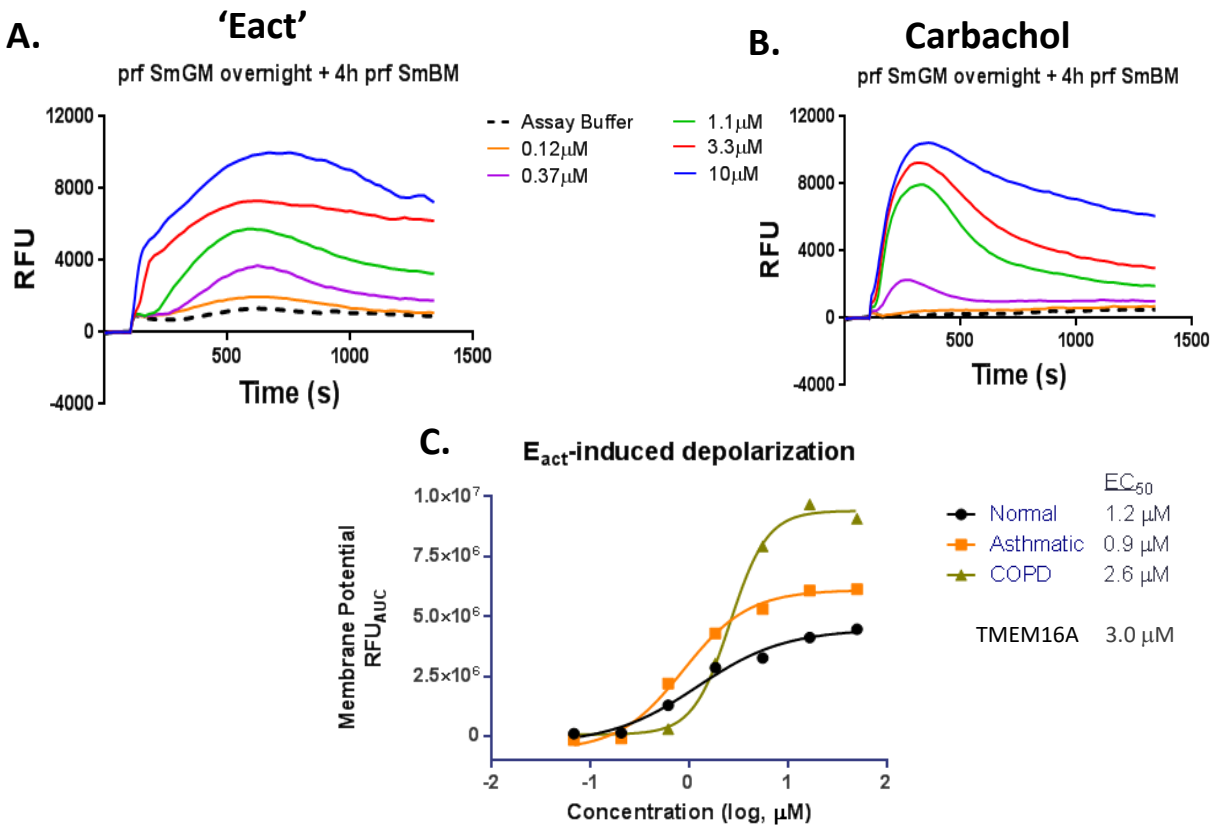

Figure 2_Supplementary Figure 27. The small molecule TMEM16A activator, E_{act}, induces depolarization of primary human airway smooth muscle cells like the contractant carbachol. Kinetic traces from the FLIPR membrane potential assay indicate E_{act} (**A**) and carbachol (**B**) elicit a concentration dependent depolarization of human ASM cells which were serum starved for 4 hours [prf SmGM overnight + 4h prf SmBM]. The E_{act} depolarization of ASM cells is similar to that reported by ***Danielsson et al. (2015)*** earlier. The potency for E_{act} depolarization of ASM cells isolated from a normal, asthmatic or COPD patient is shown in panel (**C**). The average EC_{50} of 1 – 3 μM for depolarizing human ASM cells (**C**) compares favorably to the 3.0 μM EC_{50} which ***Namkung et al. (2011)*** report for activation of TMEM16A.

RFU, relative fluorescence units. AUC, area under the curve.

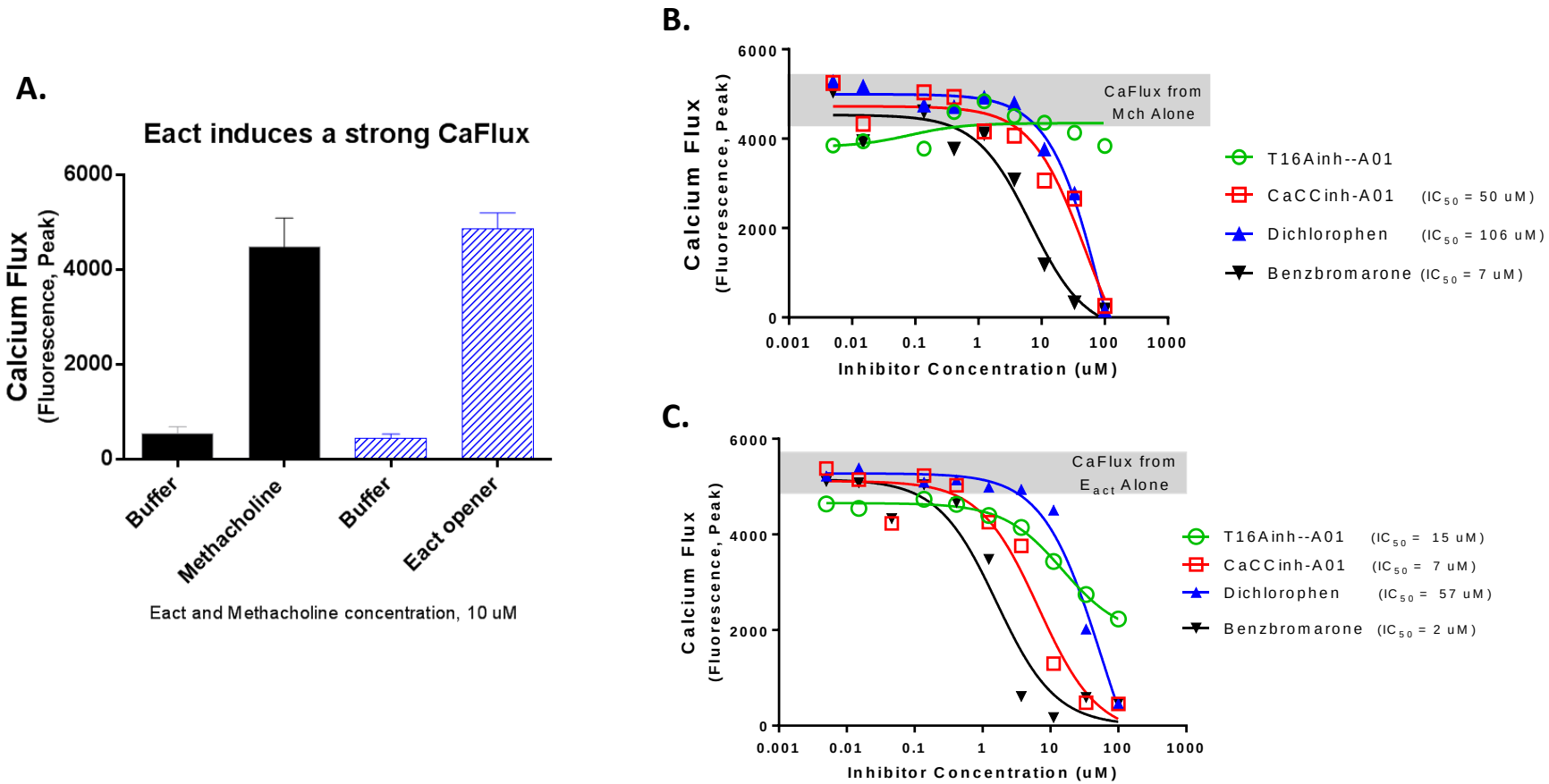

Figure 2_Supplementary Figure 28. Primary human ASM cells treated with the TMEM16A opener, E_{act}, and the cholinergic methacholine (Mch) cause similar increases in the level of procontractile intracellular calcium (**A**). The TMEM16A antagonists benzbromarone, CaCCinh-A01 and dichlorophen block both the Mch (**B**) and E_{act} (**C**) ASM calcium flux (CaFlux), while the TMEM16A antagonist T16Ainh-A01 only showed effects in blocking the CaFlux induced by E_{act}. Our findings that benzbromarone inhibited Mch CaFlux are similar to those reported earlier by ***Danielsson et al. (2015)*** who found this compound blocked histamine- and bradykinin-induced CaFlux in ASM cells.

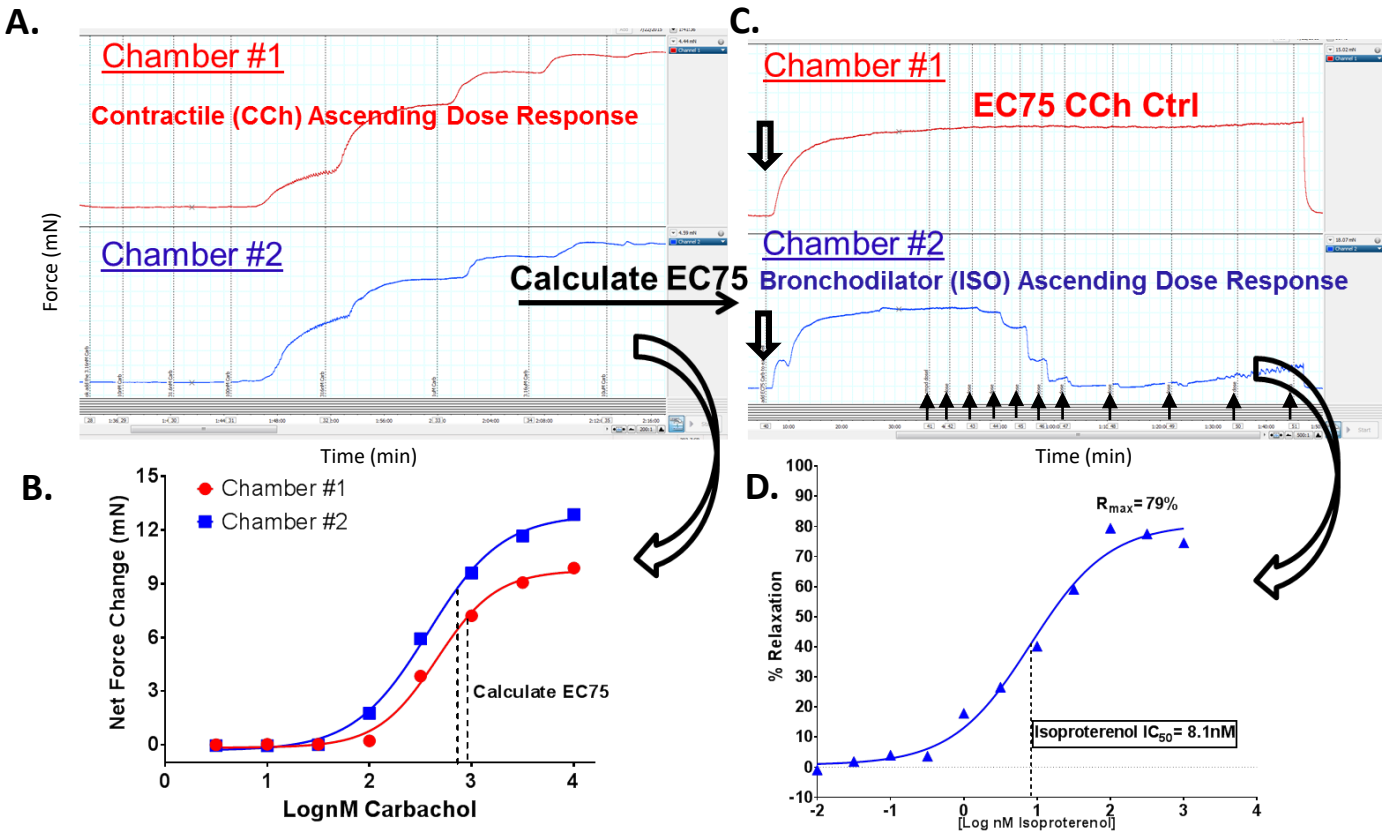

Figure 3_Supplementary Figure 1. Experimental procedure for determining the EC_{75} of carbachol for contraction of mouse tracheal rings and representative example of the efficacy of isoproterenol in relaxing carbachol pre-contracted airways. Panels (**A**) shows raw traces from the wire myograph studies on two tracheal rings showing ascending carbachol (CCh) concentrations (vertical dotted lines) cause progressive increases in force over time (each light blue block corresponds to 1 min). The calculated EC_{75} for carbachol are shown in panel (**B**). After washing tissue and resetting baseline tension, the upper trace of panel (C) shows raw traces upon addition of an EC_{75} level of CCh alone (open down arrows), while the lower trace of panel (**C**) shows force from EC_{75} of carbachol followed by level of relaxation following increasing doses (up arrows) of isoproterenol. Carbachol causes sustained contraction over time of the tracheal rings (**C**) (each light blue block corresponds to 2 min) and isoproterenol induced potent relaxation which is plotted in panel (**D**).

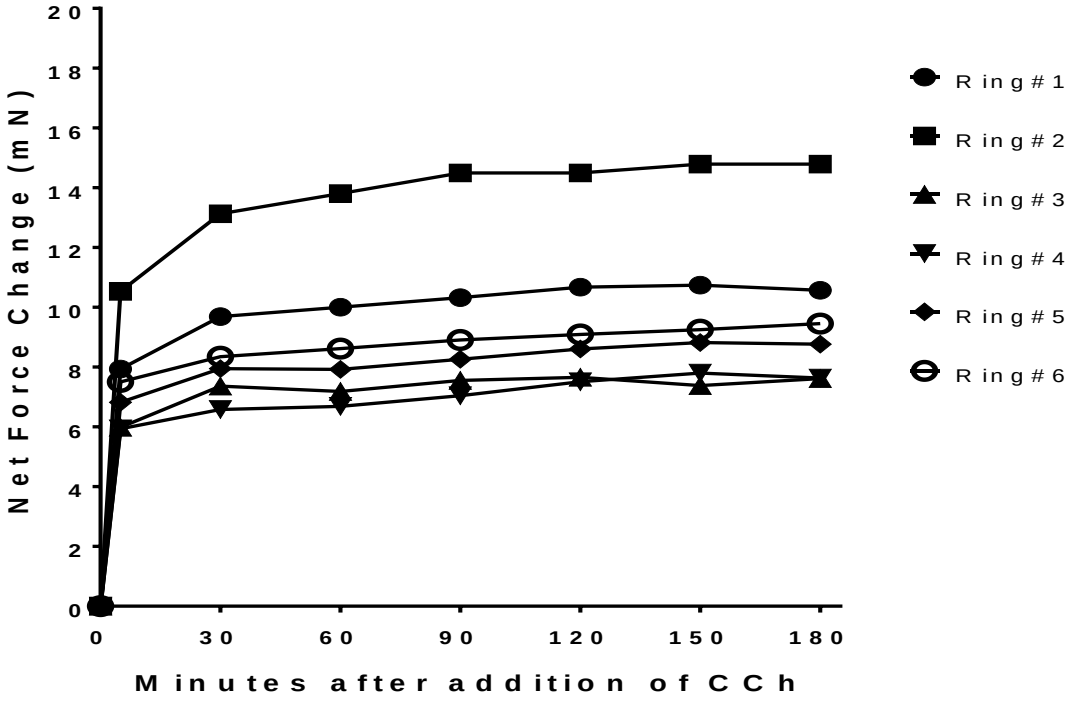

Figure 3_Supplementary Figure 2. Mouse tracheal rings do not fatigue and maintain contraction for several hours after addition of an EC_{75} level of carbachol.

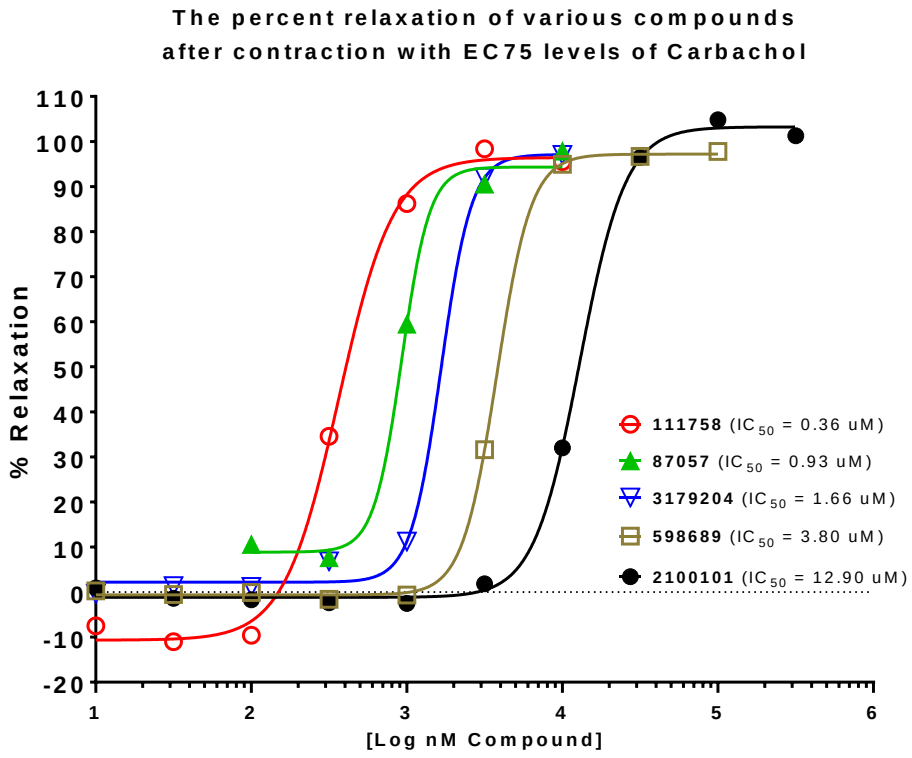

Figure 3_Supplementary Figure 3. TMEM16A antagonists bronchodilate mouse tracheal rings pre-contracted with carbachol. Compound 111758 is a structurally related analog of Compound 4 (87057), while 3179204 and 598689 are of the niclosamide series, with the former being a closely related analog of Compound 5. The compound 2100101 is a distinct chemotype from niclosamide or the Compound 4 series. As human and mouse TMEM16A are highly conserved (92% identical, 95% similar) and key pore lining residues are conserved, mouse tracheal rings represent a convenient preclinical species for testing antagonist efficacy.

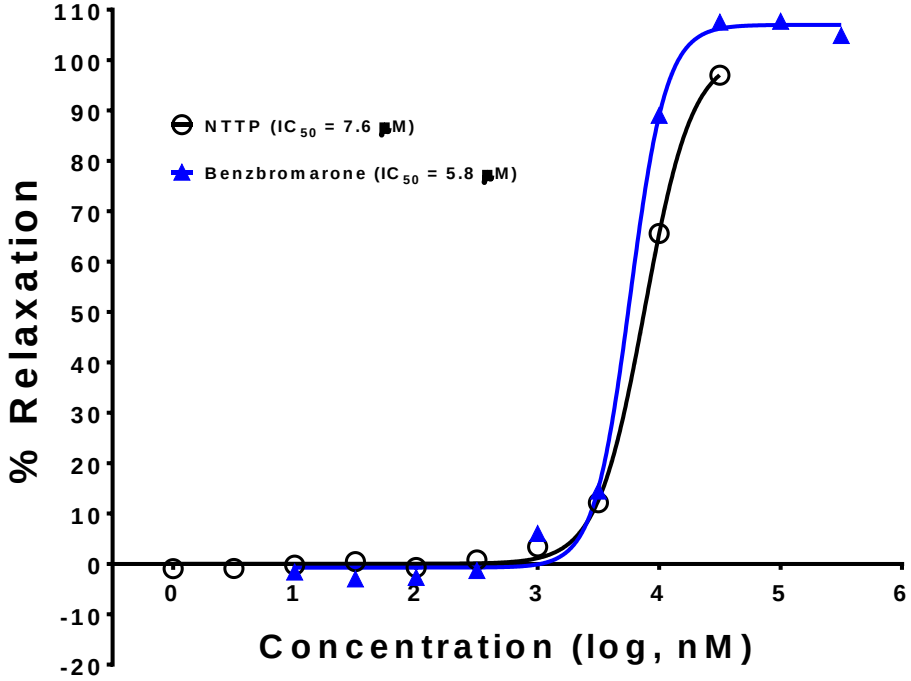

Figure 3_Supplementary Figure 4. The compound NTTP [CID: 19646] which only partially inhibits the TMEM16A iodide eYFP response but fully inhibits the calcium-activated chloride current (***Figure 2_Supplementary Figure 14***), causes full relaxation of carbachol (EC_{75}) pre-contracted mouse tracheal rings.

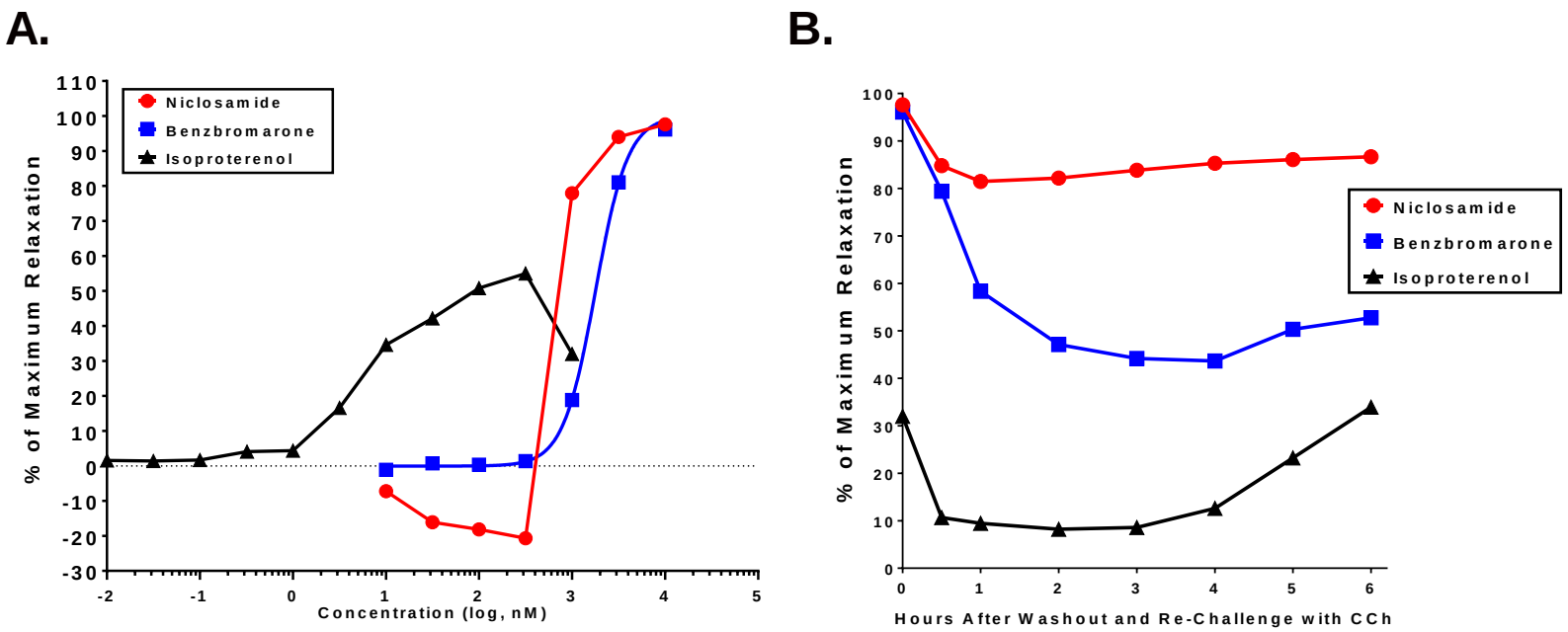

Figure 3_Supplementary Figure 5. TMEM16A antagonists fully relax mouse airways pre-contracted with carbachol and exhibit sustained action over several hours unlike the β-agonist isoproterenol that shows just transient bronchodilation. Panel (**A**) shows niclosamide, benzbromarone and isoproterenol dose-dependent relaxation of carbachol pre-contracted airways. These airways were then washed to remove compounds and re-contracted with carbachol to evaluate if any of the compounds showed sustained effects (**B**). The isoproterenol efficacy was quickly lost, but niclosamide and benzbromarone appeared to show sustained bronchodilation of the mouse airways.

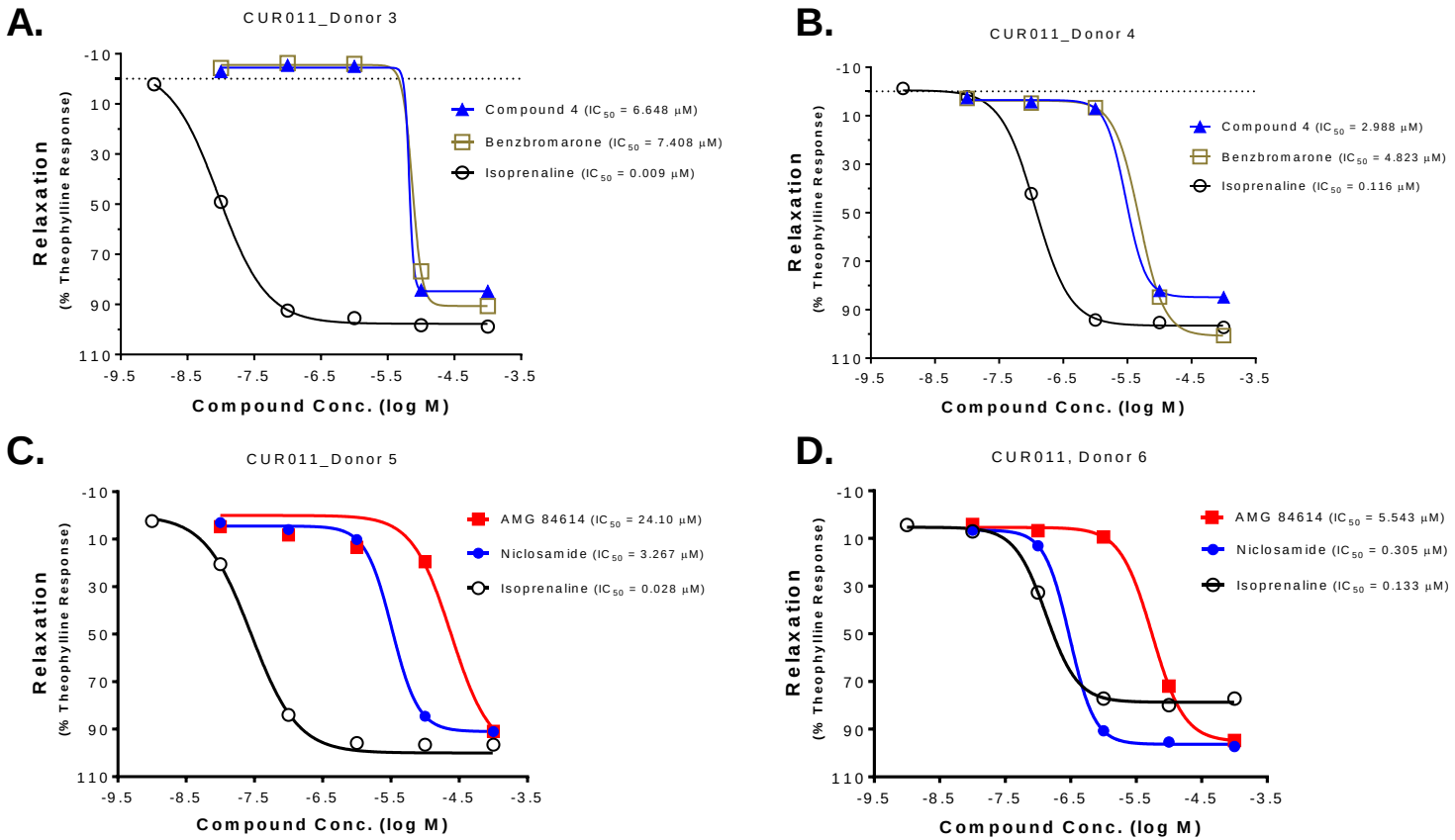

Figure 3_Supplementary Figure 6. TMEM16A antagonists relax human 4th order bronchi pre-contracted with 10 µM histamine. Each compound was tested for bronchodilation of airways isolated from two normal donors by wire myograph. Panels (**A**) and (**B**) show results for Compound 4 and benzbromarone, while panels (**C**) and (**D**) show relaxation by niclosamide and its related analog AMG 84614. The β-agonist isoproterenol run as a positive control was more potent than the TMEM16A antagonists, but showed variable responses depending on donor. The improved potency of niclosamide in panel (**D**) versus panel (**C**) may derive from improved solubility, as serial dilutions in (**D**) used DMSO versus saline which was used in panel (**C**). Vehicle controls were also tested and showed no effects on the airway tone.

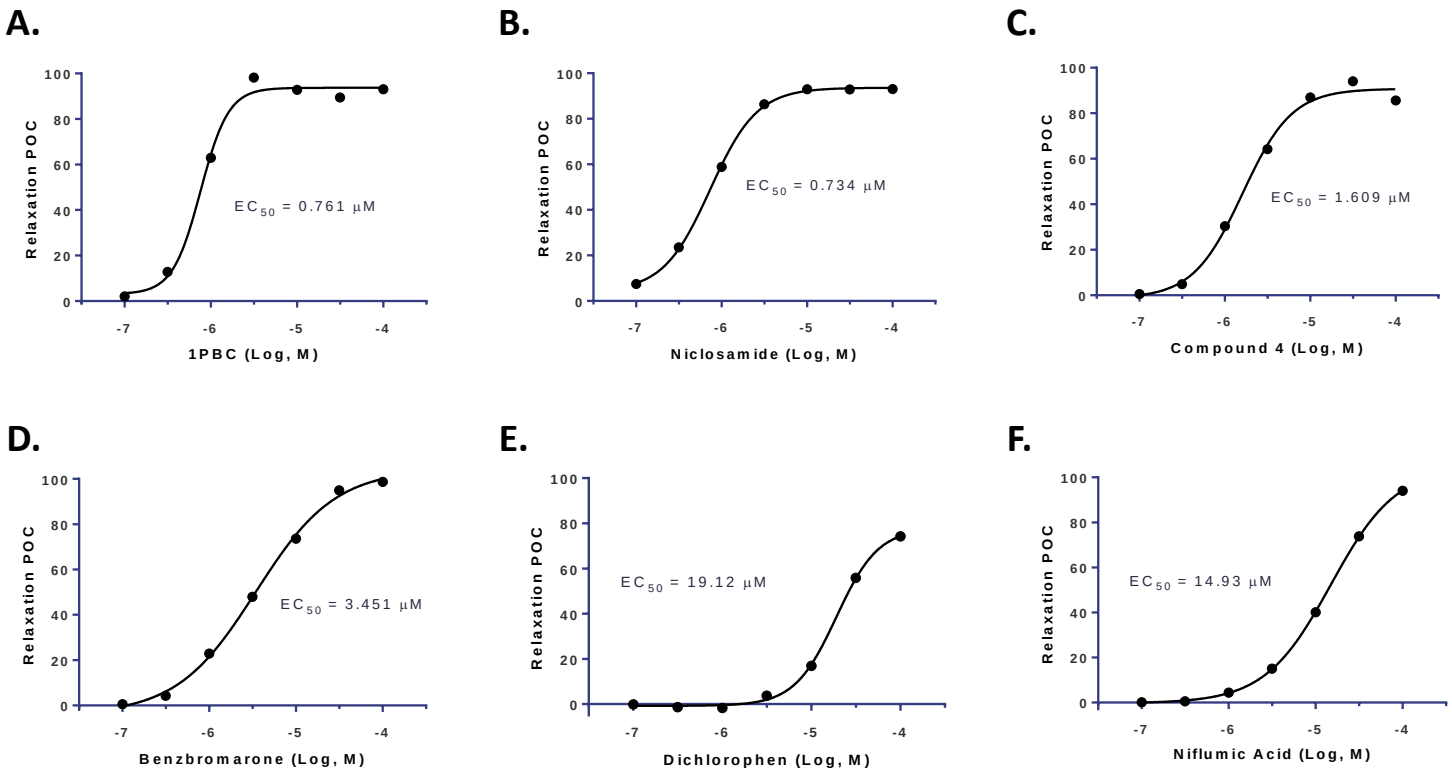

Figure 3_Supplementary Figure 7. Efficacy of TMEM16A antagonists in relaxing human bronchial rings pre-contracted with carbachol. Cumulative concentration response curves (CCRC) for 1PBC (**A**), niclosamide (**B**), Compound 4 (**C**), benzbromarone (**D**), dichlorophen (**E**), and niflumic acid (**F**) bronchodilation of airways was measured using a DMT wire myograph, with the potency (EC_{50}) of each compound being listed. At the end of each recording and CCRC, theophylline was added to 2.2 mM final to induce maximal relaxation of the bronchial ring, which was considered 100 POC and used for normalization of compound effects. As a precaution, all recordings included 5 µM indomethacin in the bath solution to eliminate any possible indirect effect due to prostaglandins.

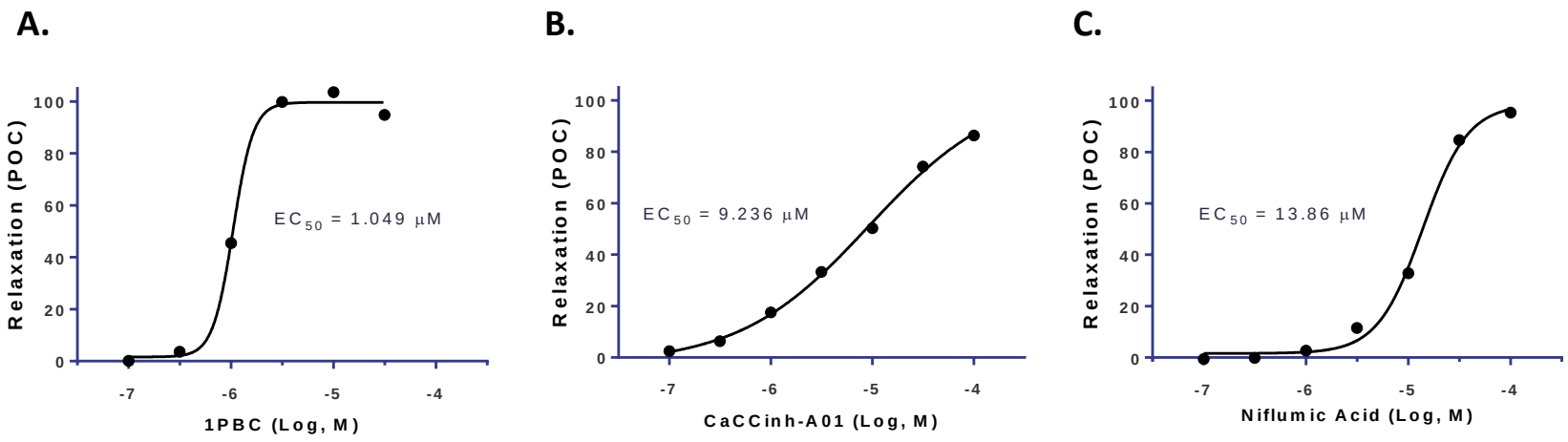

Figure 3_Supplementary Figure 8. TMEM16A antagonists offer a new mechanism for bronchodilation of airways. The efficacy of 1PBC (**A**), CaCCinh-A01 (**B**), and niflumic acid (**C**) in relaxation of human bronchial rings pre-contracted with carbachol was measured using a DMT wire myograph system. The TMEM16A antagonist 1PBC with an EC_{50} of 1.05 μM was found to be one of the most potent bronchodilators. At the end of each recording and CCRC, theophylline was added to 2.2 mM final to induce maximal relaxation of the bronchial ring, which was considered 100 POC and used for normalization of compound effects. As a precaution, all recordings included the cyclooxygenase inhibitor indomethacin (5 μM) to eliminate any possible indirect effects due to prostaglandins.

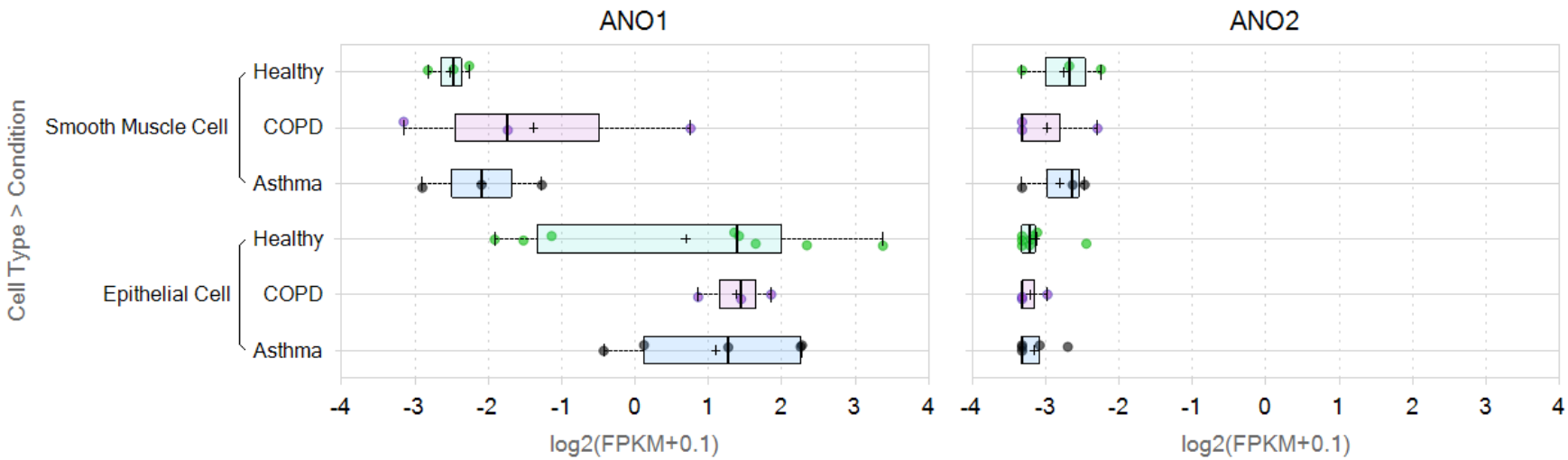

Figure 5_Supplementary Figure 1. *TMEM16A* (*ANO1*) is expressed in cultured human bronchial epithelial cells (HBE; submerged, basal cells) and human airway smooth muscle (ASM) cells from normal, asthmatic or COPD donors, while no significant expression of *TMEM16B* (*ANO2*) was detected. The RNA-seq data shown are from the Amgen Lung dataset described earlier (***Aisenberg et al., 2016***). The results for ASM cells (normal or diseased) are from 3 separate donors each, while the results for HBE cells are the average response from 8 normal, 5 asthma and 3 COPD donors.

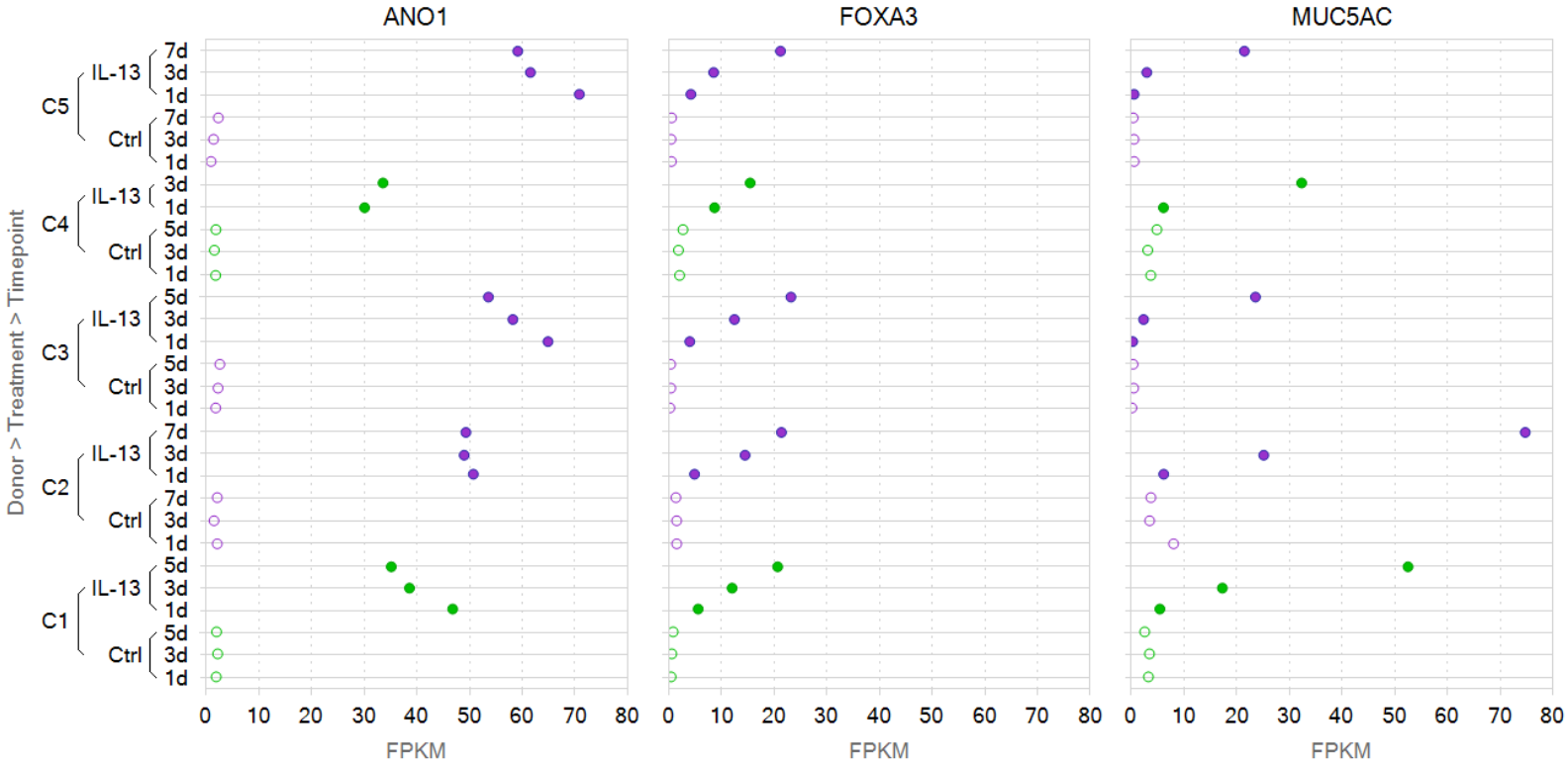

Figure 5_Supplementary Figure 2. *TMEM16A* (*ANO1*; left panel) expression is strongly and quickly upregulated after IL-13 treatment of mature bronchial epithelial ALI cultures reaching a maximum level after 1 day, while increases in *FOXA3* (middle panel) and *MUC5AC* (right panel) occur more slowly from day 1 to day 5/7. The data shown are from ALI cultures from two normal (green) and three COPD (purple) donors, untreated (Ctrl, open circles) or treated with IL-13 (closed circles). Further details on this dataset are provided in the Materials and Methods.

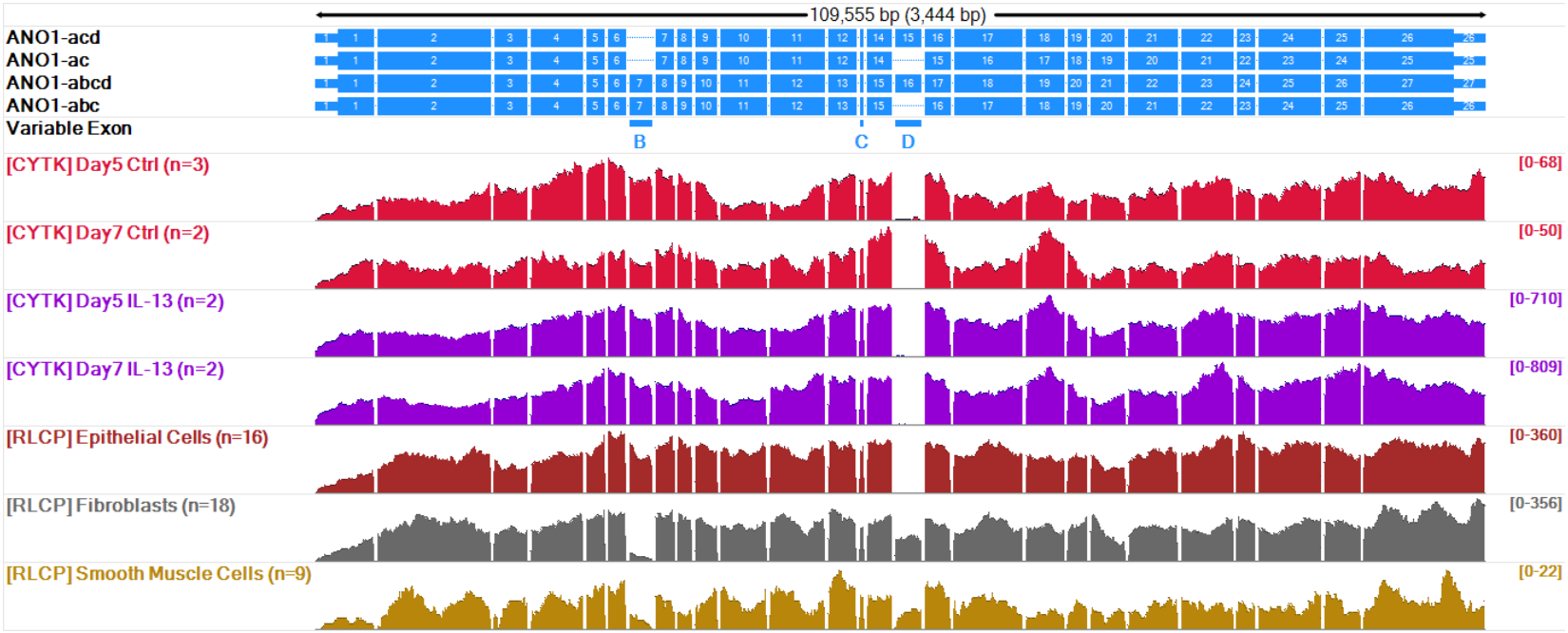

Figure 5_Supplementary Figure 3. Array Studio visualization of RNA-Seq read coverage indicates submerged bronchial epithelial cells (RLCP Epithelial Cells) and fully differentiated bronchial epithelial cells (CYTK) from untreated (red; Day5-or Day7-Ctrl) or IL-13 treated (purple; Day5 or Day7) ALI cultures predominantly express the 'abc' splice variant of *TMEM16A* (*ANO1*). In contrast, cultured (RLCP) human airway smooth muscle cells (ocher) and fibroblasts (gray) show a mixture of splice variants, with segments A and C detected in nearly all, but variable expression of segments B and D. Since ASM cells express lower levels of *ANO1* than the bronchial epithelium, it is difficult to decipher the exact variants expressed in ASM cells. The track entitled 'Variable Exon' shows the location of segments B, C and D. The four transcripts (blue) diagrammed at the topic of the image represent the most common permutations of segment B, C, and D inclusion (segment A appears to be almost universally retained). Thick bars denote exon sequences, and thin bars denote UTR sequences, which have been truncated to emphasize coding exon coverage. Intronic regions common to all transcripts are omitted. The individual RNA-Seq coverage tracks show aggregate read coverage for samples from the Amgen Lung dataset (RLCP) described earlier (***Aisenberg et al., 2016***) and the ALI culture IL-13 dataset (CYTK) described in the Materials and Methods. The scale on the right side of the track indicates the maximum coverage of any base within the region. This visualization was made using the Array Studio gene browser (Omicsoft, NC).

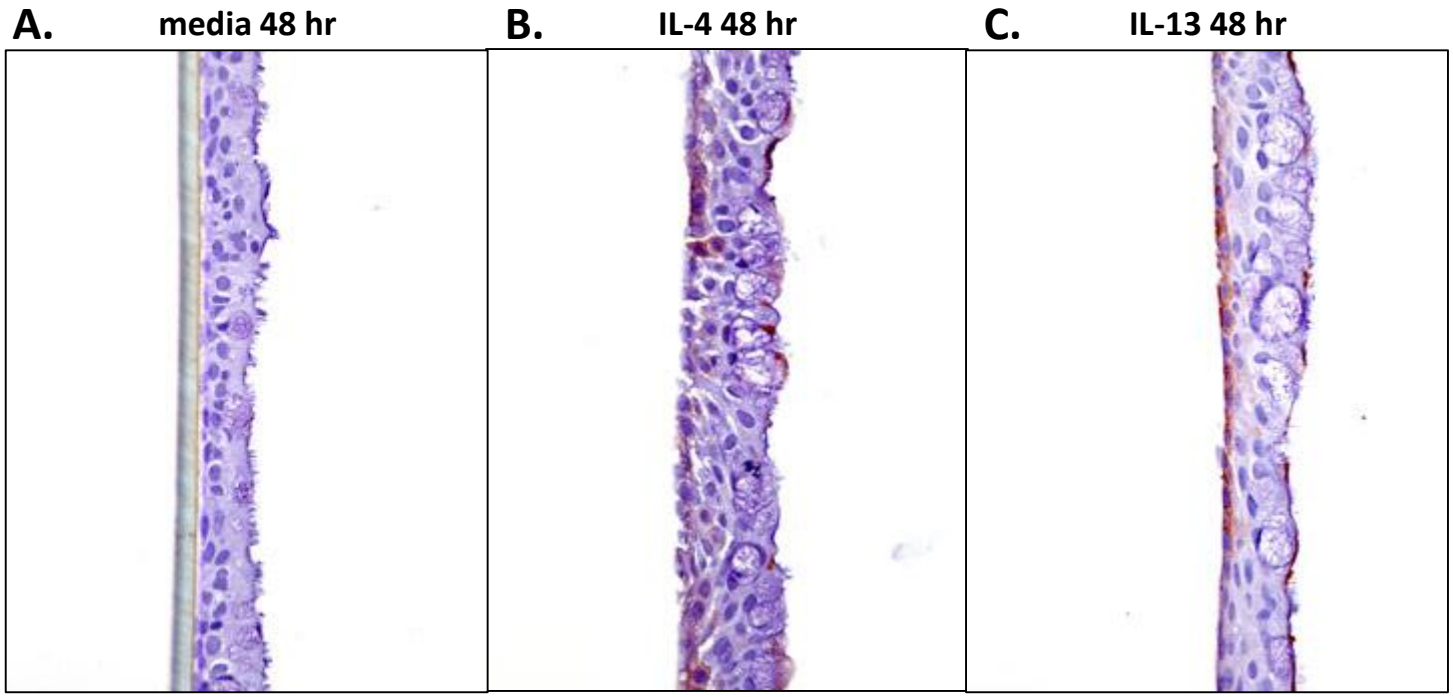

S14WR-00279

Figure 5_Supplementary Figure 4. Th2 cytokines upregulate TMEM16A in human bronchial epithelial air-liquid interface (ALI) cultures and show staining of basal cells and goblet cells. Fully differentiated human bronchial epithelial ALI cultures were untreated (**A**) or treated for 48 hours with IL-4 (**B**) or IL-13 (**C**), fixed and stained with a rabbit anti-TMEM16A monoclonal antibody from Abcam (Ab64085).

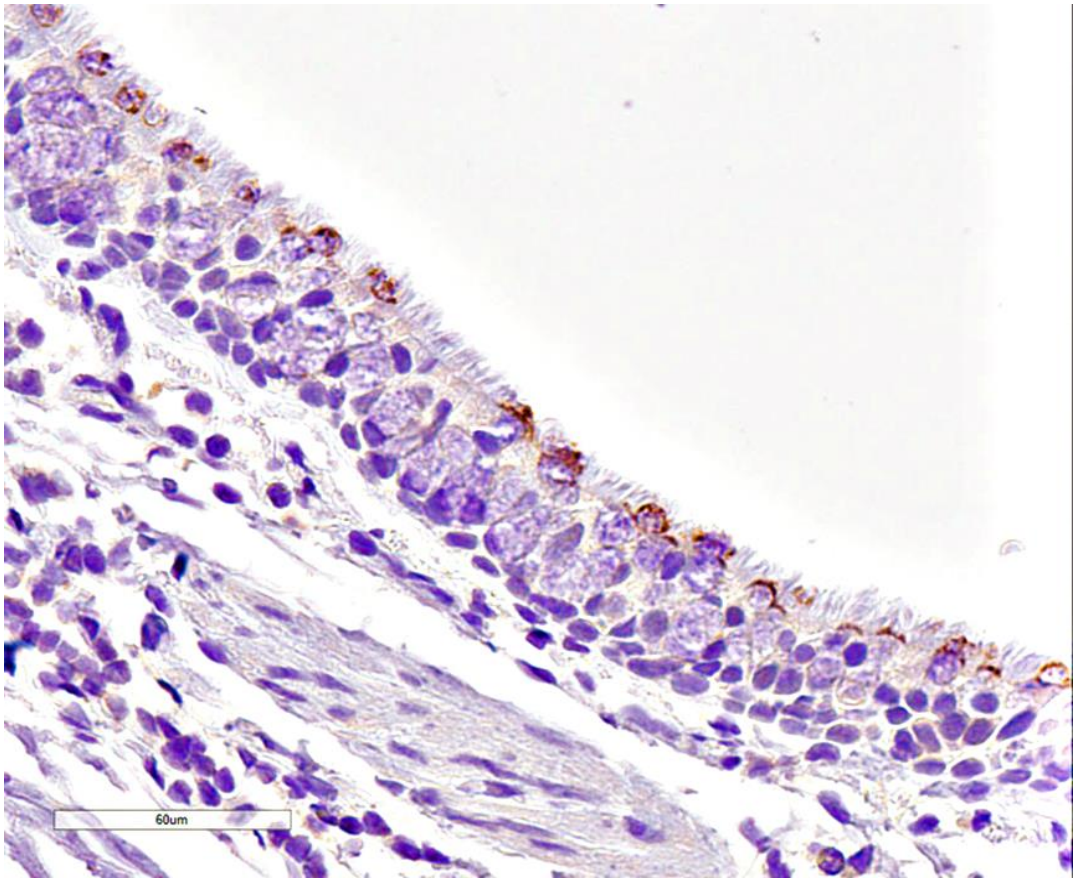

Figure 5_Supplementary Figure 5. TMEM16A expression on the apical surface of goblet cells of *Ascaris suum* challenged cynomolgus monkeys. Lung specimens from asthmatic cyno #384750 were collected 24 hours post *A. suum* challenge. Immunohistochemical staining with the anti-TMEM16A polyclonal antibody Ab53212 (Abcam) indicates TMEM16A is expressed selectively on the apical surface of goblet cells within the bronchial epithelium.

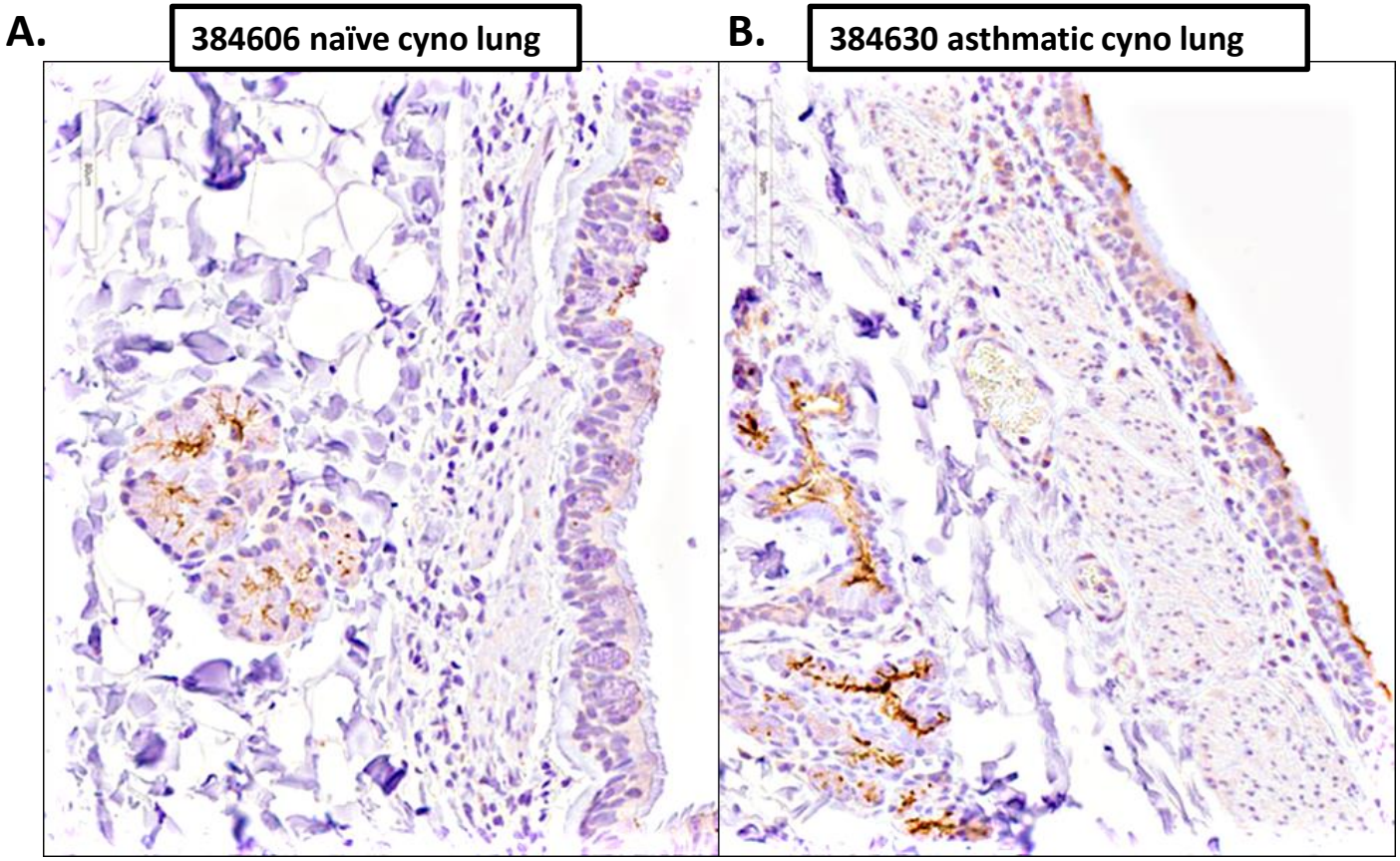

Figure 5_Supplementary Figure 6. Elevated TMEM16A expression is detected in the bronchiolar epithelium and submucosal glands of asthmatic monkeys. Cynomolgus monkeys repeatedly challenged with *Ascaris suum* (**B**) were compared to naïve non-allergic monkeys (**A**) for TMEM16A expression using the polyclonal antibody Ab53212 (Abcam). Increased TMEM16A staining was observed on the apical surface of the bronchial epithelium and in submucosal glands of *A. suum* challenged monkeys (**B**).

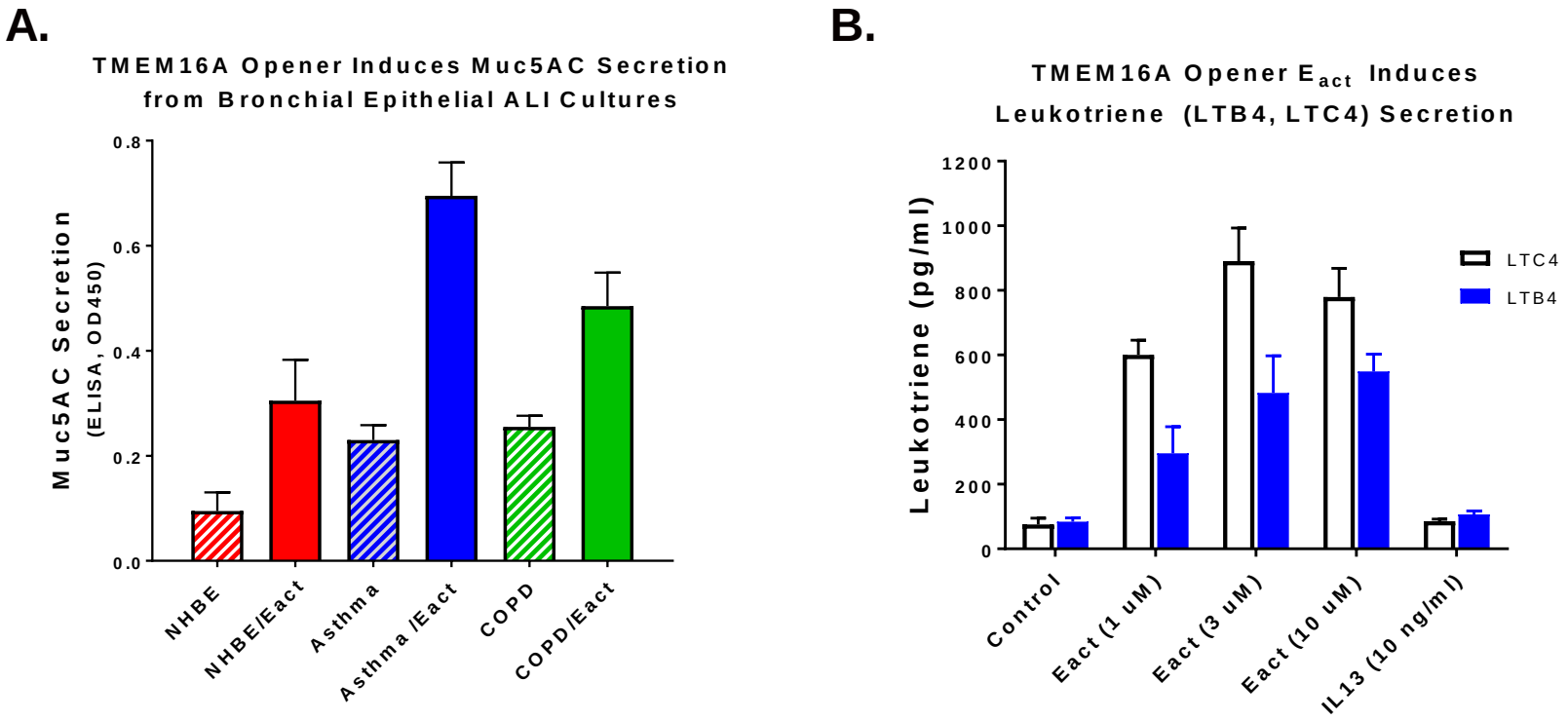

Figure 5_Supplementary Figure 7. The TMEM16A opener E_{act} induces Muc5AC and leukotriene secretion from human bronchial epithelial (HBE) air-liquid interface (ALI) cultures. Mature (14 day) HBE ALI cultures from normal, asthma or COPD patients (2 donors each, 2 ALI cultures per donor) were treated with vehicle or 5 μM Eact in basal medium for 72 hours and then the apical side of ALI cultures were washed with 10mM DTT at 37°C for 15min to collect mucus for MUC5AC ELISA analysis (**A**). To measure effects on leukotriene secretion, normal HBE ALI cultures were treated with Eact vehicle (control), Eact opener, or 10ng/ml IL13 in basolateral medium for 48 hrs (n = 3 ALI cultures per condition), after which 100 ul of basolateral medium was collected and leukotriene B4 and C4 were determined by ELISA (**B**). Shown is Mean ± SD.

Cell Line	Aliases	Tissue	Cancer	ANO1 FPKM
TE11	TE-11	Esophagus	Squamous Cell Carcinoma	396.1
MDAMB415	MDA-MB-415	Breast	Carcinoma	194.4
TT_ESOPHAGUS	T.T|T_T	Esophagus	Squamous Cell Carcinoma	162.8
SCC25	SCC-25	Tongue	Squamous Cell Carcinoma	132.7
EPLC272H	EPLC-272H	Lung	Squamous Cell Carcinoma	130.4
VMCUB1	VM-CUB1	Bladder	Transitional Cell Carcinoma	121.4
COLO201	COLO 201	Colon	Adenocarcinoma	120.5
PANC0403	Panc 04.03|Panc4.03	Pancreas	Adenocarcinoma	117.7
PATU8902	PA-TU-8902|PATU8902T	Pancreas	Pancreatic Ductal Adenocarcinoma	113.4
OE21		Esophagus	Squamous Cell Carcinoma	107.5
SW1417	SW-1417	Colon	Adenocarcinoma	103.2
LS123		Colon	Adenocarcinoma	101.6
ASPC1	AsPC-1	Pancreas	Pancreatic Ductal Adenocarcinoma	96.8
HS255T	Hs 255.T	Colon	Adenocarcinoma	96.1
CAPAN2	Capan-2	Pancreas	Pancreatic Ductal Adenocarcinoma	95.8
BHY		Head and Neck	Squamous Cell Carcinoma	94.7
MCAS		Ovary	Mucinous Cystadenocarcinoma	89.5
PANC0813	Panc 08.13|Panc8.13	Pancreas	Pancreatic Ductal Adenocarcinoma	88.9
COLO205	COLO 205	Colon	Adenocarcinoma	88.1
RERFLCAD2	RERF-LC-Ad2	Lung	Adenocarcinoma	88.0
HCC1954		Breast	Ductal Breast Carcinoma	85.9
SW480	SW-480	Colon	Adenocarcinoma	84.6
L33	L3.3	Pancreas	Carcinoma	83.3
PATU8988S	PA-TU-8988S	Pancreas	Pancreatic Ductal Adenocarcinoma	83.2
SNU324	NCI-SNU-324|SNU-324	Pancreas	Carcinoma	78.7
TE14	TE-14	Esophagus	Squamous Cell Carcinoma	75.7
5637		Bladder	Carcinoma	74.1
CORL23	COR-L23	Lung	Large Cell Carcinoma	72.3
SCC4	SCC-4	Tongue	Squamous Cell Carcinoma	72.3
BFTC905	BFTC-905	Bladder	Transitional Cell Carcinoma	72.1
T3M4	T3M-4	Pancreas	Pancreatic Ductal Adenocarcinoma	72.0
SNU899	NCI-SNU-899|SNU-899	Aerodigestive Tract	Squamous Cell Carcinoma	63.0
PECAPJ34CLONEC12	PE/CA-PJ34 (clone C12)	Oral Cavity	Squamous Cell Carcinoma	62.7
SNU1197	NCI-SNU-1097|SNU-1197	Large Intestine	Carcinoma	61.4
SW1990	SW 1990|SW-1990	Pancreas	Pancreatic Ductal Adenocarcinoma	58.0
BICR22	BICR 22	Tongue	Squamous Cell Carcinoma	56.6
SNU1196	NCI-SNU-1196|SNU-1196	Biliary Tract	Carcinoma	55.2
BICR31	BICR 31	Tongue	Squamous Cell Carcinoma	54.3
PANC0203	Panc 02.03|Panc2.03	Pancreas	Adenocarcinoma	52.7
HPAC		Pancreas	Pancreatic Ductal Adenocarcinoma	52.2
CAL148	CAL-148	Breast	Ductal Breast Carcinoma	52.0
CAL12T	CAL-12T	Lung	Non-Small Cell Carcinoma	51.4
PK59	PK-59	Pancreas	Carcinoma	49.2
PC3	PC-3	Prostate Gland	Adenocarcinoma	49.1
YAPC		Pancreas	Pancreatic Ductal Adenocarcinoma	47.9
HCC1428		Breast	Adenocarcinoma	47.4
SNU81	NCI-SNU-81|SNU-81	Large Intestine	Carcinoma	46.6
DANG	DAN-G	Pancreas	Carcinoma	46.5
A253	A-253	Submandibular Gland	Mucoepidermoid Carcinoma	45.9
SNU719	NCI-SNU-719|SNU-719	Stomach	Carcinoma	45.1
UACC893	UACC-893	Breast	Ductal Breast Carcinoma	44.5
HCC2218		Breast	Ductal Breast Carcinoma	44.4
PANC0327	Panc 03.27|Panc3.27	Pancreas	Pancreatic Ductal Adenocarcinoma	43.5
DV90	DV-90	Lung	Adenocarcinoma	43.5
HCC1500		Breast	Ductal Breast Carcinoma	43.1

Cell Line	Aliases	Tissue	Cancer	ANO1 FPKM
CL11	CL-11	Colon	Adenocarcinoma	42.1
SKCO1	SK-CO-1	Colon	Adenocarcinoma	42.0
BC3C	BC-3C	Bladder	Transitional Cell Carcinoma	41.5
TE9	TE-9	Esophagus	Squamous Cell Carcinoma	41.2
CJM		Skin	Melanoma	40.4
HPAFII	HPAF-II	Pancreas	Pancreatic Ductal Adenocarcinoma	40.4
HUG1N	HuG1-N	Stomach	Carcinoma	39.7
NCIH854	H854|NCI-H854	Lung	Adenocarcinoma	38.1
RCM1	RCM-1	Rectum	Adenocarcinoma	38.1
MDAMB134VI	MDA-MB-134|MDA-MB-134-VI	Breast	Ductal Breast Carcinoma	38.0
OCUM1	OCUM-1	Stomach	Adenocarcinoma	37.9
CAPAN1	Capan-1	Pancreas	Pancreatic Ductal Adenocarcinoma	37.8
HCC1419		Breast	Ductal Breast Carcinoma	35.4
HCT116	HCT 116|HCT-116	Colon	Carcinoma	35.3
PK1	PK-1	Pancreas	Carcinoma	35.3
OE19		Lower Third of the Esophagus	Adenocarcinoma	34.8
YD38	YD-38	Aerodigestive Tract	Squamous Cell Carcinoma	34.3
SNU620	NCI-SNU-620|SNU-620	Stomach	Carcinoma	33.6
SNUC5	SNU-C5	Large Intestine	Adenocarcinoma	31.1
LU65		Lung	Non-Small Cell Carcinoma	31.1
MDAMB175VII	MDA-MB-175|MDA-MB-175-VII	Breast	Ductal Breast Carcinoma	31.0
OE33		Lower Third of the Esophagus	Adenocarcinoma	30.9
SCC15	SCC-15	Tongue	Squamous Cell Carcinoma	30.8
SNU175	NCI-SNU-175|SNU-175	Large Intestine	Carcinoma	30.3
ZR751	ZR-75-1	Breast	Ductal Breast Carcinoma	29.9
HUPT3	HUP-T3	Pancreas	Pancreatic Ductal Adenocarcinoma	29.5
LS180	LS 180	Colon	Adenocarcinoma	29.0
CAL27	CAL 27	Tongue	Squamous Cell Carcinoma	28.9
BICR18	BICR 18	Larynx	Squamous Cell Carcinoma	28.8
JHOM2B	JHOM-2B	Ovary	Mucinous Adenocarcinoma	28.7
PC14	PC-14	Lung	Non-Small Cell Carcinoma	28.5
PANC0504	Panc 05.04	Pancreas	Adenocarcinoma	27.9
PECAPJ15	PE/CA-PJ15	Tongue	Squamous Cell Carcinoma	27.8
SW1116	SW 1116|SW-1116	Colon	Adenocarcinoma	27.8
JHUEM3	JHUEM-3	Uterus	Adenocarcinoma	26.9
BT474	BT-474	Breast	Ductal Breast Carcinoma	26.5
HT29	HT-29	Colon	Adenocarcinoma	26.7
KP2	KP-2	Pancreas	Tubular Adenocarcinoma	26.4
RERFLCAD1	RERF-LC-Ad1	Lung	Adenocarcinoma	26.3
DU4475		Breast	Ductal Breast Carcinoma	25.8
NCIH1648	H1648|NCI-H1648	Lung	Adenocarcinoma	25.7
IM95		Stomach	Adenocarcinoma	25.4
CFPAC1	CFPAC-1	Pancreas	Pancreatic Ductal Adenocarcinoma	25.1
SW837	SW-837	Rectum	Adenocarcinoma	23.7
KYSE140	KYSE-140	Esophagus	Squamous Cell Carcinoma	23.4
SNU1076	NCI-SNU-1076|SNU-1076	Aerodigestive Tract	Squamous Cell Carcinoma	23.3
RERFLCKJ	RERF-LC-KJ	Lung	Non-Small Cell Carcinoma	23.1
HS695T	Hs 695T	Skin	Amelanotic Melanoma	22.7
NUGC3	NUGC-3	Stomach	Adenocarcinoma	21.8
UMUC1	UM-UC-1	Bladder	Transitional Cell Carcinoma	21.5
HUCCT1	HuCCT1	Bile Duct	Carcinoma	20.5
TE15		Esophagus	Squamous Cell Carcinoma	20.1
NCIH2347	H2347|NCI-H2347	Lung	Adenocarcinoma	20.1
SNU407	NCI-SNU-407|SNU-407	Large Intestine	Carcinoma	20.0
LS411N		Cecum	Adenocarcinoma	20.0

Figure 5_Supplementary Figure 8. *TMEM16A* (*ANO1*) expression in cancer cell lines. The RNA-Seq *ANO1* expression level is reported for cell lines from the Cancer Cell Line Encyclopedia (***Barretina et al, 2012***), one cell line present in both CCLE and Amgen (HT-29; average FPKM shown) and a single cell lines assayed at Amgen, COLO205. The results for cancer cell lines exhibiting the highest expression (FPKM ≥ 20) are shown, and in all cases except HT-29 sample size is one.

A.

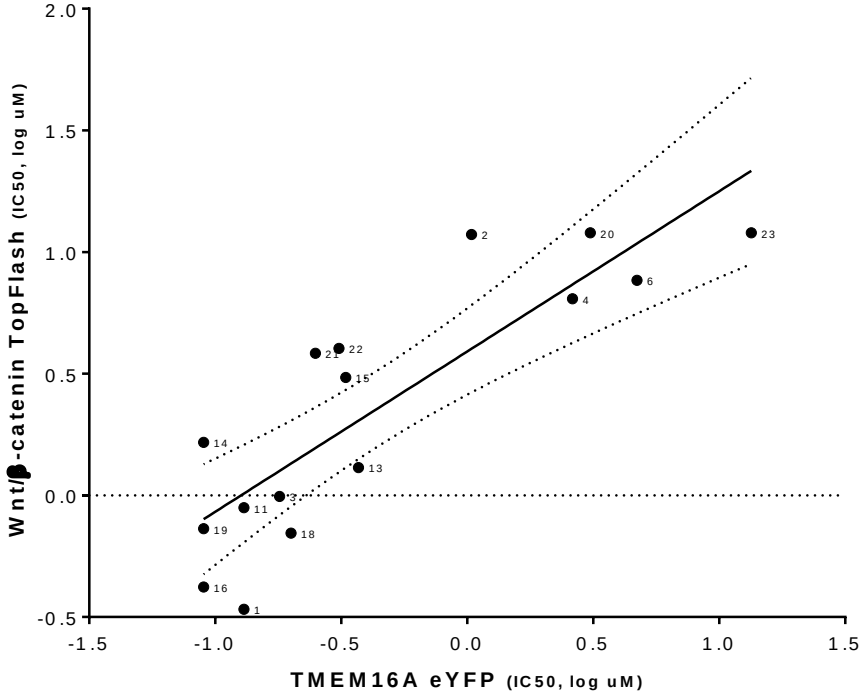

B.

Compound No.	TMEM16A eYFP Assay (IC50, uM)	Mook et al. Wnt/b-catenin TopFlash (IC50, uM)	IC50 Ratio, Wnt/TMEM16A
1	0.13	0.34	2.62
2	1.04	11.81	11.36
3	0.18	0.99	5.50
4	2.62	6.42	2.45
6	4.72	7.66	1.62
11	0.13	0.89	6.85
13	0.37	1.30	3.51
14	0.09	1.65	18.33
15	0.33	3.05	9.24
16	0.09	0.42	4.67
18	0.20	0.70	3.50
19	0.09	0.73	8.11
20	3.08	>12	NA
21	0.25	3.84	15.36
22	0.31	4.02	12.97
23	13.4	>12	NA

Figure 5_Supplementary Figure 9. Activity of sixteen niclosamide compounds on TMEM16A versus Wnt/β-catenin. ***Mook et al. (2015)*** describe the structure and activity of various niclosamide analogs for inhibition of Wnt/β-catenin transcription using a TopFlash assay. Sixteen of these compounds we have also tested for activity in our halide-sensitive TMEM16A eYFP assay and the activity is compared in the plot provided in panel (**A**). Pearson's analysis of correlation (n=14) using GraphPad Prism 7.03, provided an r of 0.8046 and P (two-tailed) of 0.0005. The raw IC_{50} values from each compound are provided in the table (**B**), where compound numbering is as provided by ***Mook et al. (2015)***, with Compound No. 1 being niclosamide.